Title of Thesis | **Digital Elevation Modeling of Inaccessible Slope by Using Close-Range Photogrammetric Data**

I, BAMBANG KUN CAHYONO

hereby allow my thesis to be placed at the Information Resource Center (IRC) of Universiti Teknologi PETRONAS (UTP) with the following conditions:

1. The thesis becomes the property of UTP.
2. The IRC of UTP may make copies of the thesis for academic purposes only.
3. This thesis is classified as:

[ ] Confidential

[X] Non Confidential

If this thesis is confidential, please state the reason:

_____

The contents of the thesis will remain confidential for _____ years.

Remarks on disclosure:

_____

_____

Signature of Author

Endorsed by

Signature of Supervisor

Assoc. Prof. Dr. Abdul Nasir Matori
Associate Professor
Civil Engineering Department
Universiti Teknologi PETRONAS
Bandar Seri Iskandar, 31750 Tronoh
Perak Darul Ridzuan, MALAYSIA

Permanent Address:
Dept. of Geodesy and Geomatic Engineering
Gadjah Mada University
Jl. Grafika No.2, Yogyakarta
Indonesia

Date: 16 March 2009

Permanent Address:
Civil Engineering Department
Universiti Teknologi PETRONAS
Bandar Seri Iskandar, Perak
Malaysia

Date: 16. 3. 2009

UNIVERSITI TEKNOLOGI PETRONAS

Approval by Supervisor

The undersigned certify that they have read, and recommend to

The Postgraduate Studies Programme for acceptance, a thesis entitled

Digital Elevation Modeling of Inaccessible Slope by Using

Close-range Photogrammetric Data

submitted by

Bambang Kun Cahyono

for the fulfillment of the requirements for the degree of

Masters of Science in Civil Engineering

_____

Date

Signature : _____

Main Supervisor : Assoc. Prof. Dr. Abd. Nasir Matori

Date : 16. 3. 2009

Co-Supervisor : _____

Assoc. Prof. Dr. Abdul Nasir Matori
Associate Professor
Civil Engineering Department
Universiti Teknologi PETRONAS
Bandar Seri Iskandar, 31750 Tronoh
Perak Darul Ridzuan, MALAYSIA

UNIVERSITI TEKNOLOGI PETRONAS

Digital Elevation Modeling of Inaccessible Slope by Using Close-range Photogrammetric Data

By

Bambang Kun Cahyono

A THESIS

SUBMITTED TO THE POSTGRADUATE STUDIES PROGRAMME

AS A REQUIREMENT FOR THE

DEGREE OF MASTERS OF SCIENCE IN CIVIL ENGINEERING

CIVIL ENGINEERING

BANDAR SERI ISKANDAR,

PERAK

JANUARY, 2009

ACKNOWLEDGEMENT

First and foremost, I would like to thank ALLAAH the almighty, for HIS blessing enabling me to complete this thesis. I am very grateful to my parents, who taught me the meaning of struggle in this life. Also I would like to express my deep indebtedness to my lovely wife Vita Puspita and my son Hafid Miftahul Azzam for their true love and support. Their loves becomes my power in my life and always make my life more meaningful.

Special acknowledgement goes for my supervisor Dr. Abd. Nasir Matori, for all of his knowledge, experience, critical thinking, and also his innumerable and invaluable contribution in this work as well as his ongoing support to complete this work. Under his supervision, I grew professionally to face new challenges in my career.

Thanks and gratitude must be given to Dr. Mohd. Fadhil Nuruddin, and all lecturers of Civil Engineering Department whom contributed their ideas, expertise and advices. Thanks to Dr. Indra Sati Hamonangan Harahap, the coordinator of Grant Assistantship in the department. Special thanks for Civil Engineering Technicians: Mr. Zaini, Mr. Meor, Mr. Ideris, Mr. Johan, Mr. Hafiz, Mr. Iskandar, Mr. Anuar, Mrs. Suhaila, Miss. Yusyawati, Miss. Ima, Miss. Ina, and Mrs. Noor for their nice cooperation during my studies.

Thanks are extended for the staff of Post Graduate Studies Office especially Mrs. Kamaliah and Mr. Hizwan for their invaluable help and cooperation.

Last but not least, thanks are given to Mrs. Yeni, Mr.Dedi, Mr. Basith, Mr. Hendrayana, Mr. Joko and his family, Mr. Asri and his family, Mr. Martin and his family, Indonesia Community in Bandar-University and all of my colleagues and friends, who support and comfort me through the good and bad times; they have given me a lot of fun and unforgettable moments.

ABSTRACT

Digital Elevation Model (DEM) currently is extensively used extensively in various applications such as for natural hazard assessment and monitoring of high risk areas. DEM data source of inaccessible areas can be collected by using several methods, but mostly are costly and requires sophisticated instruments. Due to these conditions, close-range photogrammetry offers a low cost alternative solution. Materials presented in this thesis are based on the experiments to explain the application of close-range photogrammetry with the aid of commercial digital pocket camera as DEM data collection tools, applied on inaccessible slope areas. The analysis covers calibration of the camera and surveying instruments, DEM data collections, data processing and visualization, together with DEM quality measures. The data collections are accomplished on several study areas with different topographical characteristics by using close-range photogrammetry technique. The sampling points were selected on stereo model, by using three types of sampling methods. The DEM quality measures are assessed by following elevation interpolation error and volumetric difference error analyses. The representation of the DEM is generated using TIN-based (Triangular Irregular Network) approach. The result shows that the method is able to be applied for three dimensional (3D) modeling of potentially unstable slope areas, with accuracy of less than 15 cm in RMS for elevation error and is less than 1% in volume error. The result has indicated that topographical condition has not affected the accuracy of generated DEM. Improvement of point density radically enhances the DEM's quality, up to a certain level of point density beyond which the increment of the accuracy is not significant. The difference setting of focal length has also influences the quality of captured images, and drastically affects the accuracy of the DEM. If the accuracy of the DEM is a matter of concern, the preferred sampling method is selective sampling, while if accuracy and DEM's time generation are the concern the most effective sampling method is regular sampling method. Since there was no permanent points on the observed slope surface, velocity and direction of landslide could not be accurately determined. However the distribution of mass-movement and elevation changed on the slope surfaces can be modeled through spatial-calculation of overlaying DEMs together with profiling of cross-section and longitudinal-section of the generated DEMs.

ABSTRAK

Model Ketinggian Berdigit (DEM) amat meluas digunakan pada masa ini dalam pelbagai penggunaan seperti untuk taksiran kawasan merbahaya semula jadi dan pemantauan kawasan berisiko tinggi. Sumber data DEM di kawasan yang tidak dapat dilalui, dapat diperolehi melalui beberapa kaedah tetapi memerlukan kos yang tinggi dan penggunaan peralatan yang canggih. Oleh itu, fotogrametri jarak dekat menawarkan satu penyelesaian alternatif dengan kos rendah. Bahan-bahan yang disampaikan dalam tesis ini dilandasi beberapa eksperimen bagi menerangkan penggunaan fotogrametri jarak dekat sebagai alat pengumpulan data DEM, digunakan pada kawasan lereng yang tidak dapat dilalui. Analisis itu terdiri dari penentu ukuran bagi alatan, pengumpulan data DEM, pemprosesan dan paparan data, dan pengiraan kualiti DEM. Pengumpulan data dibuat pada beberapa kawasan kajian dengan ciri-ciri topografi yang berbeza, menggunakan tiga jenis kaedah persampelan data. Kualiti DEM ditaksir oleh analisis ralat penentu dalaman ketinggian dan analisis ralat perbezaan isipadu. Penjanaan DEM dibuat menggunakan pendekatan Rangkaian Segitiga Tak Nalar (TIN). Keputusan menunjukkan bahawa kaedah itu mampu untuk digunakan untuk pemodelan tiga dimensi (3D) kawasan lereng tidak stabil, dengan hasil RMS kurang daripada 15 cm untuk ralat ketinggian dan kurang daripada 1% dalam ralat isipadu. Hasil uji kaji menunjukkan, keadaan topografi tidak menjejaskan ketepatan DEM. Peningkatan kepadatan titik menambah kualiti DEM dengan ketara, hingga satu tahap tertentu dimana kepadatan titik tidak lagi mempengaruhi peningkatan ketepatan. Perbezaan jarak fokus juga mempengaruhi kualiti imej, dan memang secara drastik meningkatkan ketepatan DEM. Persampelan memilih adalah yang terbaik jika ketepatan DEM adalah perkara utama, manakala persampelan nalar adalah lebih sesuai jika masa penjanaan dan ketepatan DEM yang dipentingkan. Bagaimanapun ketiadaan titik-titik kawalan pada permukaan lereng mensabitkan halaju dan arah tanah runtuh tidak dapat dihitung dengan mutlak. Tetapi taburan pergerakan jisim dan perubahan ketinggian di permukaan cerun itu boleh dimodelkan melalui pengiraan DEM dan penghasilan susuk keratan-rentas dan keratan-membujur dari pada DEM yang dihasilkan.

TABLE OF CONTENT

LIST OF TABLES

LIST OF FIGURES

CHAPTER 1

INTRODUCTION

1.1. Background

Digital Elevation Model (DEM) presently is extensively used in various applications. Some investigation (especially for spatial analysis) can be performed easily by using this data. The DEM data is comprised of easting, northing, and height from selected area, and can be visualized in three dimensional (3D). In civil engineering applications, the data is required for some structural constructions, and necessary for geotechnical engineering applications, such as construction of infrastructures, defining of power distribution and public utilities, defining of offshore pipeline routes. Further more, it can be applied for assessment of natural hazard, and monitoring of high risk areas.

A Digital Elevation Model (DEM) can be expressed as a digital and mathematical representation of an existing or virtual object and its environment within a selected area [1]. Idea about the DEM was initiated in 1958 by C. Miller and Laflamme from the Massachusetts Institute of Technology. They derived a 3D model of the earth surface by using stereo aerial photogrammetry method [2]. To date, a DEM can be generated from several methods; such as by using digitizing of topographic map, conventional terrestrial survey (Theodolite, Total Station), satellite positioning systems (GPS, GLONASS, GALILEO), radargrammetry (Linear SAR, Interferometry SAR), laser ranging (Airborne Laser Scanning, Terrestrial Laser Scanning), and by using stereo-pair images (nadir-backward satellite images, stereo aerial photogrammetry, and terrestrial photogrammetry). With respect to terrestrial photogrammetry it uses of close-range photogrammetry technique.

Close-range photogrammetry is a technique for obtaining 3D information of any object that was imaged on the 2D (two dimensional) photos, [3]. In the beginning period,

development of aerial photogrammetry and close-range photogrammetry were virtually identical until the First World War, when the aerial photogrammetry was expanded to be the most possible method to create a complete coverage map of entire continent, without directly contacting to the earth surface. In 1926 this method was initiated for terrestrial, architectural, and engineering photogrammetry and then in the next period it was known as non-topographic photogrammetry. The camera, lenses, and stereo-plotter of aerial photogrammetry was adopted to develop close-range photogrammetry technique [4].

Basic concept of close-range photogrammetry method was adopted from stereo aerial photogrammetry, and then continuously developed parallel with the advancement of digital technology and the expansion of computer technology. The 3D position of any objects that lie in the overlapping images can be calculated by space intersection of two rays of respective object projected on left and right photos. Images in close-range photogrammetry can be captured by using three types of camera; metric camera, semi-metric camera, and non-metric camera (pocket camera) [5]. Measurement by using a digital pocket camera offers a low cost alternative in mapping's data collection tools.

As mentioned previously, a DEM is a representation of an observed object in 3D view derived from set of 3D points' coordinate. In general photogrammetry technique, a 3D measured point is acquired from positional measurement of a certain point on a stereo model, in which the stereo model is calculated and transformed from 2D stereo overlapping images by following a certain stereo restitution method [6]. Selection of sampling points in photogrammetry methods can be performed by automatic and manual selection processes. Point selection for all pixels in manual sampling is impossible to be carried out, because it is impractical due to time consuming and possibly poorer accuracy. By using the sampling points, characteristic of the observed object can be represented well.

Inaccessible unstable slope area is one of the risky areas that is important to be monitored for safety and maintenance purposes, especially if the location is closed to residential area or infrastructures. Monitoring of the slope area can be carried out easily by using DEMs

derive from several epoch data. Landslide and mass-movement on the slope area can be detected well by calculation of DEMs derived from at least two difference epoch data, or by profiling of longitudinal-section or cross-section over the DEM of observed slope area. Measurement of the landslide is very essential to be performed in order to identify its velocity and volume. By knowing the velocity and the volume of the landslide some actions can be taken to rescue the surrounding area, such as terracing the slope area, wrapping the slope by net or waterproof covers, providing better drainages on the slope area, and excavating the unstable slope. Slope area can be measured and monitored by using various methods. One of them is by using close-range photogrammetry method. The method is preferred because of its reasonably low cost and its suitability for measuring inaccessible and risky areas.

1.2. Problem Statement

The utilization of DEM within entire civil engineering community has been practiced for various spatial analysis, especially in hydrological, structures, and geotechnical fields. Strength of constructions and structures stability is one of the most important factors that should be given attention, moreover if the structures are located close to an unstable slope area. Hence measurement and monitoring of the slope area is necessary to be performed for safety and maintenance purposes.

Terrestrial survey method by using normal total station is the most familiar and accurate technique that has been applied in civil engineering projects. Distances and coordinates measurement of target points by using this method requires placement of prism-pole on the observed objects. Application of this technique on inaccessible areas is barely to be performed due to the difficulties in placement of the prism. This condition therefore requires practitioners to use another method that is able to be applied for measurement of inaccessible area, without direct contact to the observed objects.

There are several methods that can be utilized for a DEM data collection tool to be applied on inaccessible areas such as Interferometry Synthetic Aperture Radar, Airborne

Laser Scanner, Terrestrial Laser Scanner, and GPS/GLONAS/Galileo, but all the techniques are expensive and require sophisticated instruments. In civil engineering projects, all methods and applications have to be assessed from technical and financial point of view. Hence close-range photogrammetry technique offers an alternative low cost solution to these problems.

1.3. Research Objectives

The main purpose of this research is to experimentally study the application of close-range photogrammetry as a data acquisition tool in the DEM generation, applied for inaccessible unstable slope areas. The main objectives of the research are:

i. To explore deriving DEM of observed area from overlapping photographs using close-range photogrammetry method.
ii. To determine characterizing accuracy of the close-range photogrammetry (due to topographical condition and selection of sampling method issues) as a DEM data collection tool.
iii. To verify the suitability of close-range photogrammetry method in slope monitoring.

1.4. Scope of the Research

The scope of this thesis is to study the application of close-range photogrammetry as DEM data collection tool, applied on inaccessible slope areas. Yet, to acquire a comprehensive analysis of this application, the whole process of digital elevation modeling by means of close-range photogrammetry is performed. It covers the calibration of instruments, DEM data collection, data processing and visualization, and also DEM quality measures.

Images exposure for camera calibration's pattern is carried out at the same time when unstable slope's images capturing are performed, to avoid different setting of focal length and different position of principle point because of instability in lenses. The calibration is

accomplished to get information of the camera parameters, which is required to remove systematical errors (caused by lens' distortions) in interior orientation process. Calibration of reflector-less total station is conducted on set of standardized permanent calibration bench-marks, and then calculated by using least square adjustment method. Total Station calibration was performed to correct the measurement data from systematical errors, as well as to check weather the instrument is still in a good condition for distances measurement process or not.

DEM data collection using close-range photogrammetry is accomplished on several study areas with different topographical characteristics, by using three different types of data sampling methods (regular, progressive, and selective sampling methods). Reflector-less total station is used to measure Ground Control Points (GCPs) of stereo images, check points, and also data of reference DEMs. Those GCPs are used to correct geometric of images and then transform it into ground coordinate system, while the check points and reference DEMs are used to measure quality of derived DEM by means of close-range photogrammetry. This is due to the fact that Total Station is the conventional technique that can provide higher accuracy of millimeter level. DEM quality measures are carried out by taking elevation interpolation error analysis together with volumetric difference error analysis. The representation of the DEM is generated using TIN-based (Triangular Irregular Network) approach.

Application of close-range photogrammetry in slope monitoring is accomplished based on at least two different epoch data. Landslide and mass-movement detection on the unstable slope area is detected by spatial-calculation of overlaying derived DEMs, and profiling of longitudinal-section and cross-section of the derived DEMs.

1.5. Outline of Thesis

The overview of digital elevation modeling by means of close-range photogrammetry has been given at the background section of this chapter, continued by problems statement, objectives, scope of study and then outline of the thesis.

Chapter 2 describes the literature review on digital elevation modeling concepts and theories of close-range photogrammetry, as well as best practices and guidelines adopted. Other important reference sources such as text books and standards are also consulted.

Chapter 3 explains the experiment procedures and processes applied on the research. Essential fundamental concept and theories pertaining to the research methodology are also highlighted.

Chapter 4 focuses on the results and discussions of the work accomplished by this research work.

Chapter 5 gives an overall summary of the research, followed by the conclusion of the work done and recommendations for future work.

CHAPTER 2

LITERATURE REVIEW

2.0. Introduction

This chapter reviews some relevant literatures on digital elevation modelling and its application for unstable slope monitoring by means of close-range photogrammetry method, many of which has been published internationally. Special note has been made of those papers discussing about unstable slope area, close-range photogrammetry, digital elevation modeling, data processing, representation and quality measure as well as related cases and relevant issues.

Digital elevation modeling has been in existence for years. Its applications have been constantly evolving, developing and adapting to the changing needs of a multi-discipline workplace. As the use of this grew, it is now widely used in many scientific, commercial and industrial applications one of them is applied for unstable slope area.

2.1. Unstable Slope Area

Unstable slope area needs serious attention because of its hazard potential to the surrounding environment. Due to this condition, measurement and monitoring of the area is furthermore essential if the location of the slope is close to public infrastructures and residential areas. By measuring the displacement, evolution of the slope failure can be observed, and the triggering factors can be analyzed to reduce velocity of the landslide. It is essential to recognize the type of slope and some techniques in slope monitoring.

2.1.1. Classification of Slope

According to the importance of slope measurement, it is crucial to recognize classification of slope surface. Based on the inclination angle, slope can be categorized into gentle, moderate, steep, and very steep slopes classes as presented on Table 2.1. By recognizing inclination angle of the slope as one of its characteristics, certain measurement can be taken to reduce velocity of mass-movement and landslide potential on the surface. Inclination of slope can be expressed into percentage of slope gradient or inclination angle. Illustration about the slope was given in Figure 2.1.

Table 2.1. Slope Classification based on the inclination angle (source: [7], [8], and [9]).

Slope ranges	Classes	Characteristics of slope
$< 15^{\circ}$	Gentle	Routine planting techniques for any kinds of plant and grass are able to be applied
$15^{\circ} - 30^{\circ}$	Moderate	Low difficulty in planting
$30^{\circ} - 45^{\circ}$	Steep	Increasingly difficulty to plant small trees or turf; routine application for hydro seeding
$> 45^{\circ}$	Very steep	Planting small trees and shrubs on benches is recommended

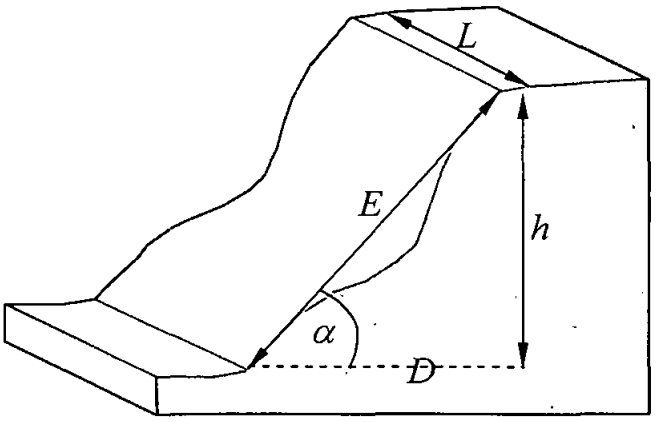

Where:
h is height (m)
E is extension (m)
L is width (m)
α is inclination angle ($^{\circ}$)
D is horizontal distance (m) between top and bottom parts of the slope

Figure 2.1. Illustration of slope surface (source: [7])

Based on the Figure 2.1, inclination angle of the slope (α) also can be expressed as Equation 2.1 [10]:

$$\alpha = \tan^{-1}\left(\frac{h}{D}\right) \tag{2.1}$$

Commonly, beside expressed as slope angle the slope inclination also can be represented in a percentage value, as given by Equation 2.2 below:

$$\% = \left(\frac{h}{D}\right) * 100\% \tag{2.2}$$

If the ability to be accessed on its surface is being a considered matter, slope area can be classified into accessible and inaccessible slope [7]. Accessible slope is a kind of slope area in which measurement and other activities can be conducted on it. Usually it covers on a large area, has a thick sliding layer, and inclination is categorized as gentle until moderate slope. Inaccessible slope is a type of slope area in which conventional terrestrial survey which required direct contact on its surface cannot be performed. Conventionally it happened on a small area, the slope is classified as steep until very steep slope, and physically it is easy to be recognized.

2.1.2. Classification of Landslide

There are several modes of landslide and slope failure that can exist within a steep slope area. Differences in landslide mechanism need to be understood in order to assist design process of any monitoring scheme to be implemented for monitoring of the particular slope. Landslide on the slope surface can be categorized in various form determined by different movement mode and type of material. It classifies slope movement into falls, topples, slides, lateral spreads, and flows. Combination of two or more types of the slope movements is called complex. The material of the moving mass is divided into rock and soil classes, latter split further into debris (mostly coarse material) and earth (mostly fine materials) [11]. The detail classification is presented on Table 2.2.

Table 2.2. Classification of Mass Movements (source: [11])

Type of Movement		Type of Material		
		Bedrock	Engineering Soil	
			Mostly Coarse	Mostly Fine
Falls		rock fall	debris fall	earth fall
Topples		rock topple	debris topple	earth topple
Slides	Rotational	rock slide	debris slide	earth slide
	Translational			
Lateral Spreads		rock spread	debris spread	earth spread
Flows		rock flow (deep creep)	debris flow (soil creep)	earth flow
Complex		combination of two or more principal types of movement		

Brief descriptions about principal type of those displacements are given [12] and [13]. Fall is a very rapid movement of the slope material that separates from steep slopes or cliffs. Most of falls' movements happen due to free fall or by rolling and bouncing. Topple is a block of rock which is tilted or rotated forward on a pivot, then separates from the main mass afterward falls down on the slope, and subsequently bounce and roll further down-slope. Slide is a movement characterized by shear failure along one or more discrete surfaces of fracture. Vector of relative motion are parallel to the surface of rupture. There are two main types of slide, they are rotational and translational. It is called rotational if the movements are rotated on an axis parallel to contour of the slope, while translational is indicated by sliding on a planar surface. Spread is a movement caused by liquefaction, the process whereby saturated, loose, cohesion-less sediments are transformed from a solid into a liquid state. Commonly it occurs on a very gentle slopes or flat terrain. Flow is a rapid movement of materials dominated by granular materials slides down over shear surface. Illustration about the categories can be seen on Figure 2.2.

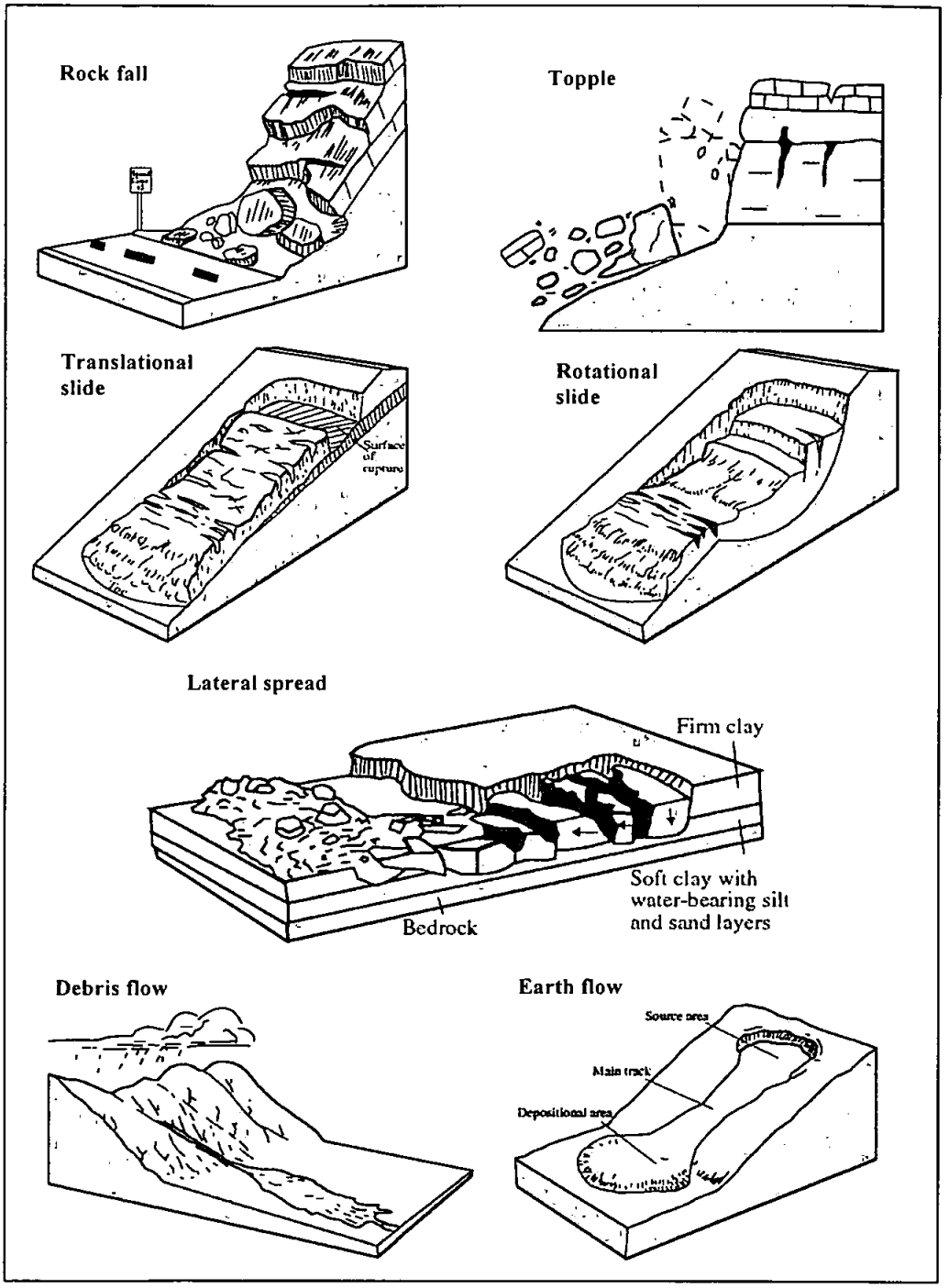

Figure 2.2. Illustration of mass-movement classification (source: [13])

2.2. Some Techniques in Slope Measurement

The measurement of steep slope area can be accomplished using several different techniques. Different modes of deformation will affect the choice of stability analysis

undertaken by the geotechnical engineer and consequently the type of deformation monitoring strategy employed. The techniques that are commonly used to measure the steep slope area can be broadly classified as instrumentation techniques and observational techniques [14].

Instrumentation technique include the use of movement indicators such as crack-meters, fixed and portable borehole extensometers, fixed and portable inclinometers, deflectometers and piezometers. Generally those mentioned methods are able to measure the slope deformation accurately (until sub-millimeters level of accuracy), but unfortunately it represents the movement only in one axis direction. Details about those methods will not be discussed in this thesis. Observation technique usually measures the slope displacement at the exposed areas. One type of these measurement methods require direct contact on the slope surface, while another types can be performed remotely. Including in observation technique is conventional terrestrial surveying (such as Theodolite, auto level, and Total Station), remote sensing techniques (such as photogrammetry, satellite imaging, radar interferometry, and laser scanning), and the use of satellite-based positioning techniques (such as GPS, GLONASS and pseudolites). The main techniques commonly used are discussed in the following sections.

2.2.1. Conventional Terrestrial Surveying

Total Station instruments consist of a device to measure horizontal and vertical angles, and some form of Electromagnetic Distance Measurement (EDM) capability to measure distances. These instruments allow the surveyor to measure 3D coordinates of points remotely (typically targeted by the placement of reflective prisms). They also permit the recording of the data in a digital format to be later downloaded or transmitted to a central processing site. The latest type of the Total Station instruments is the reflector-less Total Station, survey with prisms are no longer required at the slope surface. This, however, may result in a loss of coordinate precision due to imprecision in the repeatability of the reflecting surface. Each material and color of the observed objects has different characteristic in signal repeatability. Therefore calibration for this instrument and the

related materials is necessary to be accomplished before data collection is performed [58]. Recently there are Total Station that is equipped with servo-motors and automatic target recognition algorithms that reduce the need for personnel to physically record the observations [14].

One advantage of using total stations to monitor surface deformation is that the measurements can provide 3D position solutions of the point of interest. Coordinate precision in the vertical domain, however, is typically worse than in the horizontal domain and may not provide the precision required for the monitoring of deformations. Possibly the observations consist a systematic error that cannot be mitigated or removed completely, except by adding the correction value calculated from the calibration. The value was given to all the data measured by the Total Station. If correction values can be given to the measurements data this technique will be the best method applied for an inaccessible slope monitoring [15].

Beside the Total Station measurement, there is another conventional terrestrial surveying technique that can be used to monitor a land deformation. It is a precise levelling technique. This technique is able to provide only one dimension information (elevation or difference height) but until the date time, it is the most precise method of monitoring local vertical deformations This technique can provide a vertical component precision of 0.2 to 1 parts per million (ppm) of the level run length. Disadvantages of the technique are the survey crews must be traverse directly on the unstable surface, and it must also be initiated from a stable monument situated outside the zone of deformation. Due to the ineffectiveness, recently this method is leaved [14].

2.2.2. Satellite-based Positioning Method

Included in satellite-based positioning methods are Global Positioning System (GPS), Global Navigation Satellite System (GLONASS), and Galileo. Actually they have the same basic concept in range intersection, but characteristics of their signals and number of operating satellite is different. Principally to determine an unknown position in 3

dimensional (3D) space, three distances from three known points are needed. In this case, the positions of satellites are all known at any time because the orbit of each satellite is monitored and controlled by ground stations [16]. Therefore to determine position of the receiver, at least three satellites are observed. Observation to more than three satellites is suggested, to get an accurate measurement result.

Application of satellite-based deformation monitoring methods in slope monitoring requires less man-power, and can provide a solution to these problems by providing a continuous or quasi-continuous 3D time-series data, while also maintaining a high level of precision, and operating with minimal user intervention. GPS here is being the primary system of interest, while other systems (GLONASS and Galileo) currently failing to provide the level of operational capability needed for high-precision deformation monitoring [17].

Table 2.3. Main characteristics of RTK-GPS and FS-GPS methods compared with static method (source: [17]).

Method	**Observed time per point**	**Post-process**	**Strength against loss of signal**	**Typical max. base line (km)**	**Typical baseline planimetric error**
Static	1-several hours	Yes	Robust	50-100	5-1mm ± 1-0.1 ppm
FS	8-20 minutes	Yes	Robust	15-20	5 mm ± 1 ppm
RTK	1-10 seconds	No	Sensitive	10	10 mm ± 2 ppm

For deformation monitoring, the use of GPS techniques can be divided into two broad areas. The first area involves high precision static methods such as Continuously Operating Reference Systems (CORS) that are used to (typically) monitor regional scale deformations such as subsidence and geotechnical movements. These continuous systems are normally combined to form permanent networks. The second class of GPS technique is the use of episodic GPS data, commonly used for monitoring on a smaller scale area (with baselines up to a few kilometres), such as monitoring of dams, open-pit mine walls and landslides [14]. GPS observation methods that are usually applied for deformation of

small area are Fast Static (FS-GPS) and Real Time Kinematics (RTK-GPS) methods. Both techniques need shorter time in observation but able to yield high accurate result (until millimeters level). Comparison about characteristics of FS, RTK, and CORS by static method was given on Table 2.3. All of those mentioned techniques still require directly observation on slope surface, it still impossible to be conducted on high risk areas and unstable slope surfaces.

2.2.3. Remote Sensing Technique

Remote sensing is the best method applied for inaccessible area, because it does not require direct measurement conducted on the observed object. Moreover it can be used for small scale until large scale areas. There are some methods included in remote sensing technique, they are photogrammetry, satellite imaging, laser scanning (LIDAR), also radargrammetry & SAR. In the beginning all those methods were initiated for aerial-based systems, but since it needs sophisticated instruments and requires an expensive platform in the applications therefore ground-based method were developed.

Aerial photogrammetry and satellite imaging techniques in slope monitoring require multi-temporal data in which coverage of the observed object should be captured on at least two overlapping images. Some Ground Control Points (GCPs) well distributed on the coverage area is needed in both methods. Position of the GCPs can be recognized on the images based on relative position with other objects. GCPs were needed to rectify images from geometric errors. Spatial resolution and flight height is significant because it influences the resulted accuracy. One of advantages from these techniques is real condition of slope area can be examined well, so image interpretation can be performed to joint with the resulted elevation model. By using multi epoch data deformation and land coverage changing on the slope surface can be analyzed. Vertical accuracy for aerial photogrammetry with flight height 900-1500 m above mean sea level (2.5 μm in pixel size) reaches until 20 cm, while by using SPOT-5 panchromatic images vertical accuracy that can be achieved is 2-3 m [18] and [19].

Due to advancement in reliability of application of laser in remote sensing over the past decades, the Airborne Laser Scanning (ALS) system is becoming an important operational tool in remote sensing and mapping. The ALS system usually called airborne LIDAR (Light Detection and Ranging) in the commercial sector. It is an active remote sensing system [16]. Application of this technique in landslide monitoring should be integrated with a laser range finder (LRF), a computer system to control the on-line data acquisition, a storage medium, a scanner, and a GPS system for determining the position and orientation of the system. As an active system, it sends off electromagnetic energy and records the scattered back signal from the slope surface, as well as every object on it. Every type of materials hit by the pulse determines different intensity of the returning signals [20].

2.3. Digital Elevation Modeling in Slope Monitoring

Slope monitoring cannot be separated from Digital Elevation Model (DEM) because by using this DEM condition of the observed slope can be represented well moreover with multi-series data elevation changes on the surface can be analyzed easily. Most of the observation techniques as mentioned in the previous sub-chapter generate a DEM as a measurement result. In slope monitoring application, those techniques can be combined each others to get best DEM and to define the best analysis method, such as application of GPS and Total Station for GCPs establishment in aerial imaging system, GPS for determination of sensor's position in LIDAR system, DEM resulted form SAR system used to create ortho-images [16].

2.3.1. Definition of Digital Elevation Model

Digital Elevation Model is a digital and mathematical representation of an existing or virtual object and its environment within a selected area [21], while Digital Elevation Modeling is a process for the construction of a Digital Elevation Model. In such a process, points are sampled from the terrain to be modeled with a certain observation accuracy, density, and distribution. A digital surface can be formed by a certain

interpolation method based on the sampled data points [16]. Modeling the slope's surface is a central issue in slope monitoring. Digital Elevation Model (DEM) is a valuable data source for many applications. In this context, a clear distinction has to be made between DEM, digital surface model (DSM) and digital terrain model (DTM) [22]

DTM describe the earth surface in the sense of the bald earth, without human artifacts (such as buildings or bridges) and vegetation. DSM describe the surface in the sense of the first point of intersection by a projecting ray, includes points on buildings and vegetation as well as terrain points. The term DEM describes a 2.5 dimension (2.5 D) model that contains the elevations of points with respect to a reference surface, without any restriction on what the object is like. This term, thus, characterizes a modeling technique rather than the data which are described by an elevation model. In topographic mapping, both DSM and DTM can be described by DEM. Most systems of DEM generation yield the terrain surface in 2.5 D [22]. Beside those terms, there are some other terms used in earth surface modeling such as Digital Height Model (DHM), Digital Ground Model (DGM), as well as Digital Terrain Elevation Model (DTEM). Each of the previous mentioned terms is being used as a standard term of earth surface modeling in certain country, for example, DEM is widely used in America, DHM in Germany, DGM is used in United Kingdom, while DTEM is introduced and used by USGS and Defense Mapping Agency [23].

2.3.2. DEM Data Acquisition Methods

Most of the observation techniques as mentioned in the previous sub-chapter can be used to generate a DEM as a measurement result. Beside those techniques, map scanning and map digitization can also be used as a DEM data source. In slope monitoring application, those techniques can be combined with each other to get the best DEM and to define the best analysis method, such as application of GPS and Total Station for GCPs establishment in aerial imaging system, GPS for determination of sensor's position in LIDAR system, DEM resulted form SAR system used to create ortho-images, and application of time series DEMs resulted from two different methods.

It should be indicated that all those stated techniques have advantages and disadvantages. Therefore when choosing a method in this application various aspects should be considered, such as accuracy requirements, conditions of the equipment, condition of the slope area, and availability of source materials. To assist in the decision making, a comparison between these methods in various aspects such as efficiency, cost, and accuracy would be useful. The comparison methods are given on Table 2.4.

Table 2.4. Comparison of various DEM acquisition methods (source: [16]).

Acquisition methods	Accuracy of data	Speed	Cost	Application domain
Conventional surveying	High (cm-m)	Very slow	Very high	Small areas
GPS survey	Relatively high (cm-m)	Slow	Relatively high	Small areas
Photogrammetry	Medium - high (cm-m)	Fast	Relatively low	Medium to large areas
Satellite imaging	Low to medium (m)	Very fast	Low	Large areas
In-SAR	Low (m)	Very fast	Low	Large areas
Radargrammetry	Very low (m)	Very fast	Low	Large areas
LIDAR	High (cm)	Fast	High	Medium to large areas
Map digitization	Relatively low (m)	Slow	High	Any size of area
Map scanning	Relatively low (m)	Fast	Low	Any size of area

2.4. Digital Elevation Modeling by Means of Close-range Photogrammetry

According to the Table 2.4, photogrammetry is one of the most efficient methods to be used in DEM data collection. It has a high accurate result, good rapidity in processing, can be applied on medium until large scale area, furthermore it can be used on inaccessible slope area. Because of a flying platform (such as plane, helicopter, and balloon) is required in images capturing process, some people feel that a lower-cots alternative technique should be developed. Therefore close-range photogrammetry is innovated to solve the problems.

Basic concept of close-range photogrammetry method was adopted from stereo aerial photogrammetry, and then continuously developed parallel with the advancement of digital technology and the expansion of computer technology. 3D position of any objects lie in overlapping images can be calculated by space intersection of two rays of respective object projected on left and right photographs. Images in close-range photogrammetry can be captured by using three types of camera; metric camera, semi-metric camera, and non-metric camera (such as pocket camera) [24]. Measurement by using a digital pocket camera is offering a low cost alternative in mapping's data gathering tools [15].

2.4.1. Camera Calibration in Close-range Photogrammetry

Camera calibration is usually carried out for several objectives, such as for evaluation of the camera's performance, evaluation of lenses system's stability, and also determination of optical and geometric parameters of a lens. Calibration procedure for any kinds of camera is similar, with only minor modifications in the procedures. Elements of interior orientation are determined in this calibration by making precise measurements of the target images and comparing the actual image locations with the ideal positions as a perfect perspective view of the camera [3].

In perfect lenses system condition, light rays would pass from object space to image space and form a sharp image on the plane of focus according to the fundamental physical laws of optics. Unfortunately this condition cannot be fulfilled in field practices, aberrations (or deviation) from theoretically exact models is happen, event though it may be ignored for applications requiring a low accuracy [29].

Included in the aberration are *radial* and *tangential* lens distortions, these kinds of aberration affect in displacement of images location [30]. Wolf, 2000 [3] and Brown, 1971 [31], divided lens distortion of the camera into *symmetric radial* and *decentering* lens distortions, (included in decentering lens distortions are *asymmetric radial* and

tangential lens distortions). However even though there are differences in those definitions, the calculation procedures in camera calibration process are perfectly the same.

Radial lens distortion is an unavoidable product of the lens manufacture even with careful design. It occurs along radial lines from principal point, positive value indicating outward displacement and vice versa [3]. Decentering lens distortion is caused by imperfections in the manufacture and alignment of lens system, or because of position of curvature's center of the lens surface not being strictly collinear [30] and [3].

Effects of those lens distortion can be reduced to a very small amount by using a certain mathematical model, as called camera calibration by following Equations 2.3 to 2.6 [30]. The radial distortion can be calculated using the following equation as shown in Equation 2.3, while the calculation for tangential distortion is given by Equation 2.4.

$$\begin{bmatrix} \delta u_i^{(r)} \\ \delta v_i^{(r)} \end{bmatrix} = \begin{bmatrix} \tilde{u}_i(k_1 r_i^2 + k_2 r_i^4 + k_3 r_i^6 + \ldots) \\ \tilde{v}_i(k_1 r_i^2 + k_2 r_i^4 + k_3 r_i^6 + \ldots) \end{bmatrix} \tag{2.3}$$

$$\begin{bmatrix} \delta u_i^{(t)} \\ \delta v_i^{(t)} \end{bmatrix} = \begin{bmatrix} 2p_1\tilde{u}_i\tilde{v}_i + p_2\left(r_i^2 + 2\tilde{u}_i^2\right) \\ p_1\left(r_i^2 + 2\tilde{v}_i^2\right) + 2p_2\tilde{u}_i\tilde{v}_i \end{bmatrix} \tag{2.4}$$

$$r_i = \sqrt{\tilde{u}_i^2 + \tilde{v}_i^2} \tag{2.5}$$

Where: $\delta u^{(r)}$, $\delta v^{(r)}$ are radial distortion for *columns* and *rows* component; $\delta u^{(t)}$, $\delta v^{(t)}$ are tangential distortion for *columns* and *rows* component; $\tilde{u}_i, \tilde{v}_i$ are position of pixel in *column* and *row*; k_1, k_2, k_3, ... are coefficients for radial distortion; p_1 and p_2 are coefficients for tangential distortion; and r is radial distance from the principal point as expressed by Equation 2.5. In normal air condition, lens distortion is strongly influenced by radial distortion, while tangential distortion is significantly smaller. Usually some researchers in some applications neglect the tangential one, but in a certain condition (e.g. in underwater condition or when some lenses were combined) this distortion should be considered.

A distorted image can be corrected (or at least minimized) based on both values of radial and tangential lens distortions. By this refinement, all objects captured on the image have a correct geometrical character. Image refinement formula is given by Equation 2.6, [30].

$$\begin{bmatrix} u_i \\ v_i \end{bmatrix} = \begin{bmatrix} D_u s_u \left(\tilde{u}_i + \delta u_i^{(r)} + \delta u_i^{(t)} \right) \\ D_v \left(\tilde{v}_i + \delta v_i^{(r)} + \delta v_i^{(t)} \right) \end{bmatrix} + \begin{bmatrix} u_0 \\ v_0 \end{bmatrix} \tag{2.6}$$

Where: u_i, v_i are corrected pixel position in *column* and *row* components; D_u, D_v are pixel size in *column* and *row* components; s is a scale factor; and u_0, v_0 are principal point in column and row components. In this model, the set of intrinsic parameters (f, s_u, u_0, v_0) is augmented with the distortion coefficients k_1, k_2, k_3, ... , k_n, p_1, *and* p_2. These parameters are also known as physical camera parameters, since they have a certain physical meaning. However, the calibration procedure as presented by those formulas is carried out with a known target. After all intrinsic parameters are derived, correction for distorted images can be performed and metric information from the images is corrected.

2.4.2. Strategies for Image Processing in Close-range Photogrammetry

Close-range photogrammetry is a technique for obtaining geometric information (such as position, size and shape) of any object that was imaged on photos as mentioned previously. To achieve a restitution of a 3D point, the intersection between at least two rays (from photo to object point) in space is needed, or between one ray and the surface. If more than two rays are available (the objects shows on three or more photos) a bundle solution is possible to be carried out. These cases initiate different approaches for the photogrammetric restitution of an object. Restitution is the procedure of establishing appropriate functional and stochastic models for describing the relationship between ground and photo coordinate systems.

2.4.2.1. Single Image Restitution

A very common problem is that we know the shape and attitude of an object's surface in space (digital surface model) but we are interested in the details on this surface (patterns, texture, additional points, etc.). In this case single image restitution can be appropriate. There are two conditions in this restitution: with known camera orientation parameters, and without information of the camera orientation parameters.

If camera parameters and exterior orientation are given, so the points can be calculated by intersection of rays from camera to surface with the surface known for its shape and attitude. Interior orientation does not mean only the calibrated focal length and the position of the principal point but also the coefficients of a polynomial to describe lens distortion (if the photo does not originate from a metric camera). If the camera position and orientation is unknown at least 3 control points on the object (points with known co-ordinates) are require to compute the exterior orientation by using spatial resection of camera position [24].

Generally in close-range photogrammetry by using non-metric camera, parameters of the camera are unidentified. Due to this condition, at least four control points in two dimensional coordinates have to be available. This approach can be applied if shape of the object surface is restricted to planes only. The relation of the object plane to the image plane is described by the projective equation of two planes as given by Equation 2.7 and 2.8 [24].

$$X = \frac{a_1 x + a_2 + a_3}{c_1 x + c_2 y + 1} \tag{2.7}$$

$$Y = \frac{b_1 x + b_2 y + b_3}{c_1 x + c_2 y + 1} \tag{2.8}$$

Where X and Y are the co-ordinates on the object's plane, x and y the measured co-ordinates on the image and a_i ,b_i, c_i the 8 parameters describing this projective relation The measurement of a minimum of 4 control points in the single photo leads to the

evaluation of these 8 unknowns (a_1, a_2, a_3, ... , c_2). As a result the 2D co-ordinates of arbitrary points on this surface can be calculated using those equations. This is also true for digital images of facades. Digital image processing techniques can apply these equations for every single pixel and thus produce an orthoimage or orthophoto

2.4.2.2. Stereographic Processing

Single image restitution process of a 3D object is impossible to be performed if its geometry is completely unknown. In this case the use of at least two images is necessary. According to the stereographic principle a pair of stereo-images can be viewed together which produces a spatial (stereoscopic) impression of the object. This effect can be used to achieve a 3D restitution. Using stereo pairs of images arbitrary shapes of a 3D geometry can be reconstructed as long as the area of interest is shown on both images. The camera directions should be almost parallel to each other to have a good stereoscopic viewing. Cameras with well known parameters and free from lens distortion are commonly used in this approach. To guarantee good results the ratio between stereo base (distance between camera positions) and the camera distance to the object should lie between 1:5 and 1:15 [24]. Detail about stereo restitution will be discussed in the following sub-chapter.

2.4.2.3. Bundle Restitution

In many cases the use of one single stereo pair will not be sufficient to reconstruct a complex object. Therefore a larger number of photos will be used to cover a whole object. To achieve a homogenous solution for the entire building (as an example of the observed object) and also to contribute additional measurements, a simultaneous solution of orientation of all photos used in close-range photogrammetry project is necessary. By using the bundle restitution, on-site camera calibration is possible to be performed. In general photogrammetry, calibration of the camera traditionally was accomplished before image gathering is carried out or at the same time of image collection (if the camera used in the project is a non-metric camera).

On-site calibration of the camera is also useful to increase the accuracy when the images were captured by an uncalibrated camera. Therefore this approach is not any more restricted to metric or even calibrated cameras, which makes the application of close-range photogrammetric techniques a lot more flexible. It is also adjustable concerning the geometry of camera positions, meaning observer is not forced to look for parallel views and stereo pair configuration. Different configuration of the photographs (convergent, horizontally, vertically or oblique photos) as presented on Figure 2.3, are now well suitable, moreover combination of different cameras or lenses can easily be done by this technique [24].

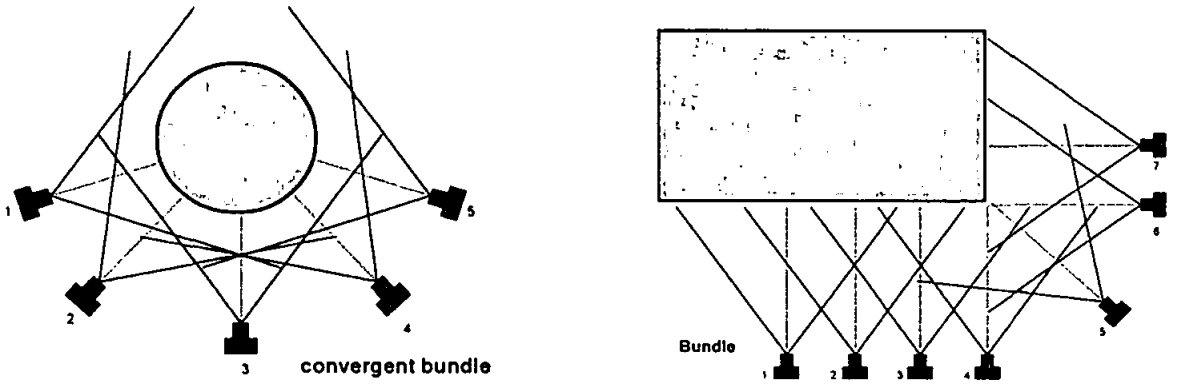

Figure 2.3. Examples of different configurations for bundle solution (source: [24])

Bundle adjustment is a wide spread technique in digital close-range photogrammetry of today. It possibly combines the application of non-metric cameras, convergent photos and flexible measurements in a common computer environment. The entire number of measurements and the full range of unknown parameters can be computed within a statistical least squares adjustment. Due to the high redundancy of such a system it is also possible to detect blunders and gross errors. Because of the adjustment process, the results are more reliable, more accurate, and readier to be used for further analysis.

2.4.3. Stereo Model Restitution

As mentioned previously, restitution a simple explaination is the procedure to describe the relationship between ground and photo coordinate systems. In many software systems analytical photogrammetry is the basis for the restitution. Analytical photogrammetry entails the formulation of the mathematical relationship between measured ground and photo coordinates, and camera parameters.

2.4.3.1. Space Intersection

A simple principle of space resection can be used to determine elements of exterior orientation for both stereo photographs. There are two conditions that can be used in photogrammetry: coplanarity and collinearity conditions, but the collinearity condition is more familiar to be applied. The object points coordinates that lie in the stereo overlapping area can be calculated using those techniques. The procedure is known as space intersection, so called because corresponding rays to the same object point from the two photos must intersect at the point as shown on Figure 2.4. The coordinates of point *A* can be calculated by space intersection formulas, as given in Equation 2.9, and 2.10 [3].

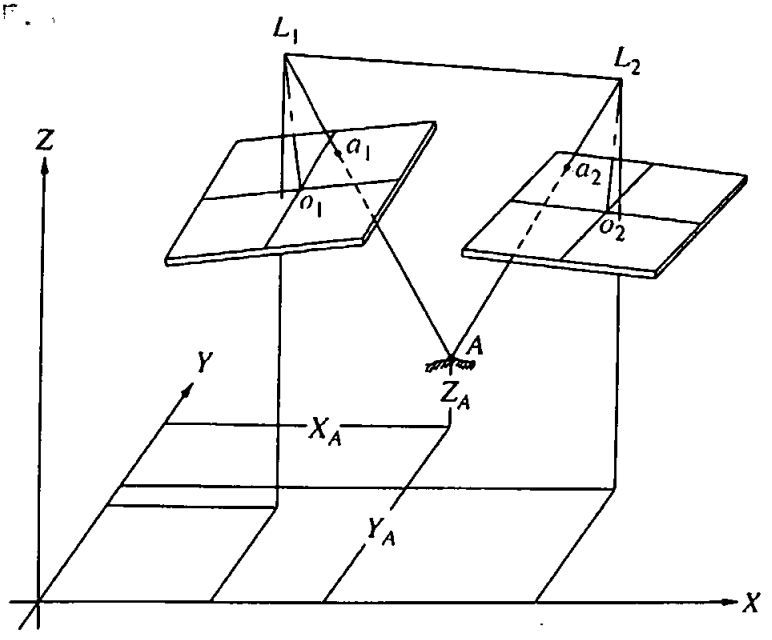

Figure 2.4. Space intersection with a stereo-pair images (source: [3])

$$x_a = x_o - f\left[\frac{m_{11}(X_A - X_L) + m_{12}(Y_A - Y_L) + m_{13}(Z_A - Z_L)}{m_{31}(X_A - X_L) + m_{32}(Y_A - Y_L) + m_{33}(Z_A - Z_L)}\right] \quad (2.9)$$

$$y_a = y_o - f\left[\frac{m_{21}(X_A - X_L) + m_{22}(Y_A - Y_L) + m_{23}(Z_A - Z_L)}{m_{31}(X_A - X_L) + m_{32}(Y_A - Y_L) + m_{33}(Z_A - Z_L)}\right] \quad (2.10)$$

Where, x_a and y_a are photo coordinate of point a on the photograph; X_A, Y_A, and Z_A are object space coordinates of point A; X_L, Y_L, and Z_L are object space coordinates of the exposure station; f is the camera focal length; x_o and y_o are the coordinate of the principal point; and the m_{pq} are fuction of three rotation angles (omega, phi, and kappa)

2.4.3.2. Analytical Stereo Model

All points that appear in the overlapping area construct a stereo-model. In most application of close-range photogrammetry, adjacent photographs should be overlapped more than 50 percent. Transformation of points from 2D left-right photo coordinate systems into 3D ground coordinate system is calculated by an analytical stereo-model. There are three primary steps in analytical stereo-model; interior orientation, relative orientation, and absolute orientation. Those mentioned orientation steps can be performed as distinct mathematical operation, or combined each other in a simultaneous calculation. Combination between relative and absolute orientation is called exterior orientation, while combination of those three orientations is called as analytical self-calibration [3].

Interior orientation is the step which mathematically reconstructs the geometry of the camera when a particular photograph was taken. It requires camera calibration information, as resulted from camera calibration process (for non-metric camera) or given by the constructor (if type of the camera is a metric camera). The process is began with measurement of fiducial mark's positions and image point coordinates by a comparator. A 2D coordinate transformation is used to relate the comparator coordinates system to the fiducial coordinate system as well as to correct for image distortion. The lens distortion and principal-point information from camera calibration are then used to refine the

coordinates so that they are correctly related to the principal point and free lens distortion [3]. Illustration about image coordinate system, fiducial coordinate system and machine coordinate system is given in Figure 2.5.

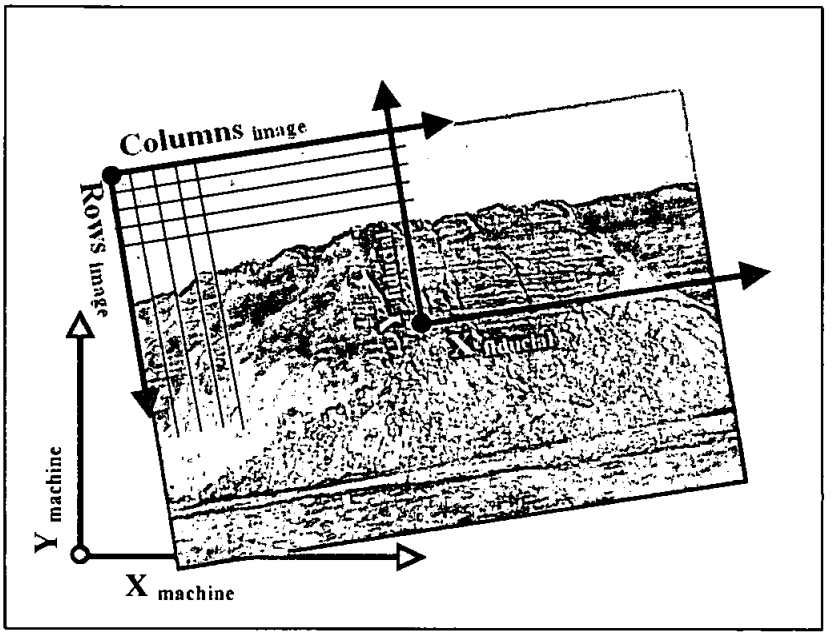

Figure 2.5. Illustration of image coordinate system, fiducial coordinate system, and machine coordinate system

Relative orientation is the process of determining the relative angular orientation and positional displacement between the photographs that existed when the photos were taken. This involves defining certain elements of exterior orientation and calculating the vector of translation. The resulting exterior orientation parameters will not be the actual values that existed when the photographs were exposed; however they will be correct in a relative sense between the photos [3]. Illustration of stereo-model formed by analytical relative orientation is shown in Figure.2.6.

In practice of relative orientation, commonly to fix the exterior orientation elements the ω, ϕ, κ, X_L, and Y_L, of the left photograph are set to be zero. Also for convenience, Z_L of the left photo (Z_{L1}) is set equal to f, and X_L of the right photo (X_{L2}) is set equal to the base b. This leaves five elements of the right photo that must be determined. Although the

coplanarity condition equation can be used for analytical relative orientation, the collinearity condition is more commonly applied for this orientation process.

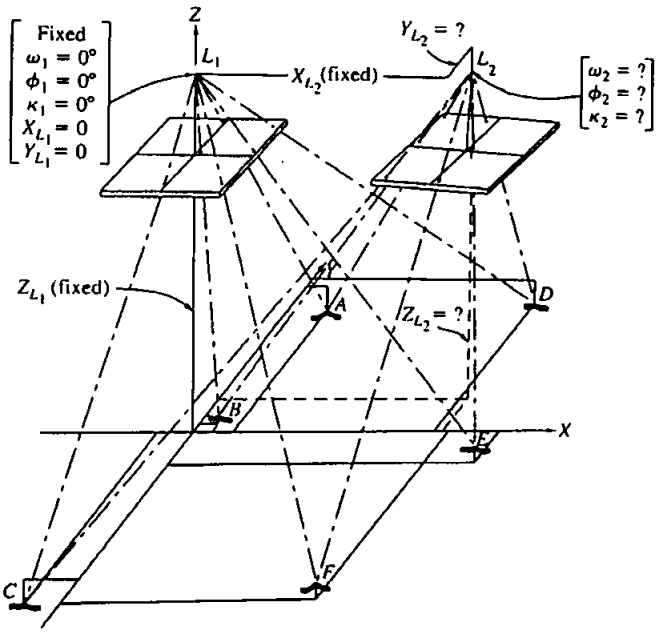

Figure 2.6. A stereomodel formed by analytical relative orientation, (source: [3])

Absolute orientation can be performed using a 3D conformal coordinate transformation. This requires a minimum of two horizontal and three vertical control points, distribution of those control points in a straight line is strictly prohibited. Additional control points provide redundancy, which enables a least squares solution, but its result is more precise. In the process of performing absolute orientation, stereo-model coordinates of control points are related to their 3D positions in a ground based coordinate system [3]. Once the transformation parameters have been computed, they can be applied to the remaining stereo-model points, including the X_L, Y_L, and Z_L coordinates of the left and right photographs. This gives the coordinates of all stereo-model points in the ground system.

2.5. Terrain Data Sampling Strategy

In this research, close-range photogrammetric data capture is based on the stereoscopic interpretation of captured imagery, using suitable photogrammetric tools. It is possible to differentiate a number of different photogrammetric sampling techniques, such as regular sampling patterns (profiling and regular grid), progressive sampling, selective sampling, and automatic sampling by digital stereo image correlation. Each of these methods tries to minimise the data collection effort, without neglecting the accuracy of the DEM [59]. Illustration about those methods can be seen in Figure 2.7, while description for each sampling strategy is discussed as follow.

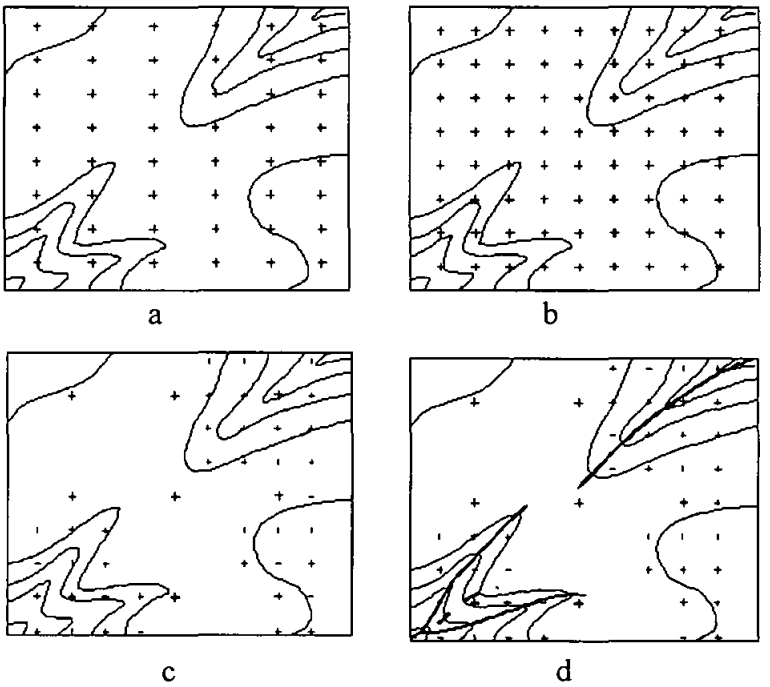

Figure 2.7. Terrain data sampling techniques by using: regular sampling profiling (a), regular grid sampling (b), progressive sampling (c), and selective sampling (d) (source: [26]).

2.5.1. Sampling with One Dimension Fixed

This kind of sampling method consists of contouring and profiling. *Contouring* means that the data sampling is along contour lines. It is exactly the same as the traditional

contour measurement on the stereo model. The only difference is that in DEM sampling, all points on the contour lines are recorded in digital form and point recording could be selective along a contour line. In contouring, height value in Z dimension is fixed, if the fixed value is in X or Y dimension it is called as *profiling* [16].

2.5.2. Sampling with Two Dimensions Fixed

Included in this type of sampling method are regular sampling and progressive sampling. Regular sampling is a selection strategy of sampling points on the stereo model, in which the selection follows regular grids with a fixed distance between points on whole stereo model. In this sampling, determination of the optimal sampling interval is important to be considered. Commonly the accuracy of DEM will increase if the sampling interval was raised. But until a certain interval value the increasing of the sampling interval does not significantly improve the accuracy of the DEM. This kind of sampling method is usually applied in semi-automatic or fully-automatic mode. It is effective to be applied in homogenous relief surfaces, but will not be efficient to be used in rugged topographical surfaces [27].

Progressive sampling is a selection method of sampling points in stereo photogrammetry, in which the sampling is carried out in a grid pattern whose interval changes progressively from coarse to fine over an area [16]. This sampling method is initiated by measuring a low intensity grid. If it is felt necessary, the sampling grid can be recursively increased until the required accuracy level is reached. High accurate DEM can be achieved by this method, but extra works have to be done to define higher/lower relief surfaces and its point density. It is usually used in manual of semi-automatic mode and effective to be applied in heterogeneous relief surfaces [27].

2.5.3. Selective Sampling

Selective sampling is a selection technique of sampling points on stereo model, in which the important regions or features (e.g. topographic breaks, watershed, and features'

border) over the areas have to be considered to improve the quality of derived DEM. This method is usually applied in manual or semi-automatic mode. It is effective to be applied in heterogeneous relief surfaces, with cover numerous abrupt relief changes. By this method discontinuities surface can be represented accurately. The selective sampling method can be combined with progressive sampling, called composite sampling, in which selective sampling is used to capture abrupt topographic changes while progressive sampling yields the data for the rest of the terrain. [26].

2.5.4. Automatic Sampling

Another method in terrain data sampling strategy is an automatic sampling. This sampling technique is the fully automated extraction of elevation models through correlation of digital stereo images. This correlation can be achieved either by using correlation devices, or 'off-line', that is fully computed without involvement of any photogrammetric equipment. In digital stereo correlation, corresponding picture elements or features are matched through cross correlation in order to obtain parallaxes and derive elevations. Although this technique is fast and seems suitable for large data collection projects, data quality is generally not very high since errors may be easily introduced [27].

2.6. Approaches for Digital Elevation Modeling

Based on the basic geometric unit in elevation modeling, there are four approaches in digital elevation modeling: point-based modeling, triangle-based modeling, grid-based modeling, and hybrid modeling approaches [16]. Each of those modeling will be discussed in the following sections, and illustration about those modeling can be seen on Figure 2.8. In actual applications, the triangle-based and grid-based modelings are more widely used and are considered as the two basic approaches [16].

2.6.1. Point-based Modeling

Point-based modeling is modeling of surface or sub-surface based on the height of individual points. Theoretically it is suitable for any data pattern, regular or irregular, since it only concerns individual points. However in practical it is not widely used, due to difficulties in determining boundaries of the region of influence and discontinuous resulted DEM surface [16].

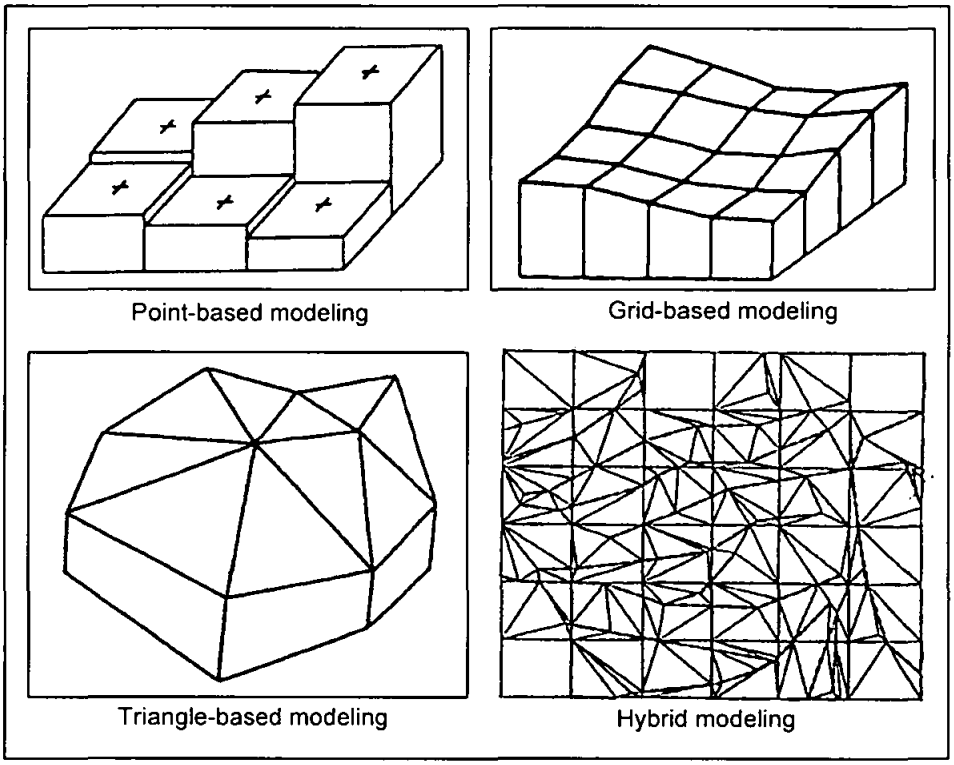

Figure 2.8. Illustration of Digital Elevation Modeling approaches (source: [16])

2.6.2. Grid-based Modeling

Grid-based modelling presents a matrix structure that records topological relations between data points implicitly. Since this data structure reflects the storage structure of digital computers, the handling of elevation matrices is simple to be performed and has many advantages [27]. Therefore elevation grid data from regular and progressive sampling, especially the square grid data are particularly suitable.Grid-based modeling is usually used to handle data covering rolling terrain over a large area, but it has less

relevance for broken surface with steep slope, numerous break-lines, and sharp terrain discontinuities [16].

2.6.3. Triangle-based Modeling

Triangle-based modeling is determination of surface model of any objects by a linked series of contiguous triangles [16]. Each triangle is used to represent only the area covered by three adjacent sampling points, as presented on Figure 2.9. In triangle-based, lines to form triangles connect the sampling points and within each triangle a plane usually represents the surface. By using triangles we are ensuring that each piece of the mosaic surface will fit with its neighbouring pieces. Irregularly space of the sample points can be represented well by using this approach, therefore this approach is usually called as a Triangular Irregular Network (TIN) [27].

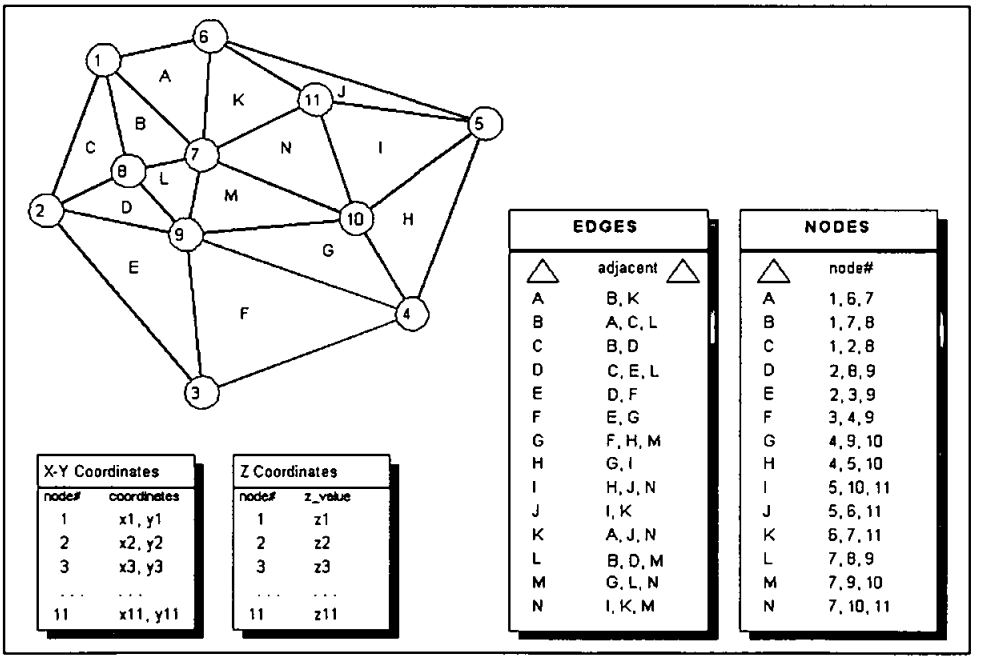

Figure 2.9. Structure of a Triangular Irregular Network (source: [27])

TIN is the approach that is feasible with any data pattern, whether it was resulted from selective sampling, progressive sampling, regular sampling, profiling, or contouring. Since triangles have a great flexibility in term of their shape and size, this approach can

easily incorporate break-lines, form-lines, and other data. Therefore the TIN has received increasing attention in terrain modelling practice and is regarded as the main approach to terrain surface modelling [16].

2.6.4. Hybrid modeling

Hybrid modeling is combination of any two of the three previous discussed modeling approaches. This kind of modeling approach is also widely used to construct DEM surfaces, but in practice the sample points usually converted into triangle-based approach. For example, a grid network would be broken down into a triangular network to form a contiguous surface of linear facet. Going in reverse condition, a grid network may be also be formed by interpolation within an irregular triangular network [16].

2.7. DEM Quality Measurement

DEM Generation by means of close-range photogrammetry requires many processing and computation, such as camera calibration, GCP selection, stereo restitution, sampling point selection, and DEM derivation. All of the previous mentioned steps contribute to the quality of DEM. Accuracy of the DEM can be defined as a degree of closeness the representation of particular surface to the real condition on the earth [28].

A significant problem of using a synthetic surface DEM (especially in high accurate application) is the definition of their quality. This is a particularly relevant issue in civil engineering where the implication of the DEM quality can entail important economic deviation during project execution as well as its technical influence [60]. There are four parameters that most frequently used to express the quality of DEM; they are elevation, curvature, roughness, and slope. All of the mentioned parameters are determined from the ability to estimate soil volume. In term of civil engineering there are two parameters that are traditionally used to determine the quality of the DEM: the volumetric difference error and the elevation interpolation error [28]. Both of the parameters has a close

correlation, because the elevation error influences to the volumetric error, and these have an obvious influence in the cost of the project.

2.7.1. Elevation Interpolation Error

The assessment of interpolation error is commonly used in civil engineering to be a quality indicator of the derived DEM, since the error in height value become volumetric errors and these have an obvious influence in the cost of the project. Some independent points is required in this assessment to be check points, at least there are 2.5 % of the total of the sample points [28]. Selection of the check points should be well distributed and represented condition of the surface. Afterward height of the check point is compared with an interpolated point on the derived DEM at the same planimetric position, by following Equation 2.11 [16]. By comparing result of all check points, statistical calculation is performed to indicate the accuracy of the DEM, as given by Equation 2.12 [16].

$$e(x,y) = f'(x,y) - f(x,y) \tag{2.11}$$

$$mse = \iint e^2(x,y)dxdy \tag{2.12}$$

Where: $e(x,y)$ is the height difference; $f'(x,y)$ is elevation of the constructed DEM surface; $f(x,y)$is elevation of the check point on the original terrain surface; *mse* is mean square error of the DEM surface.

There are four possible approaches for assessing the height accuracy of the derived DEM [32]:

i. Prediction by producing (procedures): This is to assess the likely errors introduced at the various production stages together with an assessment of the vertical accuracy of the source materials.
ii. Prediction by area: This is based on the fact that the vertical accuracy of contour lines on a topographic map is highly correlated with the mean slope of the area.

iii. Evaluation by cartometric testing: This is concerning experimental evaluation. For such a test, a set of checkpoints is required.

iv. Evaluation by diagnostic points: A sample of heights is acquired at the time of data acquisition and this set of data is used to check the quality of the model. This can be performed at any intermediate stage as well as the final stage.

2.7.2. Volumetric Difference Error

Volumetric accuracy of the DEM is calculated by comparison between volume of derived DEM and a reference model. A reference model is generated from set of correct data or measured by using other instrument which has a better accuracy. Actually it is a simple way to determine the quality of a derived DEM, but it cannot be used to detect the presence of systematical error in the sample points. It is advisable to use this method in conjunction with analysis of elevation interpolation error, due to height values have a dramatic negative impact in the quality of the derived DEM. [28].

2.7.2.1. Volume Calculation from Topographical Data

Volume of the derived DEM cannot be calculated by an integration method because topographical surfaces do not have regular shapes, which can be expressed by a mathematical function. However the volume between topographical surface and a horizontal plane in a bounded area can be calculated in different ways as presented on Figure 2.10.

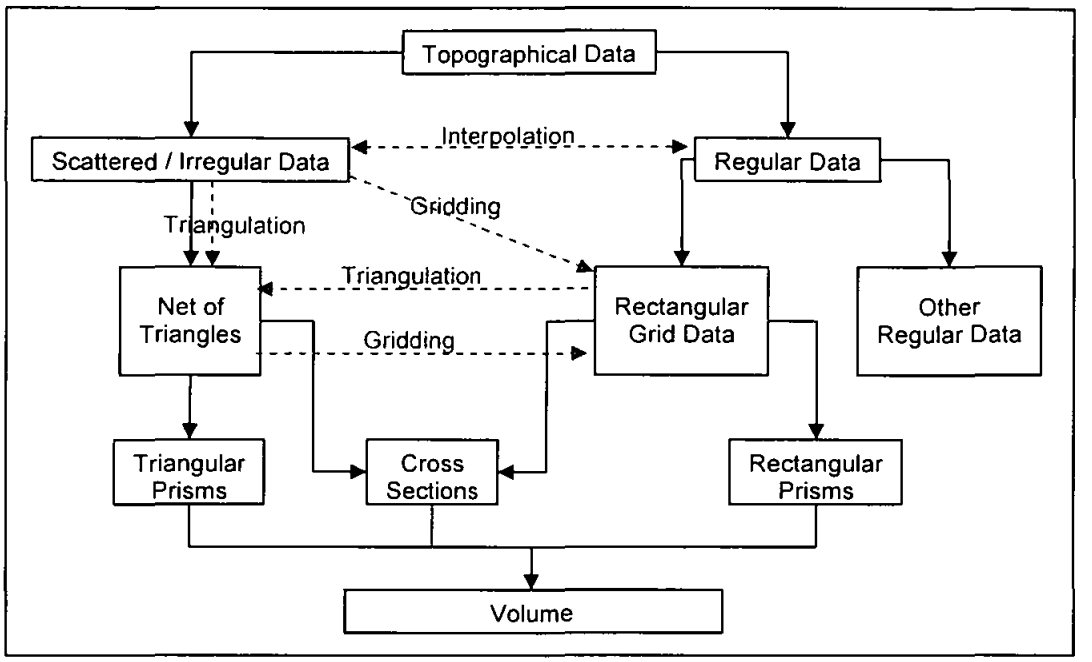

Figure 2.10. Volume calculations from topographical data (source: [33])

i. Volume calculation with triangular prisms: the data is triangulated by the delaunay triangulation method. If volume of each triangular prism is V_i; vertices elevation of each triangular facet is z_1, z_2, and z_3; elevation of height reference is z_r; and area of each triangular facet is F_t; than the volume under a triangular facet and the total volume are calculated by Equation 2.13 and 2.14 [33].

$$V_i = [\{(z_1 + z_2 + z_3)/3\} - z_r]F_t \tag{2.13}$$

$$V = \sum_{i=1}^{t} V_i \tag{2.14}$$

ii. Volume calculation with rectangular prisms: If the data are irregular or scattered, they are transformed to grid data using a certain gridding method. If volume of each rectangular prism is V_i; vertices elevation of each rectangular facet is z_1, z_2, z_3, and z_4; elevation of height reference is z_r; and area of each rectangular facet is F_g; than the volume under a rectangular grid and the total volume are calculated by Equation 2.15 and 2.16 [33].

$$V_i = [\{(z_1 + z_2 + z_3 + z_4)/4\} - z_r]F_g \quad (2.13)$$

$$V = \sum_{i=1}^{g} V_i \quad (2.14)$$

iii. Volume calculation with cross-sections: the cross-sections of the topographical surface are obtained from the DEM or directly from the original data source. If the horizontal distances between consecutive cross-sections are equal to the value l and if the area of cross-section is F_i, then the total volume can be calculated by the several approaches, such as: trapezoidal formula (as given on Equation 2.15); Simpson formula (as expressed by Equation 2.16); and average formula (as specified by Equation 2.17) [33]:

$$V = \frac{1}{2}(F_1 + 2F_2 + 2F_3 + \ldots + 2F_{u-1} + F_u) \quad (2.15)$$

$$V = \frac{1}{3}(F_1 + 4F_2 + 2F_3 + 4F_4 + 2F_5 + \ldots + 2F_{u-2} + 4F_{u-1} + F_u) \quad (2.16)$$

$$V = \frac{u-1}{u} * l * \sum_{i=1}^{u} F_i \quad (2.17)$$

2.8. Summary of the Literature Review

From these literatures review, it can be seen that, most of the work in the area of digital elevation modeling is focused on three main parts. The first part is the DEM data collection, where many authors support the finding that the DEM data collection is the most important part in digital elevation modeling. There are several techniques in DEM data collection, but only several methods are able to be applied in inaccessible slope monitoring. Each data collection technique has it own merits and pitfalls, therefore those techniques can be combined with each others to get the best DEM and to define the best analysis method. Criteria that have to be considered in selecting the most suitable technique are: scale of project, expected accuracy, speed of survey, reasonably cost, easiness to be performed and repeatability. Close-range photogrammetry technique using

non-metric camera in which GCPs were collected using reflector-less Total Station is preferred due to the previous mentioned criteria. Several preliminary researches and experiments on the application have been conducted by some researchers. Application of close-range photogrammetry in monitoring of inaccessible unstable slope area has not been investigated yet.

The second part is the data processing, included in this part are camera calibration, image processing, terrain data sampling, and digital elevation model generation. Precise measurement of focal distance, image resolution, and lens distortion data were needed in the calibration process because the camera used in this research is a non-metric. Bundle restitution is wide spread applied in digital close-range photogrammetry of today, because it possibly combines the application of non-metric cameras, convergent photos and flexible measurements in a common computer environment. Selection terrain data sampling by using several sampling methods is interesting to be investigated to evaluate the characteristics of their accuracy in digital elevation modeling. Among four main approaches in digital elevation modeling, TIN is preferred for high resolution DEM generation. Since it is feasible with any data pattern (whether it has resulted from selective sampling, progressive sampling, regular sampling, profiling, or contouring), and it has a good flexibility to incorporate breaklines and formlines (which is very useful for reconstructing structural features and abrupt changes).

The third part is the DEM quality measure. This is also an essential part of digital elevation modeling, since one of the important factors that should be considered in using DEM is the quality characterization of the DEM itself. This is a particularly relevant issue where a lack of quality in the DEM can lead importance economic deviations during project execution.

CHAPTER 3

METHODOLOGY

3.0. Introduction

This chapter describes the details of the experimental research on digital elevation modeling by using close-range photogrammetric data. The experiment presented here is based on the comparison between close-range photogrammetric method and conventional terrestrial method using Total Station as a Digital Elevation Model (DEM) data collection tool. The comparison here only covers the productivity and accuracy assessments. From this experiment, a comprehensive understanding about close-range photogrammetry especially for low-cost alternative tool in slope measurement can be projected.

Close-range photogrammetry can be considered as a low-cost alternative technique in slope measurement if the type of camera used in this technique is a commercial camera. This kind of camera has some errors, because it is not intentionally assembled for mapping purposes. To solve this problem, the errors have to be removed in order to get a proper geometric model that will be imaged on captured photographs. Systematical errors caused by lens distortion and other camera information can be modeled by camera calibration process [34]. Then using the information, undistorted images can be acquired in an interior orientation process.

As the conventional photogrammetric method, improvement of spatial accuracy from this method can be achieved by using higher accuracy sensor (camera with smaller pixel size) or by a closer capturing distance at the time of exposure. Metric capability of close-range photogrammetry can be improved by some existing control points on the target. However, if no control points exist, it must be combined with any other measurement methods for defining some of known points on the images. In this research the known points were measured by using calibrated Total Station. These points were required in

three dimensional (3D) geometrical refinement of the images, and calculated by coordinate transformations [35]. By those calculations, derived 3D model can be measured and transformed from relative coordinate system (with unknown scaling factor) into real coordinate system (with shape and dimension which are similar to the real object). The coordinate system used for particular areas is a local ground coordinate system, which was tied on two temporary bench-marks.

By the improvement of metric accuracy, the close-range photogrammetric method is able to be used in high-accuracy applications. The application of the DEMs designed in this research is for large-scale real case slope monitoring projects covering small areas. All distances from object to the camera were set shorter than 300 meter, as a requirement in terrestrial application of a close-range photogrammetry [3].

3.1. Study Area

The DEM data collections were carried out over several slopes on ex-mining pit at Bandar University, Tronoh, Perak Darul Ridzuan Malaysia. The location of the study areas are outside the UTP Complex as shown in Figure 3.1. Some areas were selected because they represent good variations of topographical conditions and surface gradient angles. Another consideration is study areas chosen are close to each other.

Dimension of the areas can be categorized as small, which is about 11-13 meters in height and 19-25 meters in width. Based on the size of the study areas, DEM data acquisition could be considered as a large scale application. Condition of the surrounding areas of the slope was inaccessible and risky. Due to those mentioned reasons, the most possible way to capture stereo images was from front site of the observed objects with the observer standing on the ground.

There are four different study areas used in this research. They area slope with different gradient and relief of the surface, as mentioned below:

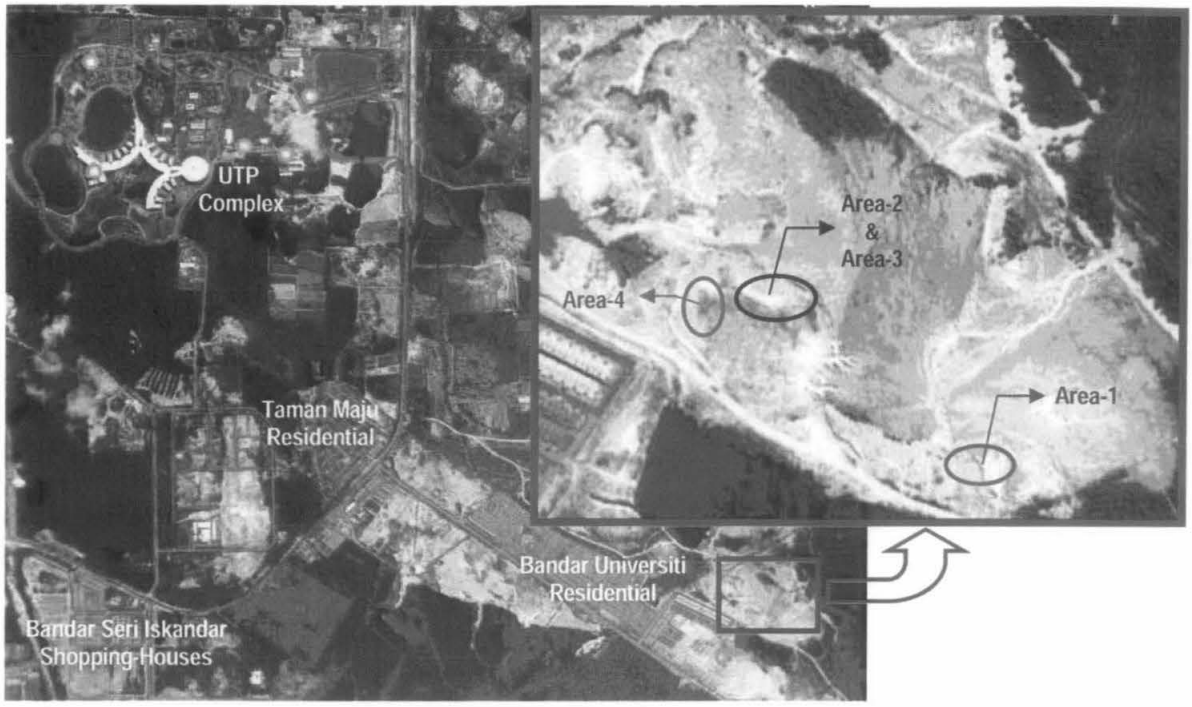

Figure 3.1. Location of the slopes (main figure), and position of all areas (inset) from satellite image [source: http://earth.google.com]

3.1.1. Area-1

Topographical characteristic of Area-1 could be described as homogeneous slope with low relief surface and slope angle is between 57.470° and 60.822°, (or 58.883° in average). Detail calculation of slope angles and slope gradient is presented on **Appendix A**. Whereas slope angle is a rising angle of the slope, while the gradient is a constant value or scaling factor of increasing of the slope surface. Dimension of the area is approximately 25 meters in width and 11 meters in height. Detailed situation of the area is shown in Figure 3.2 below.

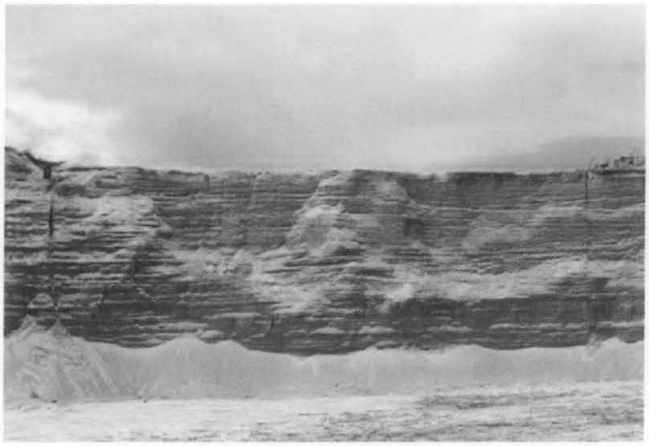

Figure 3.2. Overview of Area-1 representing an homogeneously-steep slope area

3.1.2. Area-2

Area-2 is the representative of a heterogeneous slope area. It has good variety of topographical conditions with medium gradient of the slope, being a combination of steep slope on the center area, and slightly gentle slopes on the left-right side. Slope angles of this area is 35.822° to 46.749°, (average angle is 39.740°). Along with slope angle and slope gradient calculations, some sample profiles for each study area are also presented on Appendix A. Dimension of Area-2 is roughly 19 meters in width and 13 meters in height. Detailed condition of the slope can be seen in Figure 3.3.

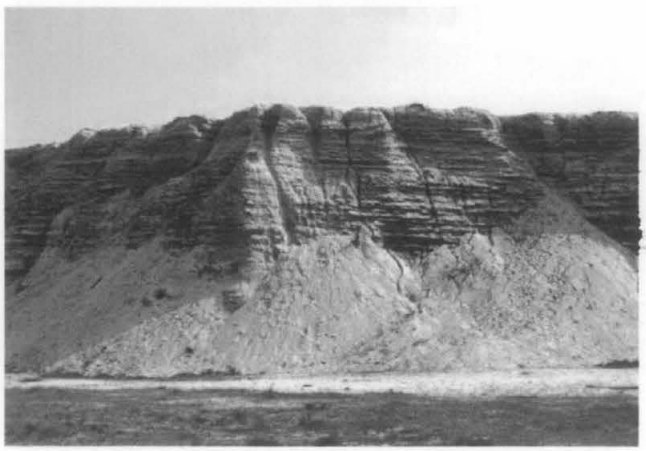

Figure 3.3. Overview of Area-2 representing the heterogeneous slope area

3.1.3. Area-3

Area-2 and Area-3 are the same area, but were measured on different epoch time. Area-2 was measured on May 13th, 2007, while measurement of Area-3 was carried out on April 07th 2008 (or 330 days after the measurement of Area-2 was performed). Area-3 has the same topographical characteristics as Area-2, which represents heterogeneous slope area, and is categorized as medium slope gradients, as shown in Figure 3.4. It was noted that there is a slight change (compared with Figure 3.3) in surface condition because of some landslides and mass movements. The average of the slope angle for this area is 39.150°, (with maximum angle is 45.941° and the minimum is 35.931°).

Figure 3.4. Overview of Area-3 representing heterogeneous slope area

3.1.4. Area-4

Area-4 is representative of a heterogeneous slope area with low gradient angles. This sample area has a good relief of topographical condition. Some extreme changes on top and middle parts of the surface, combined with homogeneous surface on the bottom made the area interesting to be examined. Detailed situation of the slope can be shown in Figure 3.5. The dimension of the area is approximately 25 meters in width and 13 meters

in height, with slope angles between 39.587° to 45.412°, (average is 41.957°). Gradient of the slope is 0.827 to 1.015 (average gradient is 0.902).

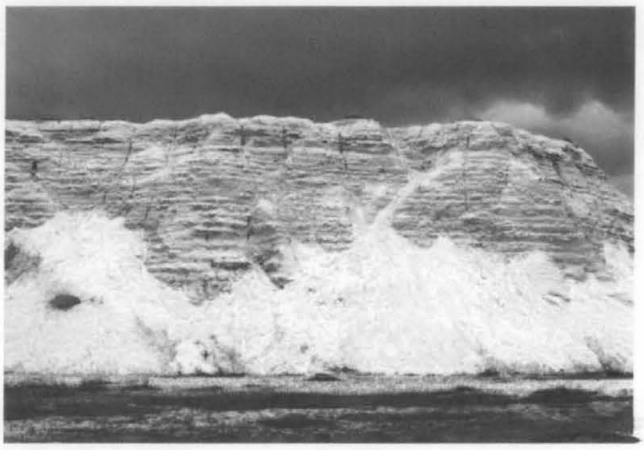

Figure 3.5. Overview of Area-4 representing heterogeneous slope area

3.2. Instrumentation and Apparatus

There were several instruments and apparatus used in the data collection survey, as given in Figure 3.6. Generally, they could be divided into two categories: the main and complementary equipments. The main equipments are set of instruments that are absolutely needed in unstable slope data collections for this research. While complementary equipments are those that were not used in unstable slope data collections, but they were used in other process such as in instrument calibration process. List of instruments used in this research are as follows:

Main equipments:
i. 1 unit Reflector-less Total Station Topcon GPT-3007 N\LN.
ii. 1 set digital pocket camera Canon A-540 6 Mega pixel.
iii. 1 unit Topcon standard single prism.
iv. 2 units tripods, for the TS and prism.
v. 1 unit tripod for the camera.
vi. 1 unit roll meter.

Complements:
vii. 1 unit pattern of camera calibration

viii. 1 set calibration plate of concrete and its special holder

ix. Permanent standardized Total Station calibration pillars.

x. Total Station-PC connection cable.

xi. Camera-PC connection cable.

xii. 1 unit personal computer.

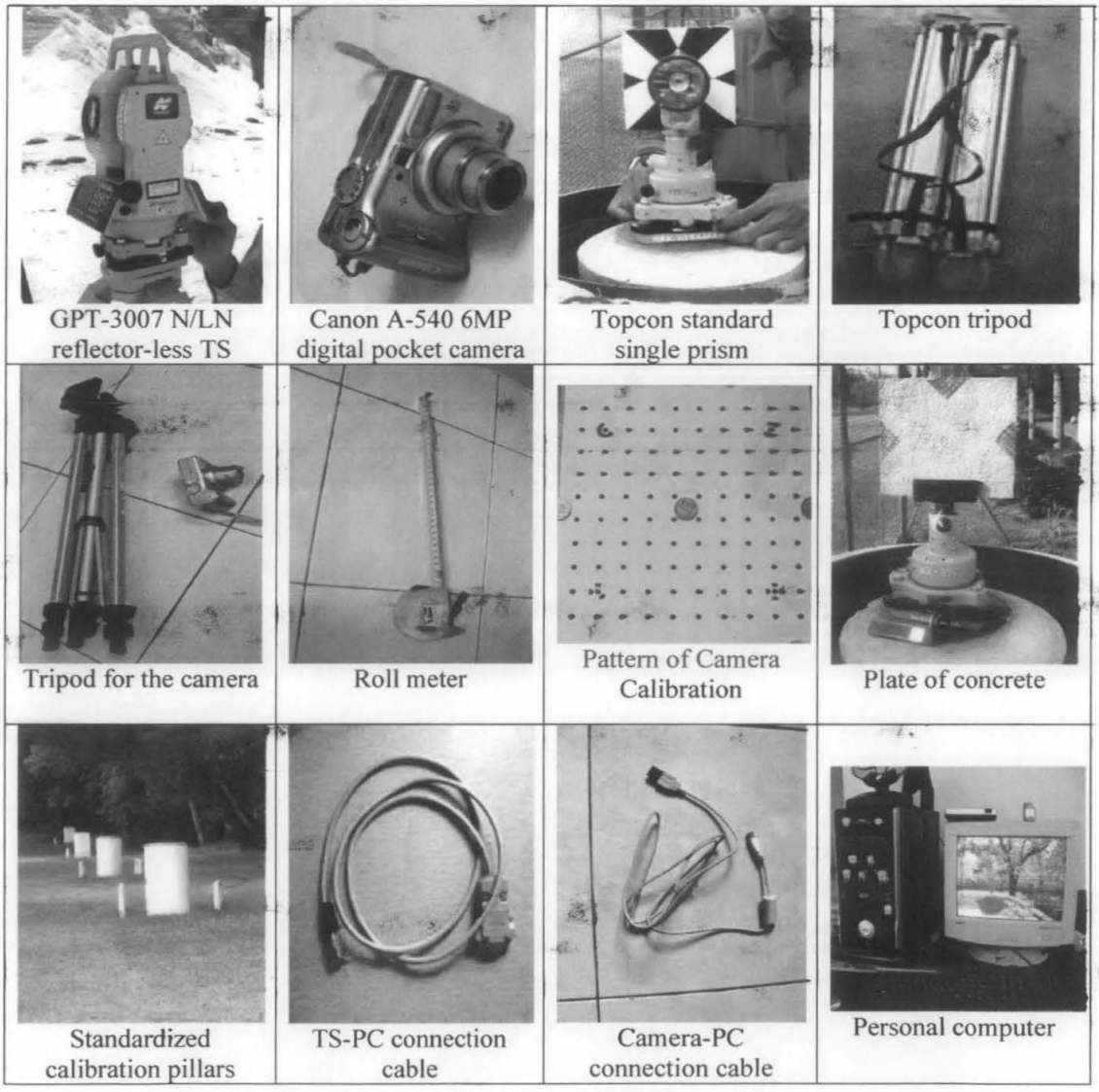

Figure 3.6. Instruments used in this research

3.3. Camera Calibration

Camera calibration is a necessary step in photogrammetry and 3D computer vision in order to extract 3D metric information from 2D images captured by camera [34]. This process determines internal geometric and optical characteristics (intrinsic parameters) of the camera, and also computes the 3D position and orientation of the camera frame relative to a certain world coordinate system (extrinsic parameters) [36]. By camera calibration, systematical errors caused by the camera can be calculated.

In this research the author only considers the error caused by lens distortions, because this kind of error significantly impresses geometrical accuracy. Other errors due to construction of the camera, atmospheric refraction, and difference refractive indexes inside and outside of the camera were neglected. Included in the systematical errors due to lens of the camera are radial and tangential distortions. Radial distortion is radial displacement of actual image point in the image plane. While tangential distortion is the displacement of actual image point caused by the position of center of lens' curvature (lens' surface) not being strictly collinear [3].

As mentioned previously, the camera used in this research was a Canon A540 6 Mega pixel. It is a digital pocket camera with a Canon 5.8 – 23.2 millimeters (mm) lens with format width and height of the camera are 5.72 mm and 4.29 mm respectively. The resolution of all captured images was set on 2272x1704 pixels. In this camera calibration, focal length of the camera was fixed at 9.8 mm (for Area-1, Area-3, and Area-4) and 11.5 mm (for Area-2), and the focus point of the camera was set at infinity. The camera calibrations have to be carried out according to the focal length of the images taken [38] and [39], because variation of focal length yields different lens distortions. Calibrator software used in this thesis was PhotoModeler Pro version 5.2.3.

Precise measurement of focal distance, recording resolution, and its distortion data were needed in this calibration because the camera is non-metric [40]. This research used a flexible camera calibration technique that required observing a calibration planar pattern from several different positions and orientations. It was performed by moving the camera,

as shown on Figure 3.7. The motion of the camera's positions was not required to be known. This research assumed that each point in the object space is projected by a straight line through the projection center into the image plane (as known as pinhole model).

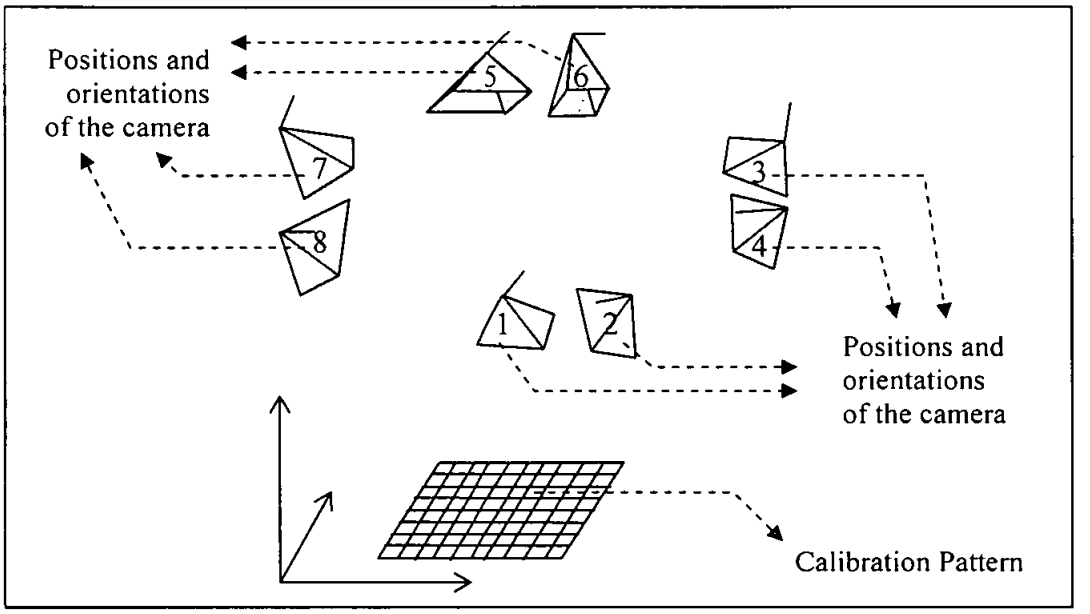

Figure 3.7. Capturing planar calibration pattern from several positions and orientations

Steps in an interior orientation process requires measurement of the fiducial marks, transformation calculation from image coordinate system (rows, columns) into fiducial coordinate system, and transformation into 2D comparator/machine coordinate system for all images. All of the processes have been accomplished by the calibrator software. Because the commercial pocket camera is not constructed as a mapping instrument, it has no fiducial marks. Alternatively, four corners of each image have been chosen as fiducial marks.

Relative and absolute orientations were completed in one process by measuring and marking one hundred common tie points on each of eight photographs. Based on the measurement and results of the previous processes, transformation from machine coordinate system (2D Cartesian) into relative 3D coordinate system, then into 3D absolute coordinate system were accomplished. By a certain mathematical resection with

bundle adjustment, location of principal point, focal length, format film, principal distance, lens distortion parameters, and also position-orientation of the camera could be achieved [38].

3.4. Total Station Calibration

The calibration data observation was obtained by measuring series of distances on one standardized baseline. The baseline was then divided into six sub-baselines defined from 21 observed distances (because only seven pillars were used in this research). The scenario of the data measurement is illustrated in Figure 3.8. Each sub-baseline was measured for ten times, therefore the standard deviation of each sub-baseline can be determined. The measurements were carried out on JUPEM's permanent standardized calibration benchmarks at Batu Gajah, Perak – Malaysia, by means of Topcon GPT-3007 N/LN reflector-less Total Station observed on a calibration plate of concrete. Detail specification for the Total Station was given in **Appendix B**

Calculation used in this research (to determine zero error and Total Station calibration) was a parametric least-square adjustment. In the parametric least-square adjustment method, observation equations are formulated by quantity of measurement related to both independent observational residuals and unknown parameters. One equation is written for each observation. If number of equations equal to number of unknowns, a unique solution of the unknowns will be given. Usually number of observations is bigger than unknown parameters. Therefore it permits determination of the most probable values for the unknowns based on the principle of least squares adjustment. Generally linear observation parametric model can be expressed as these following Equations 3.1 to 3.5 [41]:

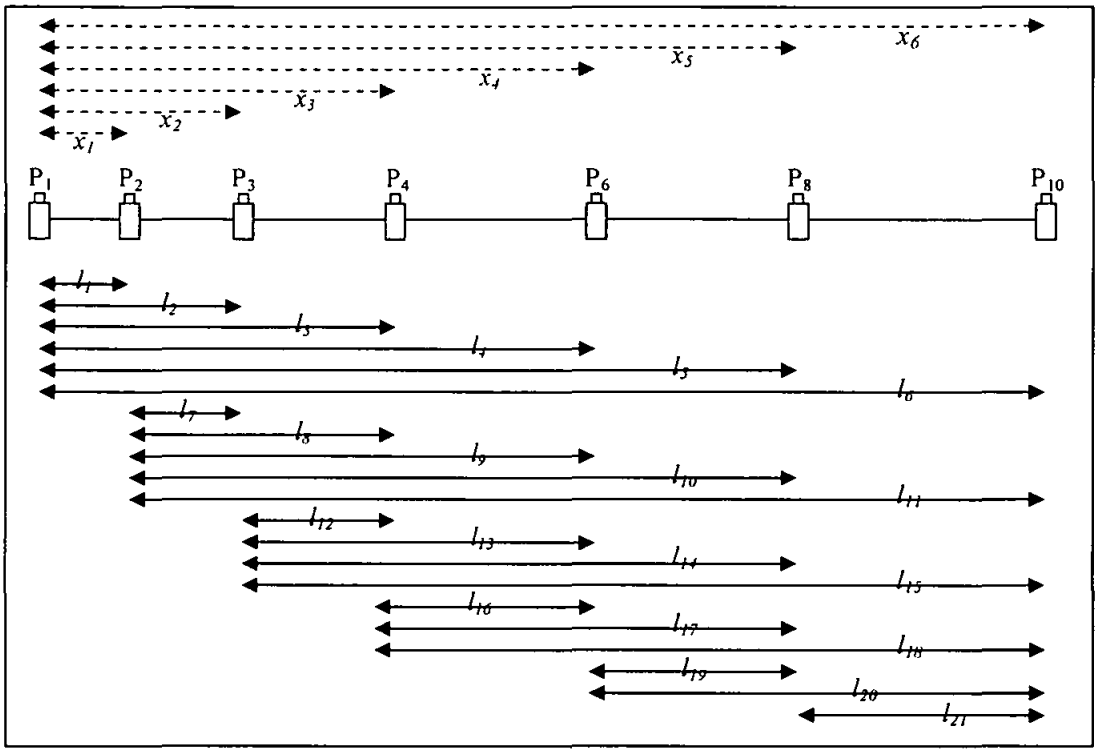

Figure 3.8. Sketch of the pillars (middle picture), with its scenario of the data measurement for all observed sub-baselines (top), and all observed distances (bottom).

$$L + V = AX \tag{3.1}$$

Where A is design matrix; X is vector of unknown parameters; L is vector of observations; and V is vector of residuals. The least-squares solution $\hat{X}$ of Equation 3.1 was given below:

$$\hat{X} = (A^T PA)^{-1} A^T PL \tag{3.2}$$

$$\sum X = \hat{\sigma}_o^2 (A^T PA)^{-1} \tag{3.3}$$

$$\hat{\sigma}_o^2 = (V^T PV)/n - u \tag{3.4}$$

$$P = \sigma_o^2 \begin{bmatrix} 1/\sigma_{l1}^2 & 0 & 0 & 0 & 0 \\ 0 & 1/\sigma_{l2}^2 & 0 & 0 & 0 \\ 0 & 0 & 1/\sigma_{l3}^2 & 0 & 0 \\ \cdots & \cdots & \cdots & \cdots & \cdots \\ 0 & 0 & 0 & 0 & 1/\sigma_{l21}^2 \end{bmatrix} \quad (3.5)$$

Where: P is weight matrix; σ_o^2 is an a-priori variance; $\sum X$ is variance-covariance matrix of parameters; $\hat{\sigma}_o^2$ is an a-posteriori variance; n is number of observation; and u is number of unknown parameter.

3.4.1 Computation of Zero Error

Computation of least square adjustment is applied for determining the zero error and the precision of materials used in this research. The number of observed distances and number of sub-baselines are required in determination of least-square equation. Number of observed distances was used to define the number of model equations, while number of unknown parameters was the same as the number of unknown sub-baseline plus zero error. Element of the zero error computation model is: n = 21 (l_1, l_2, l_3, l_4, l_5, ... l_{21}); u = 6 +1 (x_1, x_2, x_3, x_4, x_5, x_6, z_0); r = n = 21. With the linear parametric model relating the observations and unknown parameters can be written as follows:

$$l_1 + v_1 = x_1 - z_o$$
$$l_2 + v_2 = x_2 - z_o$$
$$l_3 + v_3 = x_3 - z_o$$
$$l_4 + v_4 = x_4 - z_o$$
$$l_5 + v_5 = x_5 - z_o$$
$$l_6 + v_6 = x_6 - z_o$$
$$l_7 + v_7 = x_2 - x_1 - z_o$$
$$l_8 + v_8 = x_3 - x_1 - z_o$$
$$l_9 + v_9 = x_4 - x_1 - z_o$$
$$l_{10} + v_{10} = x_5 - x_1 - z_o$$
$$l_{11} + v_{11} = x_6 - x_1 - z_o$$
$$l_{12} + v_{12} = x_3 - x_2 - z_o$$
$$l_{13} + v_{13} = x_4 - x_2 - z_o$$
$$l_{14} + v_{14} = x_5 - x_2 - z_o$$

$$l_{15} + v_{15} = x_6 - x_2 - z_o$$
$$l_{16} + v_{16} = x_4 - x_3 - z_o$$
$$l_{17} + v_{17} = x_5 - x_3 - z_o$$
$$l_{18} + v_{18} = x_6 - x_3 - z_o$$
$$l_{19} + v_{19} = x_5 - x_4 - z_o$$
$$l_{20} + v_{20} = x_6 - x_4 - z_o$$
$$l_{21} + v_{21} = x_6 - x_5 - z_o$$

Those observations can be written in matrix form, following the Equation 3.6:

$$\begin{bmatrix} v_1 \\ v_2 \\ v_3 \\ v_4 \\ \dots \\ \dots \\ v_{21} \end{bmatrix} + \begin{bmatrix} l_1 \\ l_2 \\ l_3 \\ l_4 \\ \dots \\ \dots \\ l_{21} \end{bmatrix} = \begin{bmatrix} 1 & 0 & 0 & 0 & 0 & 0 & -1 \\ 0 & 1 & 0 & 0 & 0 & 0 & -1 \\ 0 & 0 & 1 & 0 & 0 & 0 & -1 \\ 0 & 0 & 0 & 1 & 0 & 0 & -1 \\ \dots & \dots & \dots & \dots & \dots & \dots & \dots \\ \dots & \dots & \dots & \dots & \dots & \dots & \dots \\ 0 & 0 & 0 & 0 & -1 & 1 & -1 \end{bmatrix} * \begin{bmatrix} x_1 \\ x_2 \\ x_3 \\ x_4 \\ x_5 \\ x_6 \\ z_0 \end{bmatrix} \tag{3.6}$$

Based on the matrix Equation 3.6, the adjusted unknown parameter $\hat{X}$ could be obtained using the Equation 3.2 and the covariance matrix of adjusted unknown parameter was calculated using Equation 3.3. Furthermore, proper statistical test (global test) was applied in order to detect possible outlier in the processing the least square adjustment. This test was aimed to examine the compatibility of the number of estimated a-posteriori variance $\hat{\sigma}_o^2$ with the number of a-priori variance by using *Fisher* distributions with a certain significance level, α_o, and degrees of freedom, *(f=n-u)*. The *F-test* was defined in Equation 3.7. Moreover, to examine the significance of the zero error, *t*-student statistical test was carried out in this experiment. The value of the *t* is the ratio of the zero error and the standard deviation, as shown in the following Equation 3.8. The critical value of *t*-test is referred to the *t*-table with respect to the *significance level* α and the appropriate *degrees of freedom (f)*.

$$\frac{\hat{\sigma}_o^2}{\sigma_o^2} > F_{1-\alpha o, f, \infty} \tag{3.7}$$

$$\frac{z_o}{\sigma_{zo}} \leq t_{\alpha,f} \tag{3.8}$$

3.4.2 Calibration of Distance Measuring Tool in the Total Station

Value of the zero error was computed from the previous calculations. Based on this value, correction for zero error was given for all observed distances; therefore corrected observed distances were acquired. Calibration of the distance measurement tool is necessary to ensure confidence in the distances it measures. The calibration was not only applied for the instrument, but also for its related reflector. As mentioned in the previous sub-section, reflectors used in this research are standard single prism and, concrete materials. The observation equation for an electronically observed distance on a calibration base line can be expressed in Equation 3.9 below [41]:

$$(D_o - D_p) + V_{Do} = a * D_p + b \tag{3.9}$$

Where: a is the scaling factor for the Total Station; b is instrument-reflector constant; D_o is the observed horizontal distance after *correction of zero error* was given; D_p is the published horizontal calibrated distance for the sub-baseline; V_{Do} is the residual error for each observation.

Equation 3.9 is a linear equation with two unknowns (a and b), so it can be solved by using Equation 3.2. The equation can be expressed in matrix form as presented in Equation 3.10 follow:

$$\begin{bmatrix} (Do_1 - Dp_1) \\ (Do_2 - Dp_2) \\ (Do_3 - Dp_3) \\ (Do_4 - Dp_4) \\ \cdots \\ Do_{21} - Dp_{21}) \end{bmatrix} + \begin{bmatrix} v_1 \\ v_2 \\ v_3 \\ v_4 \\ \cdots \\ v_{21} \end{bmatrix} = \begin{bmatrix} Dp_1 & 1 \\ Dp_2 & 1 \\ Dp_3 & 1 \\ Dp_4 & 1 \\ \cdots & \cdots \\ Dp_{21} & 1 \end{bmatrix} * \begin{bmatrix} a \\ b \end{bmatrix} \tag{3.10}$$

3.5. Data Collection

Data collection in this research consist of stereo images data gathering by means of the Canon A-540 digital commercial pocket camera, measurement of some Ground Control Points (GCP), measurement of reference point to build a reference DEM, and measurement of check points as well. The last three of measurement processes were carried out by using calibrated GPT-3007 N/LN reflector-less Total Station.

3.5.1 Stereo Images Data Collection

As mentioned in sub-chapter of study area, the slopes of interest and its surrounding area were considered inaccessible and high risk areas. Due to those mentioned condition, the most possible way to capture stereo images of the slopes was from front site of the observed objects with the observer standing on the ground. Stereo photographs of the slopes were captured with a stereo base line of 8 meters, and at a distance of 55-65 meter (for all sampling areas), as illustrated on Figure 3.9. In close-range photogrammetry, ratio of the stereo base line and the distance between camera and the observed object should lie between 1:5 and 1:15 [5] and [61]. Stereo photographs used in this research were taken with more than 80% overlapping. Points that appear on the overlapping area construct a 3D stereo model, calculated by some steps of computation.

Camera used in this data collection was set manually before image data collection started. Similar to the setting of the camera in camera calibration process, focal length of all captured photographs on Area-2 were set on 11.5 mm. Meanwhile, focal length for all photographs on rest of the sample area (Area-1, Area-3, and Area-4) were set on 9.8 mm. Different setting of the focal length here is due to the difficulty in setting the focal length of the digital pocket camera.

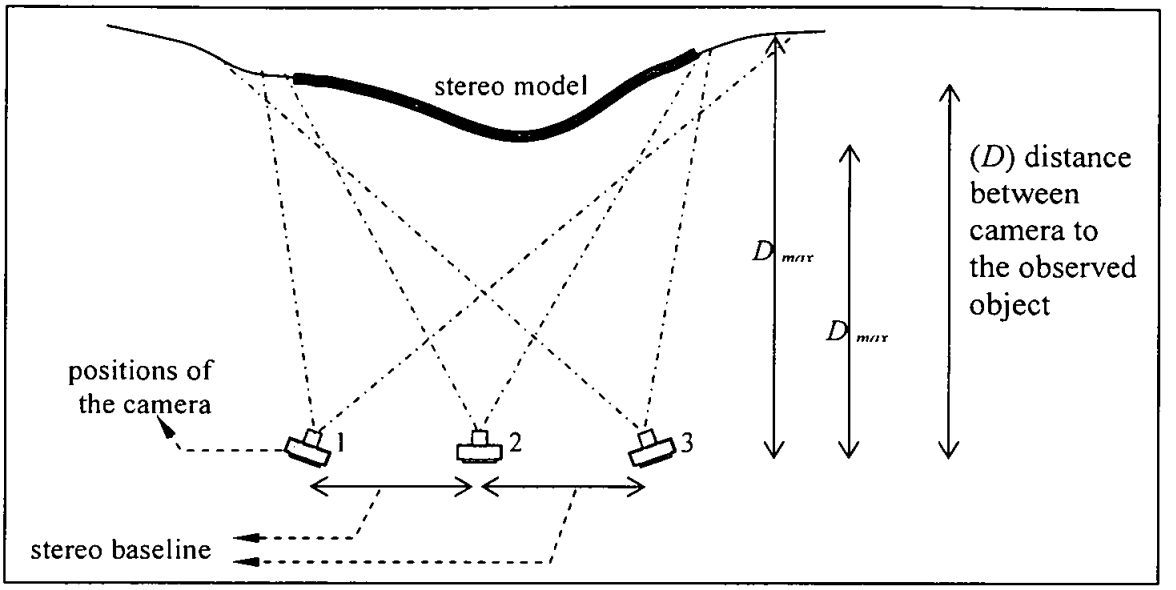

Figure 3.9. Illustration of stereo images data collection

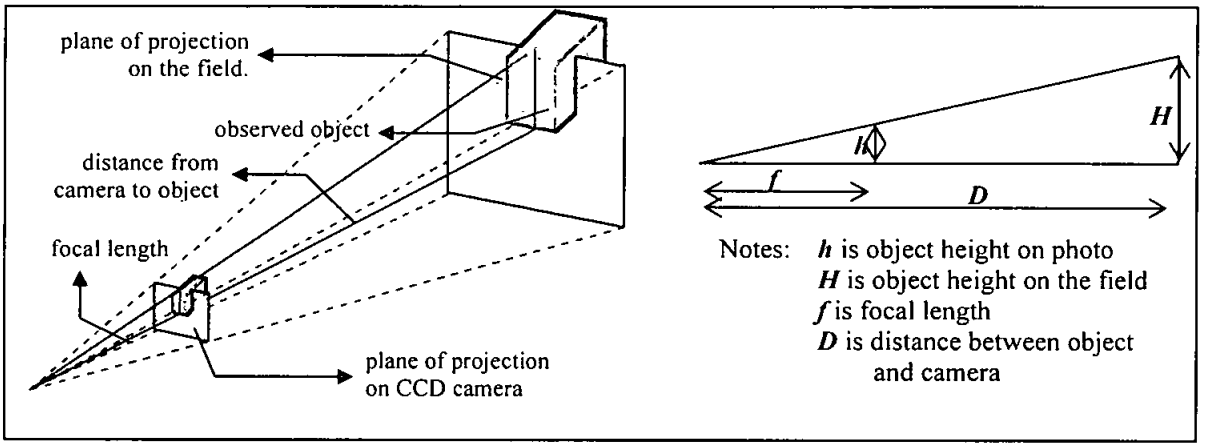

Figure 3.10. Scaling factor calculation illustrated in 3D (left), and in 2D projection by following simple triangles formula (right)

Format height and format width of the CCD camera were still be the same (5.72 mm and 4.29 mm respectively), because the same camera was used on camera calibration and image data capturing processes. All captured images of the study areas were set with 2272x1740 pixel resolution. Scaling factor and the spatial resolution of the images could be achieved by using a simple triangles formula. Illustration of the calculation is presented on Figure 3.10 and expressed by Equation 3.11 to 3.15 follow.

$$scaling\_factor = \frac{D}{f} \tag{3.11}$$

$$scaling\_factor = \frac{H}{h} \tag{3.12}$$

$$r_1 = \frac{fw}{pw} \text{ and } r_2 = \frac{fh}{ph} \tag{3.13}$$

$$r_m = \frac{r_1 + r_2}{2} \tag{3.14}$$

$$spatial\_resolution = scaling\_factor * r_m \tag{3.15}$$

Whereas: fw and fh is width and height of the CCD camera in millimeters unit; pw and ph is width and height of the CCD camera in pixels unit; r_1, r_2, and r_m is resolution of the CCD camera in width, height, and average respectively; while f, D, h, and H are stated in Figure 3.10.

3.5.2 GCP Measurements

Ground Control Points used in this thesis were measured by using the reflector-less Total Station, at least there were 20 GCPs for each sample area. Position of the GCPs should be well distributed on the observed area. Another requirement on GCP selection is each object (point) should be recognized clearly on the captured images and clearly observed by the telescope of the Total Station instrument. These GCPs were needed in exterior orientation, especially in absolute orientation process.

Being a conventional terrestrial survey using Total Station, this measurement also needs two Temporary Bench Marks (TBMs). First TBM was used for occupied point, while another one was used for orientation or back-sight point. The Total Station instrument was set up on the occupied point, while the single standard prism was set up on the back-sight point, as shown in Figure 3.11. Coordinates of occupied and orientation points were input after setting up of the instruments was carried out. Aiming the back-sight target and measuring its bearing and distance were carried out to set the real orientation of the Total Station. If all previous stated steps were done, the Total Station was ready to be used to

define coordinate of any targets included for the GCPs. Once a GCP was measured by the reflector-less Total Station, the corresponding target on the stereo images was marked (in this research the observer used print out of stereo photograph, and marked observed GCPs on it). It was performed to get an easier way to derecognize the GCP in the following stereo reconstruction process.

Figure 3.11. Position of the TS (on occupied point) and the standard single prism (on back-sight point) in the field measurement process

3.5.3 Reference point measurement

Several check points would be compared with the points of the derived DEM recording at the same horizontal position. It was performed to define the value of Root Mean Square (RMS) of elevation interpolation error. Measurement of these points was accomplished by the calibrated Total Station. Distribution of these points should be well, so all kinds of relief condition can be adequately represented. In this thesis, result of this measurement is assumed to be correct, considering the calibration process and corrections on the measured data.

Another parameter used in accuracy assessment process was volume difference error parameter. For this purpose, sampling points as reference data of the study areas should

be measured by using the reflector-less Total Station. Certain terrain data sampling method was used to select the sampling points. In this research, regular sampling method was chosen and applied for all study areas (Area-1 to Area-4), because of their effectiveness on the measurement and representation ability. As the check point measurement, the measured data here was assumed as a set of correct data.

Measurements of both types of points were similar to steps on GCP measurement. The differences were only in point selection and providing code of the measurements. Selection of the GCP points has been revealed on previous sub-chapter (GCP measurement). Check points were randomly selected on the slope surface, but they ought to represent all types of topographic condition, while selection of sampling points was following the selected terrain data sampling method. The sampling point was measured following horizontal and vertical array. Interval distance between one point to other adjacent points was set approximately one meter length. So formation of those measured points form a grid structure.

3.6. 3D Stereo Model Reconstruction

Reconstruction of 3D stereo model consists of three main steps: interior orientation, relative orientation and absolute orientation [3]. However, in this research, relative and absolute orientations were performed in one process, called exterior orientation. Photogrammetry workstation software used in this research was PhotoModeler Pro version 5.2.3, while number of photographs used for each sample area was three photographs.

3.6.1 Interior Orientation

Interior orientation is the mathematical reconstruction of geometric camera when a particular photograph was taken. It requires camera calibration information resulted from the previous camera calibration process. The information was used to refine all of the stereo images in this research, so the images were free from camera's systematical error

(in this case, it is free from lens distortion) and the recent coordinates were correctly related to the principal point. The process begins with measurement of fiducial marks positions and image point coordinates by a comparator. A 2D conform coordinate transformation was used to relate the comparator/machine coordinate system into fiducial coordinate system [3]. Because no fiducial marks are on all stereo images, four corners of each captured image have been selected as fiducial marks. In this software, interior orientation was automatically calculated after camera calibration information was given.

3.6.2 Exterior Orientation

Relative orientation is the process of determining the relative angular orientation and positional displacement between the images at the time of exposure. It involves the definition of certain elements of position of the cameras and its angles of orientations at the time of execution. Transformation from 2D machine coordinate system into 3D Cartesian relative coordinate system was accomplished in this process. The resulting exterior orientation parameters will not be the actual values that existed when the photographs were exposed. However, they will be correct in a relative sense between the stereo photos.

Relative orientation requires the marking of some tie points on those three overlapping photographs. In this research there are at least six marked points. Process to mark the tie points were executed manually by pointing on all overlapping photographs. Certain terrain data sampling method must be applied here to construct a 3D stereo model. In this research, a regular sampling method was applied for all sample areas. Especially for sample Area-2, three types of terrain data sampling methods were used. There were regular sampling, progressive sampling, and selective/composite sampling methods. It was performed in order to investigate the correlation between sampling method and quality of the derived DEM.

Absolute orientation can be performed using a 3D conformal coordinate transformation. This stage transforms the coordinates from 3D relative coordinate system into world

coordinate system. For stereo model computed from one stereo-pair images, analytical absolute orientation requires two horizontal and three vertical control points. In this stage additional control points are needed to achieve a better accuracy, resolved by a least squares adjustment calculation. Once the transformation parameters have been computed, this result can also be applied to the remaining stereo model points.

There are three techniques that can be used in absolute orientation process using this software: defining three transformation points; defining rotation axis, translation vector, and scaling distance; defining at least three Ground Control Points (GCPs) [39]. The last mentioned technique was applied in this thesis, but it requires processing relative and absolute orientations in one process [40], which is commonly called an exterior orientation. To get a better accuracy in resulted DEM, selection of the GCPs was carried out before sampling point selection, whereas accuracy of the GCP selection does not exceed 0.5 pixel [43].

The GCPs were measured using the calibrated reflector-less Total Station. These GCPs were well distributed covering the slope surface, and their positions were clearly recognized on all stereo photographs. Those GCPs coordinates were required in this stereo model restitution process. By these coordinates, parameters of transformation from 2D left-right fiducial coordinate system (x^L, y^L and x^R, y^R) into 3D world coordinate system (Easting, Northing, and Elevation) can be calculated using least square bundle block adjustment formula.

3.7. DEM Derivation

DEM generation requires establishment of the relationships between points' coordinates and its interpolation to approximate the real surface. The 3D coordinates of the photogrammetric sampling points were derived to be a DEM of the study area's surface using a Triangular Irregular Network (TIN). Being data structure, TIN could be decrypted since a terrain is represented by a set of point (nodes or vertices), a set of edges (lines), and a set of triangular faces (triangles areas) [44].

Interpolator and visualizing software used in this thesis is ArcView 3.2 with its 3D Analyst Extension. Almost the same as the concept of topology, a point is defined by coordinate position in 3D Cartesian system (*x, y, z* or *easting, northing, elevation*). An edge of TIN connects two adjacent points and it is described by intersection of two faces. A face is bordered by three edges, and surface condition of this triangle is assumed as a flat surface [45].

In ArcView-3D Analyst, there are five interpolation methods: TIN, *Inverse Distance Weighted* (IDW), *Spline, Kriging*, and *polynomial regression* interpolation methods [46]. TIN, IDW, and *Spline* interpolation methods are available on the *surface menu* and can be used directly under Windows Operating System. The last two mentioned methods can be accessed by typing certain commands on avenue script language. TIN was preferred in this research because of the following reasons:

i. The possibilities to represent the digital 3D model at both small and large scale resolution;
ii. This interpolation function can be adapted to the varying terrain character, as the condition of the sample areas;
iii. Volume calculation of the DEM is easier to be performed by using this method.

Sampling points coordinates of all study areas (Area-1 to Area-4), derived from close-range photogrammetric method were transformed into DEM. Apart from those DEM there was another DEM derived from conventional terrestrial survey data measured using a calibrated reflector-less Total Station. The DEM derived from Total Station data was treated as a reference DEM, and it was used in the quality measurement process of the DEM generated from close-range photogrammetric data. The Total Station was preferred in reference DEM collection data tool because the accuracy of the Total Station is in millimeters level. In addition, compared to the application of close-range photogrammetry for slope monitoring, the accuracy of Total Station is generally better.

3.8. Quality Measurement of DEM

Theoretically any level of accuracy could be achieved by increasing density of the sampling points. However, this condition is not always feasible practically, especially for a rugged surface. There are even anomalous situation where increasing the point density will decrease the quality of the DEM. Generally, there are four parameters in expressing quality of derived DEM: elevation, curvature, roughness, and slope. In term of Civil Engineering, there are two parameters that traditionally used to characterize the accuracy of DEM: elevation interpolation error and volumetric difference calculation error [28]. Both parameters were preferred, because the errors (volume and elevation errors) have significant impact in economical factor to determine duration and volume of construction project.

Quality of the DEM derived from close-range photogrammetric data was determined by: volumetric difference error calculation and elevation interpolation error computation. There were 38 independent points per each study area measured by calibrated reflector-less Total Station for check points. These points were compared with the elevation (***Y*** position) of derived DEMs against the same position of ***X*** and ***Z*** because images on photographs were projected on the *X-Z Cartesian's plane*. Elevation of every point inside each triangle of TIN (that has same planimetric position with the check point), can be interpolated by using Equation 3.16 [21].

$$V\begin{pmatrix} X_1 - X \\ Y_1 - Y \\ Z_1 - Z \end{pmatrix},\ V_1\begin{pmatrix} X_2 - X_1 \\ Y_2 - Y_1 \\ Z_2 - Z_1 \end{pmatrix},\ V_2\begin{pmatrix} X_3 - X_1 \\ Y_3 - Y_1 \\ Z_3 - Z_1 \end{pmatrix} \tag{3.16}$$

V also can be expressed as

$$V = \mu V_1 + \nu V_2, \tag{3.17}$$

$$\text{where: } \mu = \frac{(V \wedge V_2)k}{(V_1 \wedge V_2)k},\ \nu = \frac{(V \wedge V_1)k}{(V_2 \wedge V_1)k} \text{ and } k = \begin{pmatrix} 0 \\ 0 \\ 1 \end{pmatrix} \tag{3.18}$$

Thus $Z = (\mu V_1 + \nu V_2)k$ (3.19)

Accuracy of the generated DEM was shown by the value of statistical calculation results. The bigger the value of those results, the lower the accuracy of the derived DEM is, and vice versa. The statistical calculation of DEM accuracy was calculated using formulas given in Equation 3.20 to3.22 [28].

$$E_m = \frac{\sum e_i}{n} \tag{3.20}$$

$$E_{ma} = \frac{\sum |e_i|}{n} \tag{3.21}$$

$$RMS.error = \sqrt{\frac{\sum (e_i - E_m)^2}{n-1}} \tag{3.22}$$

Where E_m is mean error; e_i is individual error of one point; n is total number of points; E_{ma} is absolute mean error; *RMS.error* is root mean square error. The mean error is a good indicator of the randomness of the errors (obtained by interpolation calculation process, or errors in check points measurement), in which both errors greatly affect the quality of DEM. Modeling of the absolute mean error is the best indicator of the accuracy in elevation interpolation of the DEM, while RMS error is an indicator of the distribution of the height errors [28].

Volume of the DEM can be calculated using a simple mathematical formula of triangular prism approach as given in Equation 2.25 [47]. This approximation method computes volume of the DEM based on the volumetric calculation of numerous triangular prisms. Each volume of triangular prism is calculated using the given formula on Equation 3.23 and 3.24. Similar to the elevation interpolation error calculation, the result was also compared to the volume of reference DEM (derived from Total Station data) in order to get difference in volume. The value of volume difference (volume error) from this calculation shows the quality of the resulted DEM.

$$h_{m_i} = \frac{h_{i1} + h_{i2} + h_{i3}}{3} \tag{3.23}$$

$$V_i = F_i * h_{m_i} \tag{3.24}$$

$$V = \sum_{i=1}^{n} V_i = \sum_{i=1}^{n} F_i * h_{m_i} \tag{3.25}$$

Whereas i is name of one triangle; n is total number of all triangles; h_{i1}, h_{i2}, h_{i3} are height of each vertex of one triangle; h_{mi} is medial height of one triangle; V is volume of the object; V_i is volume of one triangle; F_i is area of one triangle.

3.9. Mass-movement Detection

Since the observed area for Area-2 and Area-3 are the same but measured at different time (13/05/2007 and 07/04/2008 respectively) therefore some analysis can be performed here. One of them is to detect landslide possibility on the slope surface. Condition of the observed objects is they have no permanent points on the surface. Therefore velocity and direction of the landslide cannot be accurately identified. The most possible way to detect the landslide is by calculating the DEMs derived from both different epochs. By this calculation the distribution of mass movement as well as its volumetric changing was able to be modeled. There are two kinds of representations that possible to be used in this research: using 3D spatial calculation of overlaying derived DEMs together with profilings along cross-section and longitudinal-section. Elevation changes on both epoch DEMs can be represented by the profiling, while distribution of gain and loss soil can be represented using DEM calculation.

3.10. Experimental Work Flow

This work is carried out in several steps of process, but generally it can be performed in five steps:

i. Preparations (consist of calibration processes for Total Station and camera);

ii. Data collection (include capturing stereo photographs by the camera, and measuring GCP check points, and reference DEM data by the Total Station);
iii. Data processing (involved in two steps: interior and exterior orientations);
iv. Quality measure and characterizing the quality;
v. Mass-movement detection.

The workflow of this thesis was presented in the following Figure 3.12.

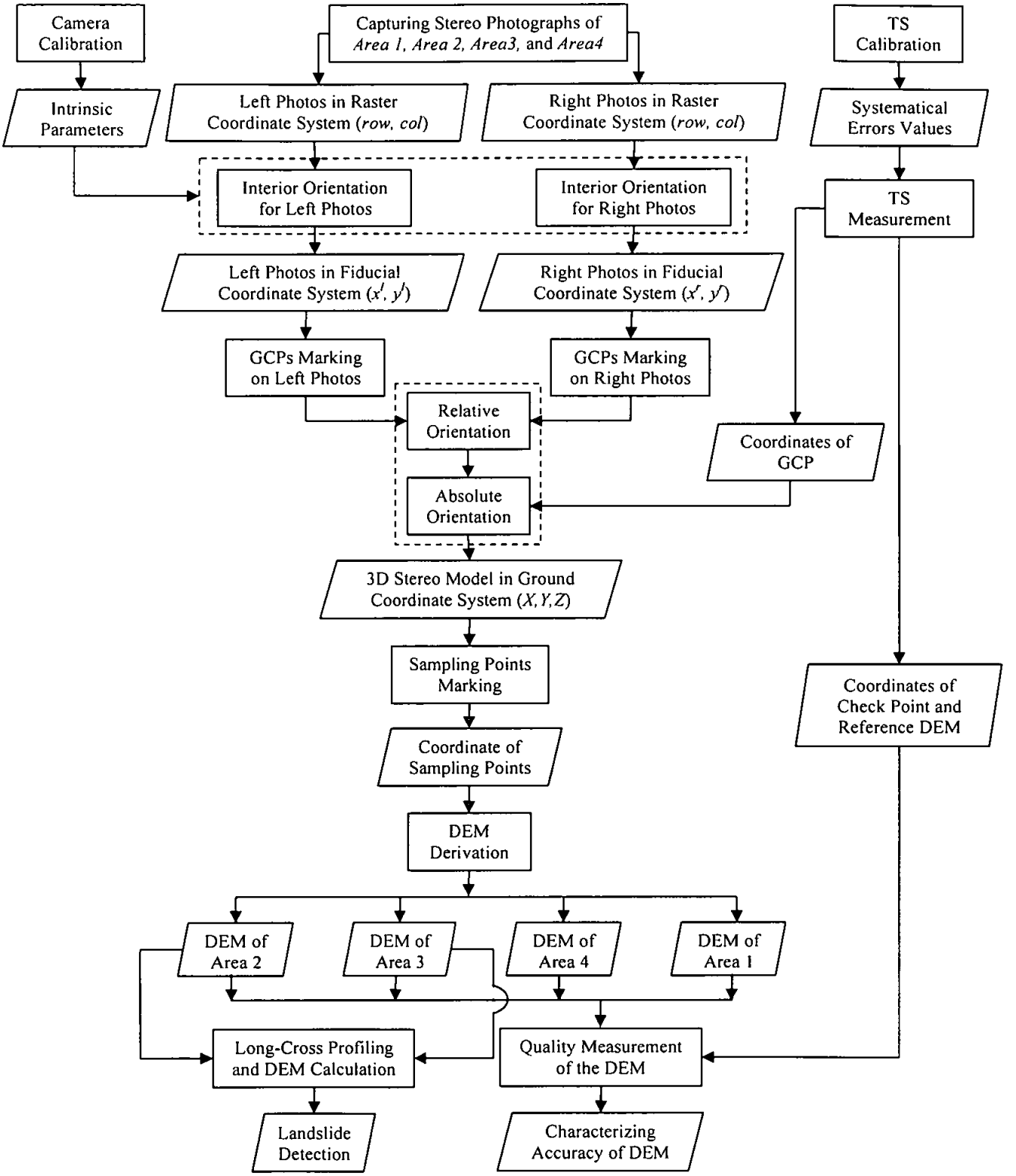

Figure 3.12. Experimental work flow of this research

CHAPTER 4

RESULT AND DISCUSSION

4.0. Introduction

This chapter shows results of experimental process described in the previous chapter. The results consist of: camera calibration, total station calibration, DEM data collection, 3D stereo model reconstruction, DEM derivation, quality measurement of DEM, and landslide detection.

4.1. Camera Calibration

Camera used in this research is a digital commercial pocket camera. As a non-metric camera, this type of camera is not designed for mapping purposes. Consequently, some essential information such as: principal point, fiducial marks, and lens distortion information are not provided by the constructor/producer. For precise analytical photogrammetric works, it is necessary to compute those mentioned information by camera calibration process.

Auto self calibration calculated using bundle block adjustment was used in this research study to define the intrinsic camera parameters. Included in intrinsic parameters are focal length, principal point, and lens distortion parameters. These parameters are needed in photogrammetric process as a requirement in image refinement when interior orientation was performed (both for aerial and close range photogrammetry). By this calibration, characteristic of the camera can be calculated, and systematical error in the camera can then be eliminated.

The camera calibration has to be carried out for each different focal length of the camera [38]. In this research, the camera calibration was carried out twice because there are two

different focal lengths used in data collections. First focal length was set on 11.49 mm for Area-2, while the second focal length was set on 9.77 mm for Area-1, Area-3, and Area-4. Result of both calibrations is presented in Table 4.1. Those calculation results show that by using different setting of focal length and different position of both principle points caused the resulted values of the lens distortion parameters are being different.

Table 4.1. Result of camera calibration calculation

Camera Parameters		**Area-2**		**Area-1, Aera-3, and Area-4**	
Focal length	*f*	11.490	mm	9.768	mm
Format size	Width	5.724	mm	5.724	mm
	Height	4.293	mm	4.293	mm
Format pixel	# of row	1704	pixel	1704	pixel
	# of column	2272	pixel	2272	pixel
Principal point	*Xo*	2.999	mm	2.984	mm
	Yo	2.190	mm	2.202	mm
Radial distortion	*K1*	0.00114		0.00161	
	K2	0.00000912		0.00000679	
Tangential Distortion	*P1*	-0.000112		-0.000120	
	P2	-0.0000189		-0.0000152	

One of the characters of the non-metric camera is that the position of principal point is not stable. This instability influences to the other camera calibration parameters [49]. Due to the condition, images acquisition of the camera calibration pattern was performed 'at the same time' with the capturing of the object images. 'At the same time' means the exposures were carried out before the camera was turned off or before the focal length was changed. Traditionally instability of the principal point for non-metric camera is caused by some of the following factors [49]:

1. Mechanical influence by the user; during the hand-held shots, different circumstances influence the camera, especially for difficultly-accessed objects.
2. Effects of gravity; it always changes relatively to the camera for each different viewing directions.

3. Heating of the camera during a long period of image acquisition, especially for large or difficultly-accessed objects

Direction and magnitude of both lens distortions of the camera can be modeled using those parameters and by the following Equations 2.3 to 2.5 as mentioned previously in Chapter 2. By these calculations, geometrical correction for all captured objects inside the image can be performed. Figure 4.1 and Figure 4.2 presents the model of these lens distortions.

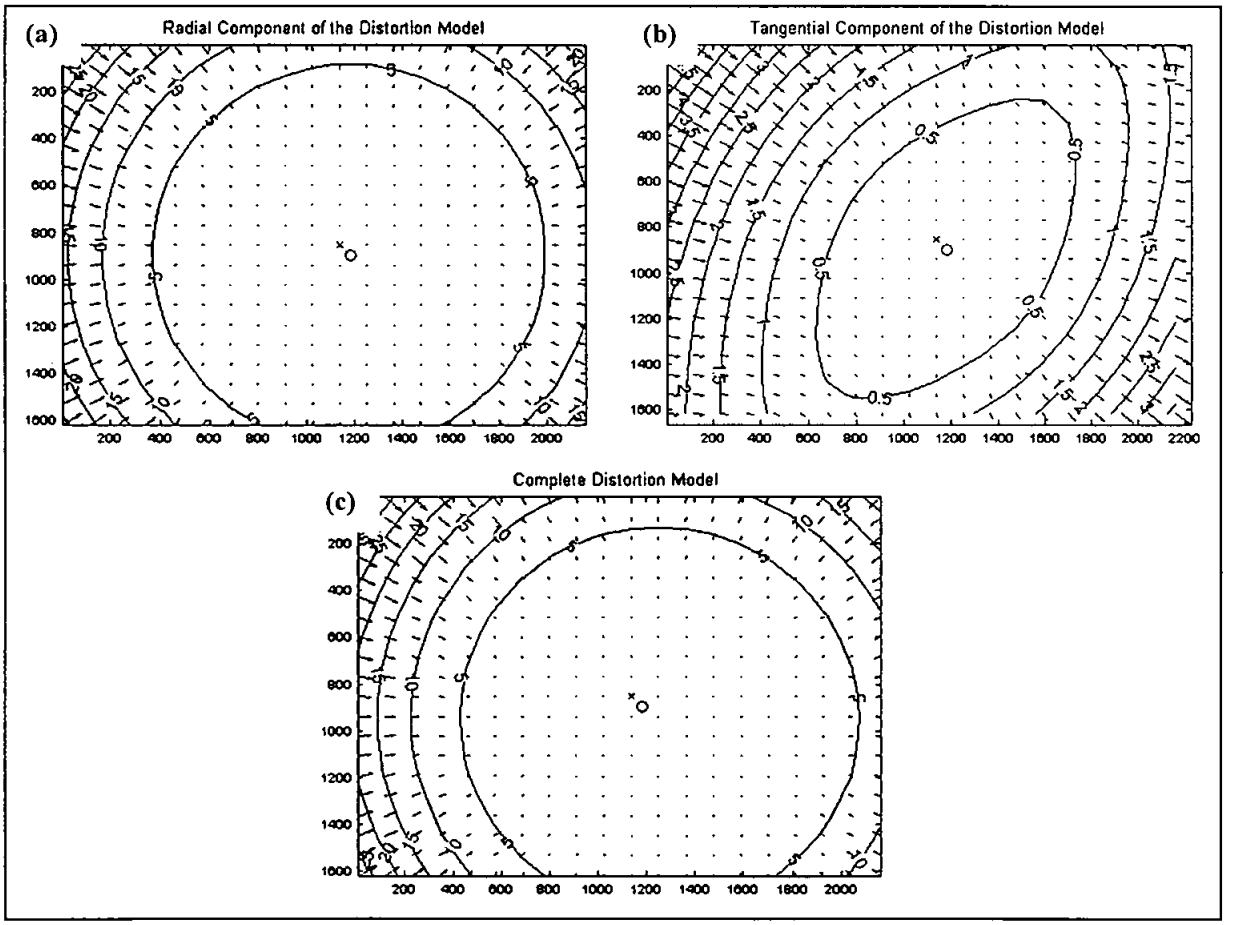

Figure 4.1. Modeling of magnitude and direction for: radial distortion (a); tangential distortion (b); and total lens distortion (c) for Canon A450 with focal length was set on 9.768 mm.

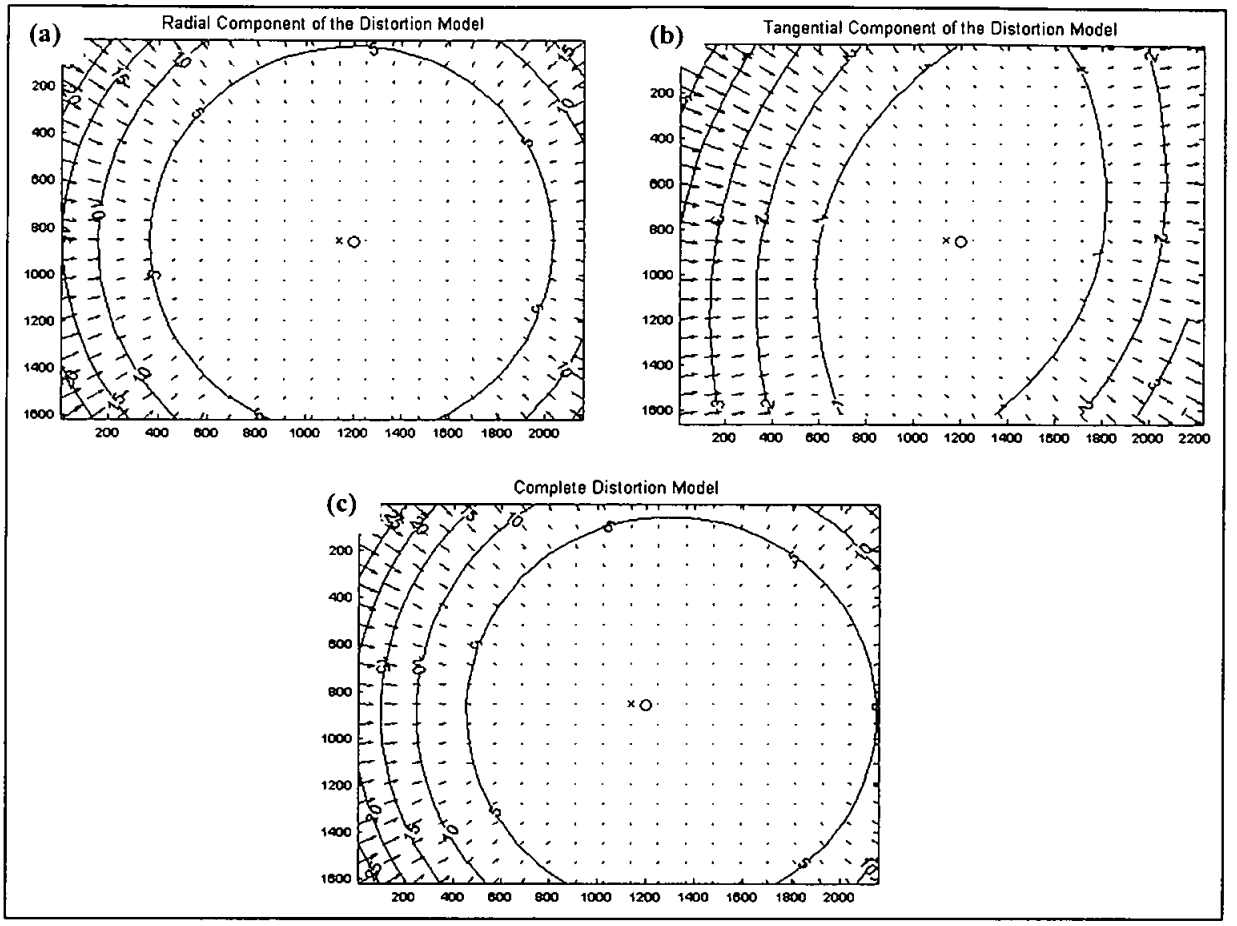

Figure 4.2. Modeling of magnitude and direction for: radial distortion (a); tangential distortion (b); and total lens distortion (c) for Canon A450 with focal length was set on 11.490 mm.

In general concept of photogrammetry, image refinement usually consists of four error corrections [3]: correction of earth curvature; correction of atmospheric refraction distortion; correction of film distortion; and correction of lens distortion. This thesis assumed that images displacement is contributed by lens distortion only, while other errors were ignored by these following reasons:

i. As common principal in surveying, at a small area of earth surface (in this case maximum distance is ±65 meters) earth curvature was negligible [50];
ii. Close-range photogrammetry was applied to measure any objects with the distance from camera of not exceeding 100 meters [4], in this distance, atmospheric condition is absolutely the same;

iii. No film distortion needs to be taken into account because it was a digital camera, so that object images were projected on a CCD (Charge-Coupled Device) and recorded as a binary image [3].

Based on the modeling of magnitude and direction of lens distortions (as presented on Figure 4.1 and Figure 4.2), it can be seen that the value of tangential distortion is lower than that of the radial one. Therefore, the tangential distortion is not significant and negligible in image displacement [52]. Commonly value of the tangential distortion is close to zero, because at the time of manufacture all elements in a lens system should be collinear to the optical axis of the entire lens system [4] and [31].

4.2. Total Station Calibration

Not only the camera, the total station used in this study was also calibrated. The calibration was accomplished on standardized permanent calibration bench marks, in which true distances between the pillars were known. In this Total Station calibration data measurement, each distance between the pillars was measured for nine times by the Total Station. The average of the measured distances was used in the next calculation. By using parametric least square adjustment method, zero error, constant value, and scaling factor of calibration-target and the Total Station (as systematical errors) can be computed.

4.2.1 Zero Error Estimation Result

Once adjustment computation was completed, the global test is then applied to ensure the compatibility of the a-posteriori and a-priori variances. The result of global test is presented in Table 4.2. The critical value is obtained from Fisher table with 95% significance level and 14 degrees of freedom. Table 2 shows the F-computed is lower than 1.70 which indicates that there is no outlier in the data. The result of the zero error and its precision is also given in Table 4.2.

Table 4.2. Result of Global test and Zero Error Calculation

Target	F-computed	Zero Error Result	
		z_0	σz_0
Standard Prism	0.592	0.093 mm	0.709e-3 mm
Plate of Concrete	0.450	3.135 mm	1.172e-3 mm

Referring to the result in Table 4.2, standard single prism yields much smaller value of zero error than concrete material target. Because the value is very small and almost zero, in some surveying application it is usually neglected. Value of zero error for concrete target based on the calculation result was significant, so it cannot be ignored and have to be taken into account in measurement.

Table 4.3. Result of significant test for the zero error

Target	t-computed
Standard Prism	2.299
Plate of Concrete	2.491

To check the significance of the zero error value, t-student statistical test was carried out in this study. The critical value of t-table is 2.145 with 95% significance level and 14 degree of freedom. Table 4.3 depicts the result of t-test for zero error. The table shows that the t-computed for both targets are larger than 2.145. It indicates that the zero error significantly exists in this baseline measurement. Since the error occurred in the instruments and/or target, the appropriate value should be directly applied to each observed baseline.

Due to statistical calculation result of significant test, all measurements data have to be adjusted to remove the zero error from the measured distances. The adjusted distance for each sub-baseline between both targets, and its published distance are given in the Table 4.4. According to the values of adjusted distance, it can be observed that the differences between adjusted sub-baselines of standard single prism and the published distance do

not exceed 3mm, while differences between concrete target and the true distances were below 5mm. If the adjusted error was yielded, it means that the data was free from zero error, rest of error is caused by scale error (as an incremental systematical error) or cyclic error (as a periodic systematical error) [53].

Table 4.4. Adjusted sub-baseline for both calibration targets based on measurement data.

Baseline	True Distances (m)	Standard Prism (m)		Plate of Concrete (m)	
P0-P1(m)	5.004	5.003	± 0.000e-3	5.007	± 0.894e-3
P0-P2(m)	10.002	10.001	± 0.548e-3	10.004	± 2.702e-3
P0-P3(m)	49.002	49.000	± 0.894e-3	49.000	± 2.881e-3
P0-P4(m)	125.000	124.999	± 0.894e-3	124.995	± 3.564e-3
P0-P5(m)	201.002	200.999	± 0.577e-3	201.007	± 3.083e-3
P0-P6(m)	300.008	300.005	± 0.577e-3	201.008	± 4.163e-3

4.2.2 Calibration Result of Distance Measuring Tool in the Total Station

Based on the adjusted sub-baseline results and computed by following parametric least-square adjustment formula as mentioned on Equation 3.9 and 3.10, the constant value and scaling factor of the reflector-less Total Station (symbolized by a and b respectively) can be acquired. Result for calibration of the distance measurement tool in the total station is presented in Table 4.5.

Table 4.5. Constant value and scaling factor in TS calibration for various material targets

Target	Constant Value		Scaling Factor	
	a (mm)	σa (mm)	b (ppm)	σb (ppm)
Standard Prism	1.031	6.202e-4	2.040	3.149e-6
Plate of Concrete	0.616	1.019e-3	5.978	9.777e-6

Referring to the calibration result in the Table 4.5, standard single prism target gives small value for the constant and scaling factors of the Total Station (1.031 mm and 2.040 ppm, respectively) but the scaling factor here is still bigger than the specification

provided by the manufacturer (2 mm ± distance * 2 ppm). Even though the scaling factor here is bigger than the specification, it is acceptable as long as it is still smaller than the maximum range of the prism (3000 m) measured by GPT 3007 N/LN total station [54]. Unlike the prism, plate of concrete used in this calibration yields both values of constant and scaling factors of below the specification (10 mm ± distance * 10 ppm).

In order to check the significance of the calibration calculation results, t-student statistical test was performed in this research. The critical value of t-table is still the same as the previous t-test calculation (2.145 with 95% significance level and 14 degree of freedom). Table 4.6 shows that the t-computed for both targets are lower than 2.145. It indicates that there is no error in the distance measurement tool in the total station, neither in the reflectors. The value difference between the adjusted distance and the corresponding published distance (as provided on Table 4.4) are tolerable, and the errors are still below the specification claimed by the manufacturer.

Table 4.6. T-computed for significant test of TS calibration

Target	T-test Result	
	Constant Value	**Scaling Factor**
Standard Prism	1.663	0.743
Plate of Concrete	0.605	0.611

From the result of this total station calibration, it can be concluded that until 300 meters length (as the maximum distance of the sub-baseline) the GPT 3007 N/LN Total Station used in this research still provides a valid distance, and can be used as a data collection tool for any surveying application.

4.3. Data Collection

Data collection was performed after calibration for both main instruments was accomplished. Included in data collection stage of this research were: stereo images data capturing using the calibrated Canon A450 digital pocket camera; and terrestrial survey

by means of calibrated GPT 3007 N/LN reflector-less total station to measure some control points, check points, and sampling points to derive a reference DEM. The data collection was carried out on all study areas (Area-1 to Area-4). Capturing images and measuring by the Total Station for each area was accomplished in a same day.

4.3.1 Stereo Images Data Collection

Stereo images used in this thesis were captured by using a Canon A540 digital pocket camera, with photo resolution of 2272 pixels x 1740 pixels. The focal length of the camera was set on 11.490 mm (for Area-2) and 9.768 mm (for Area-1, Area-3, and Area-4). Each study area was captured by three overlapping photographs, taken from different position and orientation with a length of stereo base line of 8 meters, and average distance between the target and the camera ranged between 55 and 65 meters. Each stereo photograph covers more than 80% of its adjacent coverage, as presented in Figure 4.3. When the stereo images were taken, the positions and orientations of the camera were not recognized, but these positions and orientations can be calculated based on coordinates of the Ground Control Points (GCPs) on those overlapping photographs.

Using the values of format width, format height, distance between the camera to object, and focal length, spatial resolution and scaling factor can be calculated using the Equations 3.11 and 3.12. Scale of the captured images of Area-2 was 1: 5000 (exact 1: 5217.391), while images' scale of the rest of the study area was 1: 6000 (exact 1: 6122.449). As general concept in photogrammetry that captured images can be derived to be a map with the scale can be enhance until eight times of the sources images [3]. Therefore in this study the captured images will be derived to be DEMs with the scale of 1:200. By following the calculation for spatial resolution as expressed by Equation 3.13 to 3.15, spatial resolution of the images on Area-2 was 12.458 mm, while spatial resolution of the other areas was 14.949 mm.

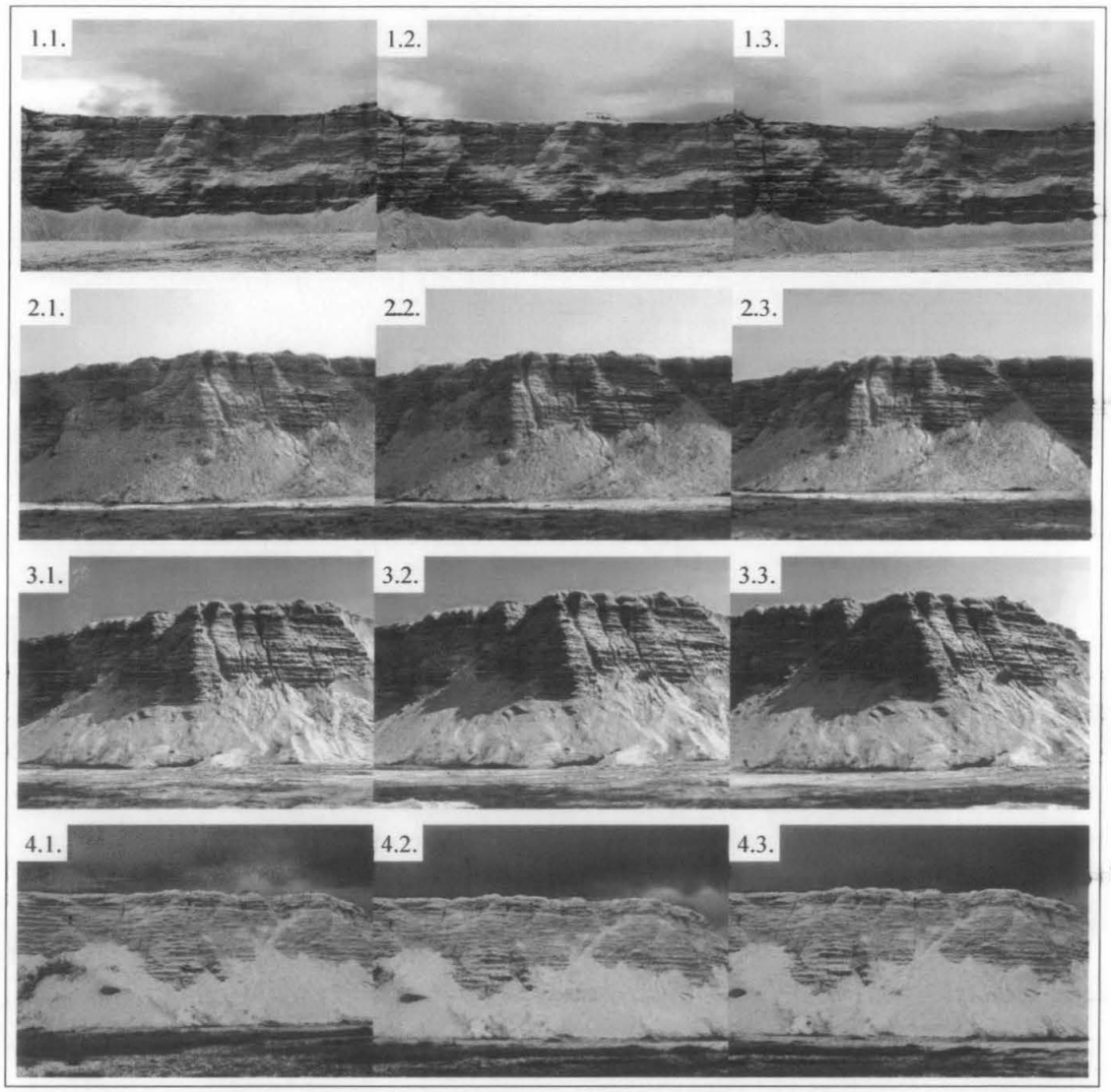

Figure 4.3. Overlapping photographs of the study areas
(in top-down arrangement: Area-1, Area-2, Area-3, and Area-4)

4.3.2 GCPs and Reference Points Measurements

The GCPs were measured by using the calibrated GPT 3007 N/LN reflector-less Total Station. Position of the GCPs were well distributed covering the observed area and the objects (points) were clearly recognized both on the photographs and on the field by telescope of the Total Station. An example of the measurement data is shown in Figure

4.4, while complete GCP measurement data for each study area is presented on **Appendix C.**

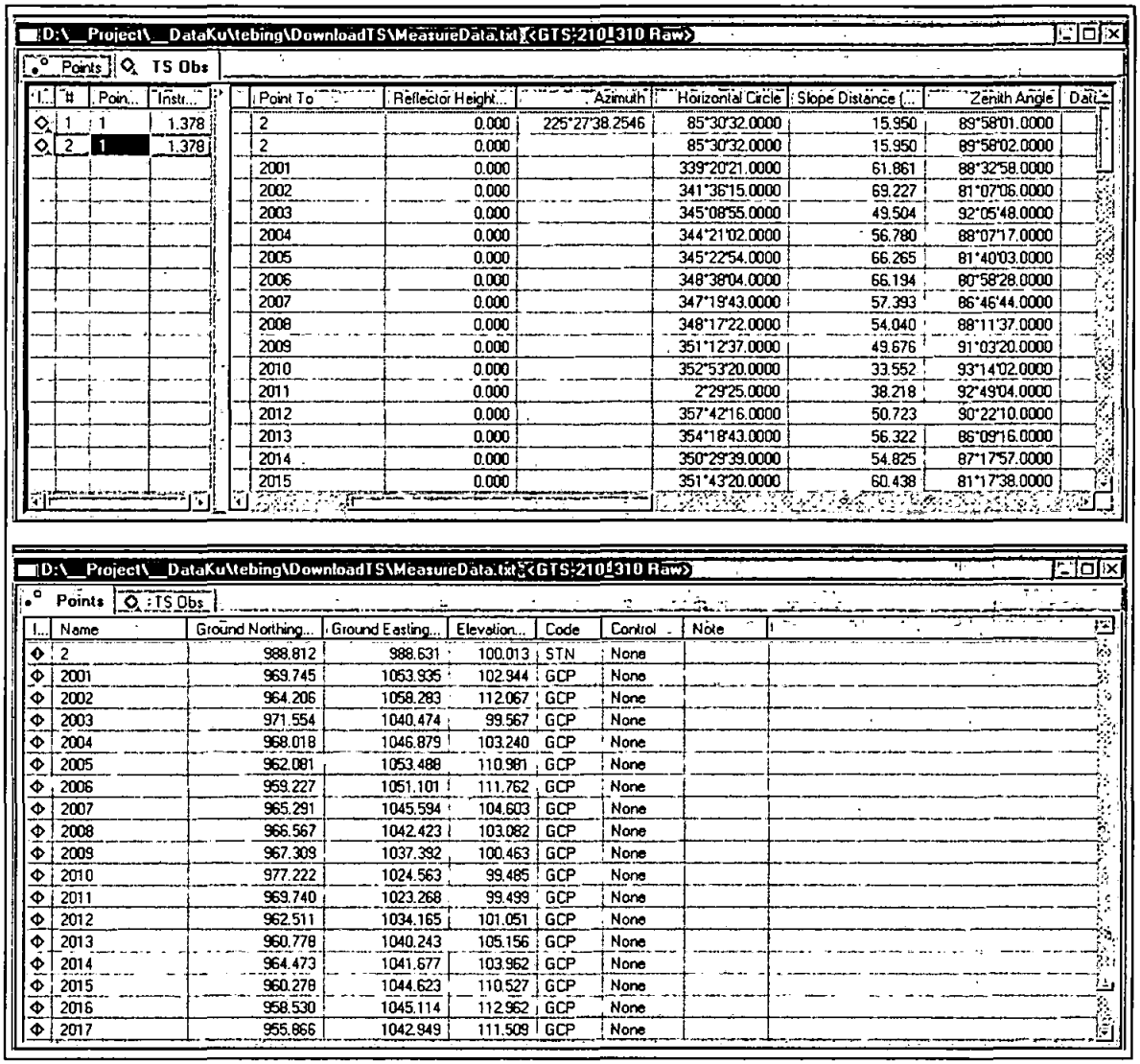

D:_Project_DataKu\tebing\DownloadTS\MeasureData.txt<GTS-210_310 Raw>

Points | TS Obs

I...	#	Poin...	Instr...
1	1	1	1.378
2	2	1	1.378

Point To	Reflector Height...	Azimuth	Horizontal Circle	Slope Distance (...	Zenith Angle	Dat...
2	0.000	225°27'38.2546	85°30'32.0000	15.950	89°58'01.0000	
2	0.000		85°30'32.0000	15.950	89°58'02.0000	
2001	0.000		339°20'21.0000	61.861	88°32'58.0000	
2002	0.000		341°36'15.0000	69.227	81°07'06.0000	
2003	0.000		345°08'55.0000	49.504	92°05'48.0000	
2004	0.000		344°21'02.0000	56.780	88°07'17.0000	
2005	0.000		345°22'54.0000	66.265	81°40'03.0000	
2006	0.000		348°38'04.0000	66.194	80°58'28.0000	
2007	0.000		347°19'43.0000	57.393	86°46'44.0000	
2008	0.000		348°17'22.0000	54.040	88°11'37.0000	
2009	0.000		351°12'37.0000	49.676	91°03'20.0000	
2010	0.000		352°53'20.0000	33.552	93°14'02.0000	
2011	0.000		2°29'25.0000	38.218	92°49'04.0000	
2012	0.000		357°42'16.0000	50.723	90°22'10.0000	
2013	0.000		354°18'43.0000	56.322	86°09'16.0000	
2014	0.000		350°29'39.0000	54.825	87°17'57.0000	
2015	0.000		351°43'20.0000	60.438	81°17'38.0000	

D:_Project_DataKu\tebing\DownloadTS\MeasureData.txt<GTS-210_310 Raw>

Points | TS Obs

I...	Name	Ground Northing...	Ground Easting...	Elevation...	Code	Control	Note
	2	988.812	988.631	100.013	STN	None	
	2001	969.745	1053.935	102.944	GCP	None	
	2002	964.206	1058.283	112.067	GCP	None	
	2003	971.554	1040.474	99.567	GCP	None	
	2004	968.018	1046.879	103.240	GCP	None	
	2005	962.081	1053.488	110.981	GCP	None	
	2006	959.227	1051.101	111.762	GCP	None	
	2007	965.291	1045.594	104.603	GCP	None	
	2008	966.567	1042.423	103.082	GCP	None	
	2009	967.309	1037.392	100.463	GCP	None	
	2010	977.222	1024.563	99.485	GCP	None	
	2011	969.740	1023.268	99.499	GCP	None	
	2012	962.511	1034.165	101.051	GCP	None	
	2013	960.778	1040.243	105.156	GCP	None	
	2014	964.473	1041.677	103.962	GCP	None	
	2015	960.278	1044.623	110.527	GCP	None	
	2016	958.530	1045.114	112.962	GCP	None	
	2017	955.866	1042.949	111.509	GCP	None	

Figure 4.4. Examples of the GCP measurement data as a raw data with distances and angles (top); and as a calculation result in local coordinate system (*N, E, Z*).

Parameters of accuracy assessment used in this research were volumetric difference error and elevation interpolation error. Both parameters are traditionally used in civil engineering, because effect of those errors directly influence the duration of project and cost of the project as well. Due to those parameters, there were two kinds of points required in this assessment: check points; and reference points.

At least 40 check points for each study area were measured using the calibrated reflector-less Total Station GPT 3007 N/LN. Row data of the check points measurement result (distances and angles), were then required to calculate the positions of those check points in 3D ground coordinate system (easting, northing, and elevation). To remove errors because of the instrument on the measurement data, these coordinates then should be simultaneously corrected with the value of zero error as yielded by the Total Station calibration process. Resulted data after this correction was assumed as a correct data. Those check points were randomly selected but well distributed covering the study area, and all those points should be representing the topographical condition on the study area.

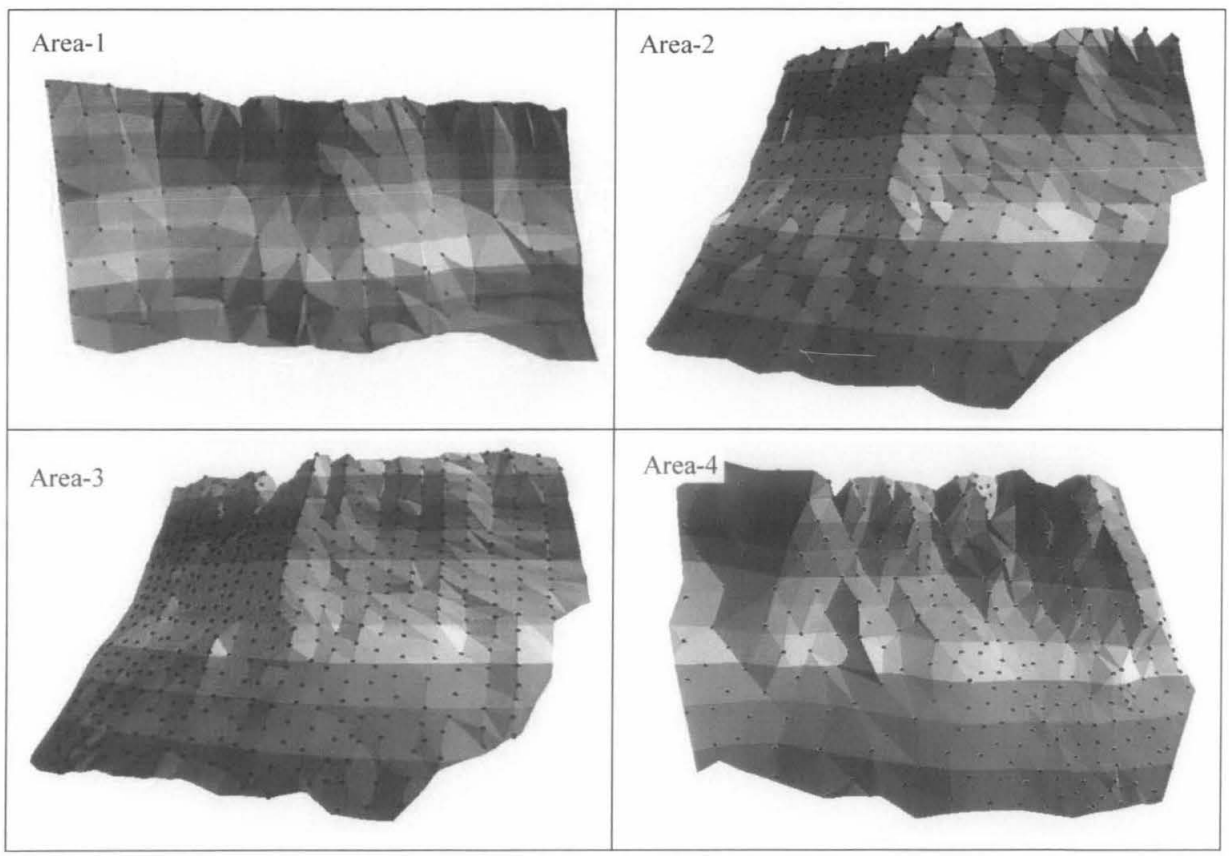

Figure 4.5. Distribution of the real DEM's sampling point measured by the calibrated TS

In addition to the measurement of the check points, the real slope on the study area was also measured using the calibrated reflector-less Total Station. Because of the ability of

the reflector-less Total Station in data measurement in which targets or objects are measured as a point, a certain terrain data sampling method was required. In this study, all of study area (real slopes) was measured by following a regular sampling method, by means of the calibrated Total Station. Distribution of the sampling points of the real objects and it's derived DEMs (generated from Total Station data) for all study areas are available in Figure 4.5, while coordinates of sampling points measured by using the calibrated reflector-less Total Station is presented on **Appendix D**. These DEMs were assumed as a reference DEMs.

4.4. 3D Stereo Model Reconstruction

Transformation process for all overlapping objects on the stereo photographs, from 2D left-right photo coordinate system into 3D ground coordinate system is called as a 3D stereo model reconstruction (also known as a stereo restitution). This stereo restitution consists of three main processes: interior orientation; relative orientation; and absolute orientation. If the relative and absolute orientations were carried out in one process it is called exterior orientation. In this research an exterior orientation was calculated by bundle block adjustment.

4.4.1 Interior Orientation

Interior orientation was carried out by inputting the camera information parameters into the software, and then it will be automatically processed. One of processes included in interior orientation stage is image refinement. The image refinement is performed because of image plane of the camera is neither completely flat, nor absolutely orthogonal to the optical axis. This condition is usually corrected via fiducial marks on a glass plate fixed to camera body at the image plane [51]. By using parameters of interior orientation, image refinement can be carried out by following Equation 2.6. Some examples in image refinements were given in Figure 4.6.

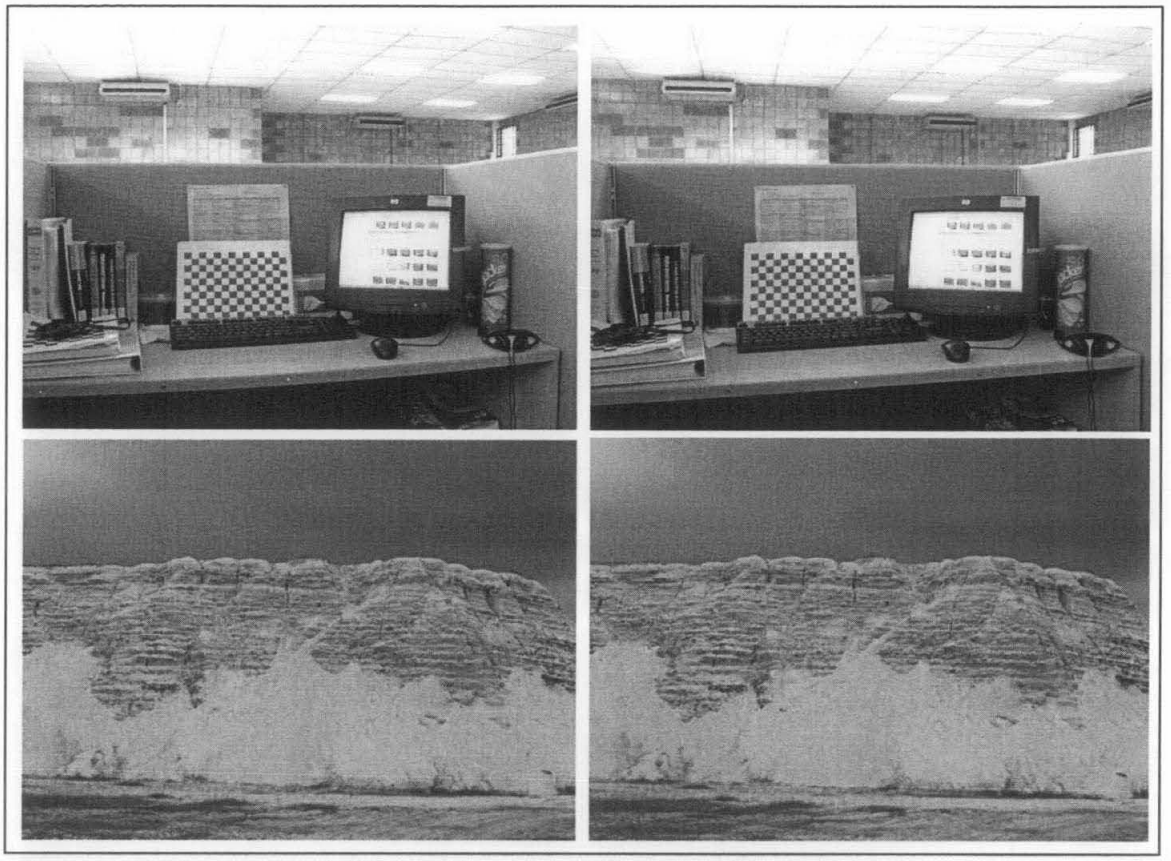

Figure 4.6. Examples of distorted images (left) and undistorted images (right) as results of image refinement from camera lens distortion.

4.4.2 Exterior Orientation

To determine the relative angular orientation and positional displacement between the images at the time of exposure, some GCPs were required. Positions and orientations of the cameras at the captured time were given on Table 4.7. GCPs selection is an essential step in photogrammetry, because the resulted stereo model will be in a right geometry if error of GCPs marking on the stereo photos is close to zero. GCPs marking means defining position of the GCPs on three stereo overlapping photos, based on its position on the field. Twenty GCPs for each area were selected to yield transformation parameters from 2D left-right photo coordinate system into a real 3D ground coordinate system, in which by this parameters position of any objects on the overlapping area in ground coordinate system can be defined. Accuracy of the GCPs marking can be examined in **Appendix C**, while distribution of the GCPs on the study area can be seen in Figure 4.7.

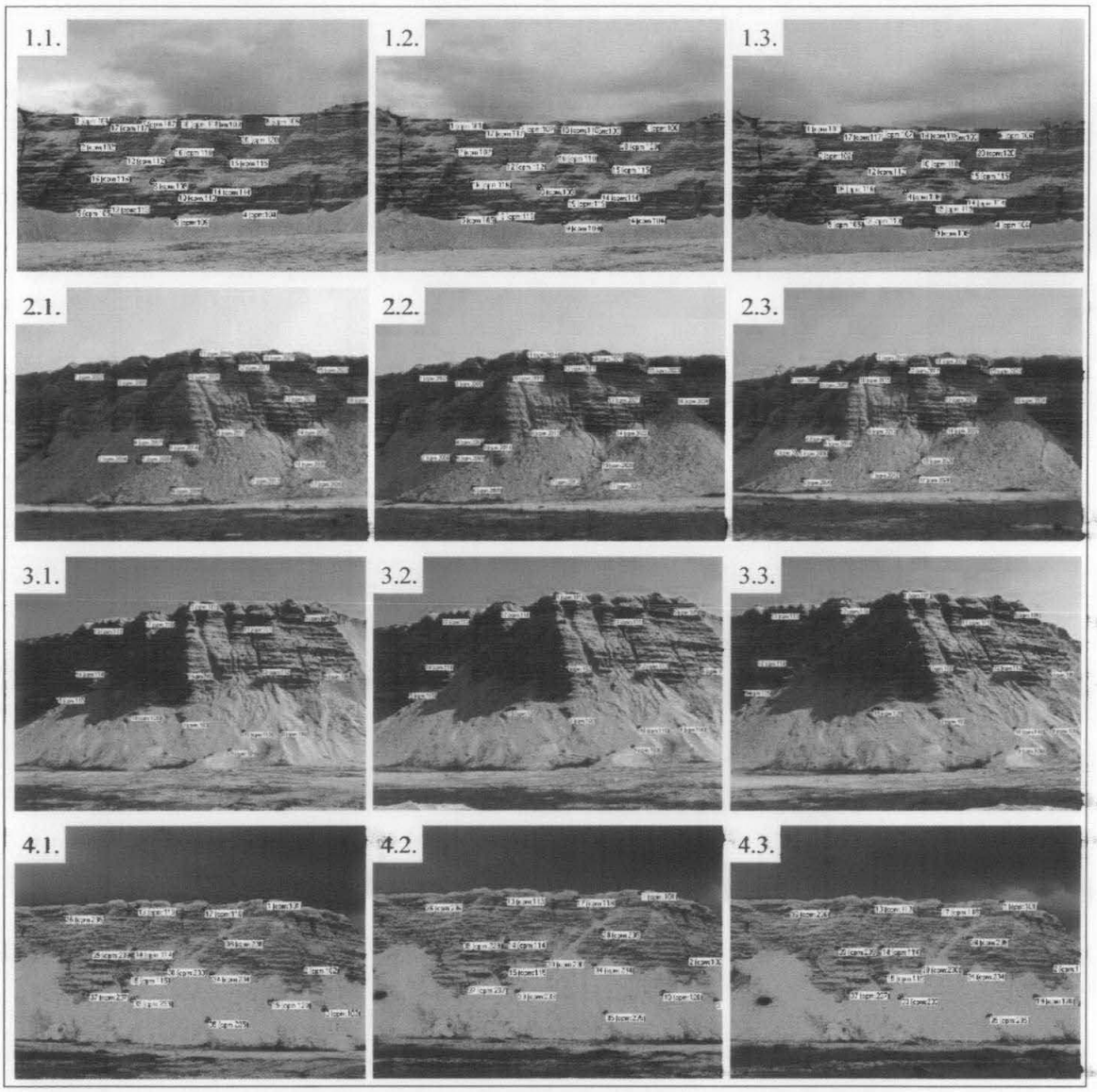

Figure 4.7. Distribution of GCPs on the overlapping photographs (in top-down arrangement: Area-1, Area-2, Area-3, and Area-4)

Table 4.7. Position and Orientation of the Camera at the Time of Exposure

Area	Photo #	Position center of the Camera			Orientation of the Camera		
		X (m)	Y (m)	Z (m)	Omega (°)	Phi (°)	Kappa (°)
Area-1	1.1.	1004.435	1004.001	101.519	96.8534	7.0787	-2.7119
	1.2.	996.279	1003.562	101.408	97.6464	0.1215	-2.1713
	1.3.	988.5026	1003.657	101.357	98.2183	-8.4292	-1.3301
Area-2	2.1.	999.109	994.380	101.717	110.2577	-76.8019	18.1929
	2.2.	1001.395	984.576	101.591	103.9181	-70.4608	12.3703
	2.3.	1002.084	971.779	101.480	98.9764	-61.4858	7.7101
Area-3	3.1.	1008.637	994.947	101.739	-265.1025	-9.6582	-0.1616
	3.2.	1002.335	999.478	101.559	-84.9752	197.1066	180.2513
	3.3.	995.324	1003.425	101.508	-84.2651	208.1516	181.6728
Area-4	4.1.	977.060	1005.486	101.355	98.6373	-39.0419	6.9885
	4.2.	972.458	1012.341	101.234	98.7513	-45.7917	7.0682
	4.3.	965.824	1016.579	101.133	100.7580	-52.6354	8.7794

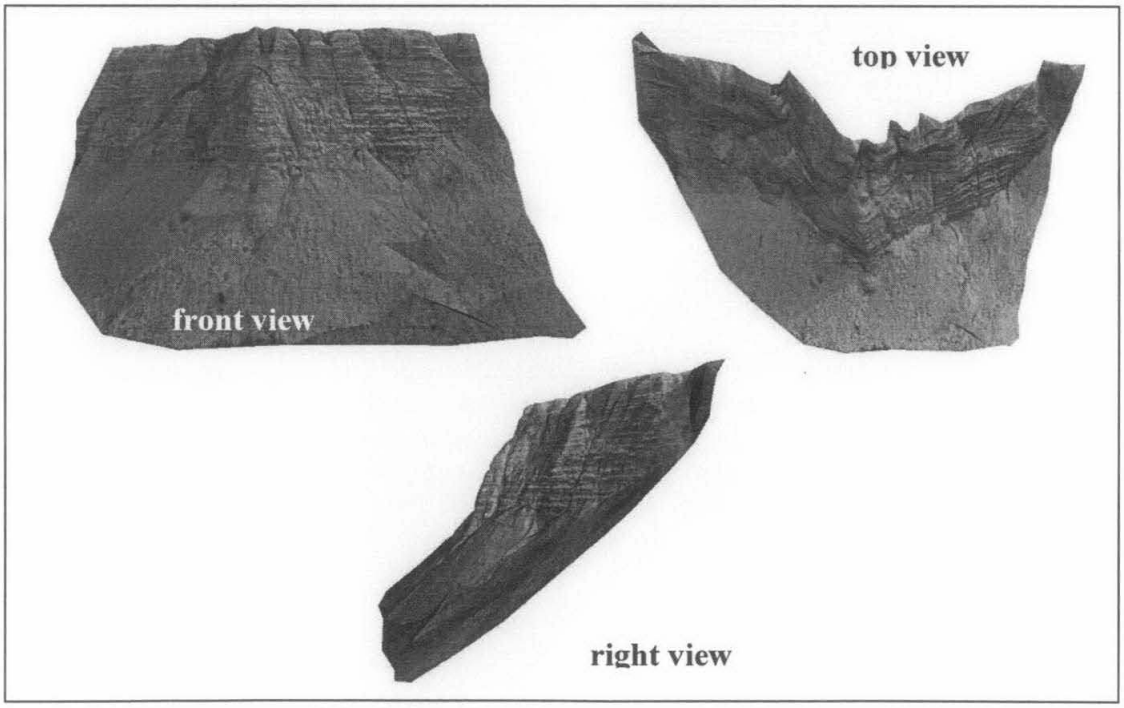

Figure 4.8. 3D stereo model of Area-2 in front, top, and right views, derived based on the stereo overlapping photographs.

Three dimensional stereo model was created after interior and exterior orientation were accomplished. By this model, real condition of observed object at the captured time can be examined virtually, so some applications and analysis can be carried out. Also, based on the created model, terrain data sampling can be selected and then Digital Elevation Model (DEM) of the observed object can be derived after that. An example of the resulted 3D stereo model derived from the stereo photographs was shown on Figure 4.8.

4.5. Selection of the Terrain Data Sampling Points

The constructed 3D stereo model from the previous process cannot automatically become a DEM, without throughout selection of the object sampling point process (that is usually called as a terrain data sampling) and interpolation process. Terrain data sampling points is a selection of the sampling points on stereo model based on interpretation, correlation, or recognition of captured images on the stereo overlapping photographs by using appropriate photogrammetric equipment [55]. Therefore, by this selection, it is not needed to measure and calculate position of all picture elements of the stereo images into 3D ground coordinate system. It is because of the efficiency in storage capacity and accuracy of the derived DEMs.

The terrain data sampling can be achieved by some different photogrammetric techniques, but in this research three different methods were used: regular sampling (Area-1, Area-2, Area-3, and Area-4); progressive sampling (Area-2); and selective sampling (Area-2). Detail of resulted coordinate selected by using those sampling technique were presented on **Appendix E,** while the derived DEMs were given in Figure 4.9, and 4.10.

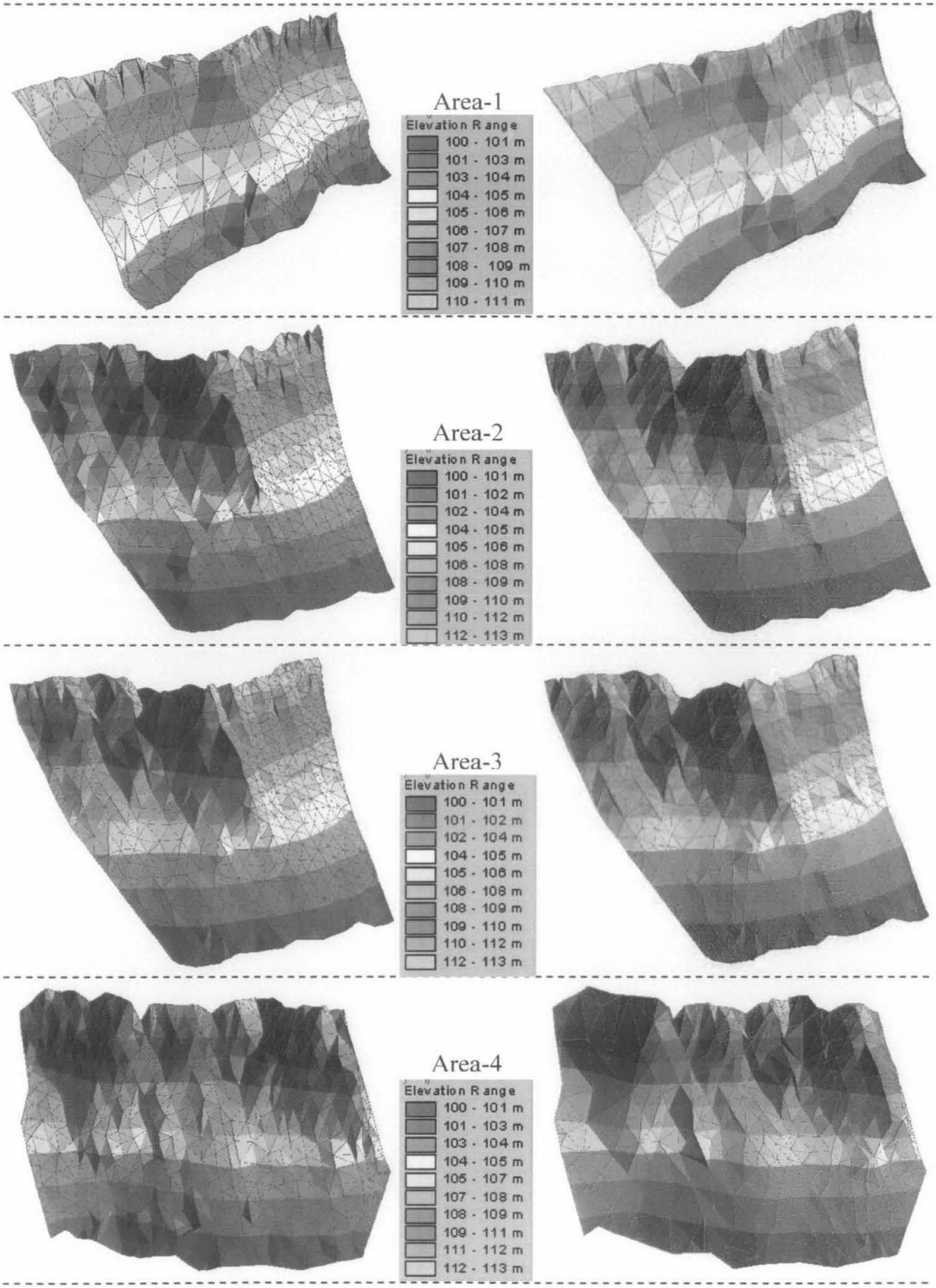

Figure 4.9. Derived DEM generated from total station data (right); and close-range photogrammetric data (left) selected by regular sampling method.

Different way in sampling point selection yields some differences in the resulted DEMs. Effect of the selection is not only on relief surfaces of the DEMs, but also in accuracy and quality of the generated DEMs. Based on the experiment, in a certain topographical condition, increasing of the point density is not significantly affecting the accuracy of DEMs. In other words, it can be said that increasing number of sampling points or point's density cannot be a guarantee for the raising quality of the derived DEMs.

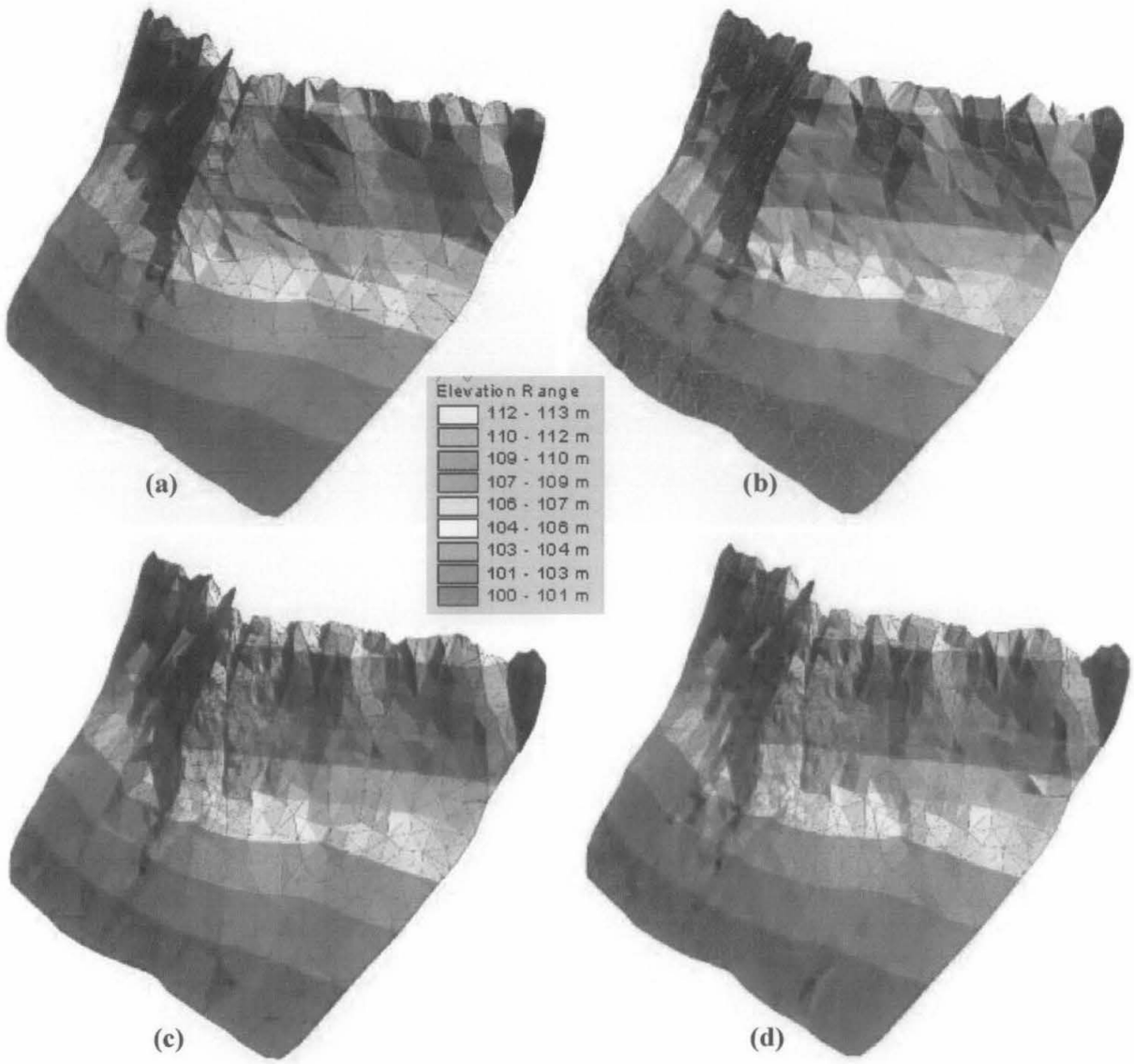

Figure 4.10. A reference DEM of Area-2 derived from total station data (a); and DEMs generated from close-range photogrammetric data in which the sampling points were selected by: regular (b); progressive (c); and selective (d) sampling methods.

4.6. DEM Derivation

The DEMs were derived based on resulted data from the previous processes. Because the data acquisition method used in this research provides sparse points measurement, those DEMs were generated by using Triangular Irregular Network (TIN) interpolation method. It was chosen because of its simplicity, flexibility and also its rapidity in the interpolation process compared to other methods [56]. The triangular modeling is also widespread and extremely popular in virtual reality and in Computer Assisted Design (CAD) systems.

Each study area produced two DEMs, one is a reference DEM derived from Total Station's data and another one is generated from regular sampling point selected from close-range photogrammetric data, as shown on Figure 4.9. Unlike the others, Area-2 produced two additional DEMs, derived from progressive sampling point data and selective sampling point data, as presented on Figure 4.10. First mentioned group of resulted DEMs were used to characterize the photogrammetric method in slope monitoring, while DEMs of Area-2 were used to characterize the correlation between sampling method and accuracy of the DEM.

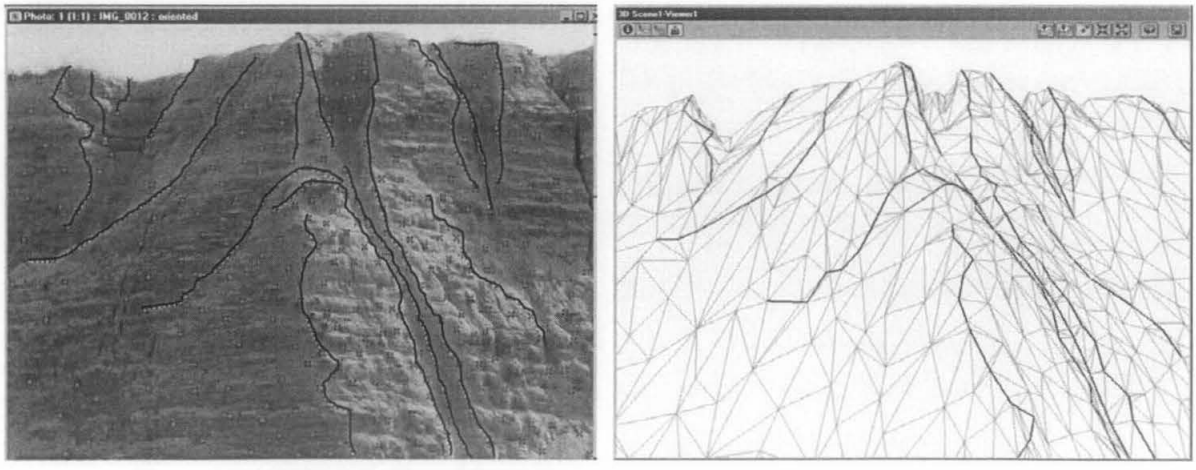

Figure 4.11. Some of digitizing breaklines on the stereo photograph (left); Constructed TIN based on 3D coordinates and breaklines data (right).

In TIN method, the triangles can be constructed from the 3D coordinates of the sampling points to their planimetric components followed by delaunay triangulation criterion. TIN can also be combined with some breaklines, as performed in selective sampling method. In this research, those breaklines were digitized based on features on the stereo photographs, as presented on Figure 4.11. By using the breaklines, the abrupt changes on topographical surfaces can be accommodated, and the TIN can be forced to follow trend of the relief surface as presented on Figure 4.12.

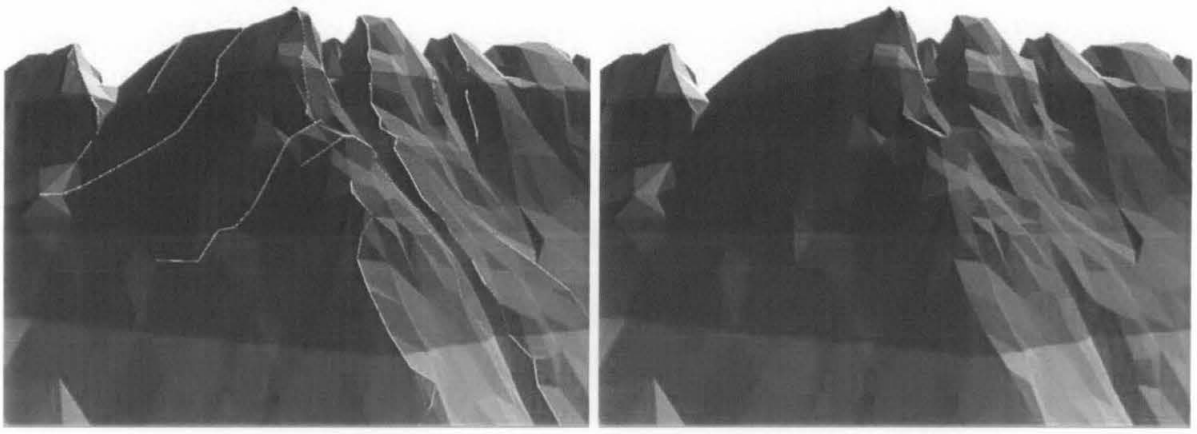

Figure 4.12. Difference results of derived DEM with breaklines (left); and without breaklines (right)

4.7. Quality Measurement of DEM

In order to assess quality of derived DEM, as mentioned in the previous sub-chapter, this thesis used volumetric difference error and elevation interpolation error as the accuracy assessment parameters. Elevation interpolation error was performed by comparison between elevation of some check points and elevation of the resulted DEM derived at the same planimetric position (*X-Z Cartesian's plane*, as mentioned in Chapter 3). Statistical calculations can be carried out for this parameter, because there are several samples (check points) for the derived DEM. Mean error, absolute mean error, and Root Mean Square (RMS) error were the indicators of DEM quality. The mean error indicates randomness of errors, both because of the interpolation calculation process and check

points measurement. The absolute mean error is an indicator of the accuracy in elevation interpolation of the DEM, while RMS error is the best indicator of the distribution of the DEM's height errors.

Volume difference error computes the difference volume between resulted DEM derived from photogrammetric data, compared with reference DEM generated from total station data on the same coverage area. This kind of parameter shows general inaccuracy of resulted DEM obtained by interpolation calculation process and point's measurement, in which both errors significantly affect the quality of DEM. In the process of the DEM quality measurement, volumetric difference error (global method) is more sensitive than elevation interpolation error (local method), but the volumetric difference error cannot be used to detect systematical errors in the sampling points. Therefore it is advisable to use both parameters of DEM quality together [28].

In elevation interpolation error, subjectivity has a larger probability to happen because the calculation was based on comparison elevation of points on the derived DEM with the check points. It means operator can substitute the certain sampling points (which provide larger difference error) with other check points to get a better result in quality assessment process. Consequently the substitution of sampling points will radically change the errors value. Apart from the subjectivity, unwell distribution of sampling points may also occur, so it cannot represent the real relief condition of the slope surface. That was another reason why the elevation interpolation error calculation only (even it has three indicators of accuracy) was not enough to illustrate quality and accuracy of resulted DEM.

Statistical calculation result of the elevation interpolation error for all study areas was given on Table 4.8, but the DEMs used here were derived from regular sampling method only. The derived DEM of Area-2 by using several sampling method data was shown on Table 4.10. Result of Volume difference error calculation was available on Table 4.9, and Table 4.11. Detail about both calculations was presented on **Appendix F**.

Table 4.8. Statistical calculation result of elevation interpolation error for all study areas

Parameters		Area-1	Area-2	Area-3	Area-4
slope angle (%)		57.5 - 60.8	35.8 - 46.7	35.9 - 45.9	39.6 - 45.4
total check points		38	38	38	38
maximum error of positive value (m)		0.132	0.179	0.103	0.177
minimum error of negative value (m)		-0.187	-0.130	-0.194	-0.167
mean error (m)		0.006	-0.010	-0.010	0.035
absolute mean error (m)		0.055	0.047	0.033	0.056
root mean square error	(m)	0.074	0.062	0.051	0.074
	(cm)	7.365	6.200	5.107	7.430

Table 4.9. Statistical calculation result of volume difference error for all study areas

Parameters			Area-1	Area-2	Area-3	Area-4
slope angle (%)			57.5 - 60.8	35.8 - 46.7	35.9 - 45.9	39.6 - 45.4
maximum elevation (m)			110	112	112	112
minimum elevation (m)			101	101	101	101
surface area	derived DEM (m^2)		233.162	354.363	356.026	420.177
	reference DEM (m^2)		226.803	352.568	354.052	415.152
	error	(m^2)	6.359	1.795	1.974	5.025
		(%)	2.804	0.509	0.558	1.210
volume	derived DEM (m^3)		574.404	1276.537	1280.848	1525.806
	reference DEM (m^3)		577.066	1274.915	1279.802	1540.940
	error	(m^3)	2.662	1.622	1.046	15.134
		(%)	0.461	0.127	0.082	0.982

According to the elevation interpolation calculation result as presented on Table 4.8 and Table 4.9, close-range photogrammetric method was able to yield a DEM of steep slope with an accuracy level of below fifteen centimeters in RMS of elevation error, and error in volume of less than one percent. Due to acceptable error in USGS standard, not more than 10% of the check points' errors are exceed one and half of contour interval of the

derived DEM [57], therefore in this research RMS should be below 15 cm (because the interval contour of the DEMs of 10cm).

Area-3 generated the best-quality DEM, while the opposite was for Area-4. If topographical characteristics of both areas were examined carefully, it can be observed that their slope angles were almost the same (39.150 degrees for Area-3 and 41.957 degrees Area 4). However, Area-4 has better relief surfaces than Area-3 (some extremely changes on top and middle parts of the surface, combined with homogeneous surface on the bottom part). Regular sampling method as applied on Table 4.8 and Table 4.9 cannot be used to represent some extremely-changed topographical condition of the slope. That condition can be approached using different sampling method which is able to accommodate those abrupt topographical changes.

Referring to both statistical calculation results, Area-2 and Area-3 are indeed located at the same area, but measurement and image exposure were performed at the different time (Area-3 were measured 330 days after measurement of the Area-2 was accomplished). Accordingly, even though terrestrial survey using the Total Station was carried out from the same stations (using same Temporary Bench Marks), positions of the camera were not like that. Image exposure of Area-3 was performed with closer distance (between camera and observed object) compared to the Area-2. It influenced image spatial resolution for both study areas (spatial resolution of the images on Area-2 was 12.458 mm, while Area-3 was 14.949 mm), images of Area-3 had better quality than images of Area-2. Objects and points recognition were easier to do on images with 12.5 mm resolution than 15 mm.

Based on calculation results are presented on Table 4.10 and 4.11, it can be seen that selective sampling method derived DEM with better quality than other sampling methods. It is due to the capability of selective sampling method to cover some extreme changes on the topographical relief using breaklines. The breaklines can be used to force TIN to follow trend of the relief surface, therefore the abrupt changes on topographical surfaces can be accommodated.

Table 4.10. Calculation result of elevation interpolation error for Area-2 using three different sampling methods

Parameters		Sampling Methods		
		Regular	**Progressive**	**Selective**
total check points		38	38	38
maximum error (m)		0.169	0.115	0.108
minimum error (m)		-0.137	-0.198	-0.125
mean error (m)		-0.012	-0.035	-0.023
absolute mean error (m)		0.048	0.049	0.039
root mean square error	(m)	0.062	0.067	0.053
	(cm)	6.208	6.703	5.299

Table 4.11. Calculation result of volume difference error for Area-2 by using three different sampling methods

Parameters			Sampling Methods		
			Regular	**Progressive**	**Selective**
maximum elevation (m)			112	112	112
minimum elevation (m)			101	101	101
surface area	derived DEM (m^2)		446.859	447.893	448.180
	reference DEM (m^2)		444.469	444.469	444.469
	error	(m^2)	2.390	3.424	3.711
		(%)	0.538	0.770	0.835
volume	derived DEM (m^3)		1570.403	1574.163	1573.016
	reference DEM (m^3)		1568.425	1568.425	1568.425
	error	(m^3)	1.978	5.738	4.591
		(%)	0.126	0.366	0.293

Calculation for study Area-2 was accomplished twice (both for elevation interpolation error and volume difference error calculations) using different number of sampling points and different boundary area. Results of all calculation are shown on Table 4.8 to 4.11, thus those results can be compared each other (Table 4.8 compared to Table 4.10, and also Table 4.9 with Table 4.11). Elevation interpolation error calculation for regular sampling data of Area-2 on Table 4.10 has much more sampling points than Area-2 on Table 4.8, but the results were not significantly different (for mean error, absolute mean error, and also for the RMS error). While in volume difference error calculation Table 4.11 calculated from the bigger coverage area than Table 4.9, but the results were not radically different (in percentage of surface area error, and percentage of volume error). Table 4.12 was provided to compare this condition easily.

Table 4.12. Comparison result for DEM of Area-2, derived from different number of points and coverage area.

Parameters		**Without add. sampling points**	**With additional sampling points**
number of points		361	475
surface area (m^2)		354.363	446.859
point density (points/m^2)		1.018	1.063
elevation interpolation error	mean error (m)	-0.010	-0.012
	abs. mean error (m)	0.047	0.048
	RMS error (m)	0.062	0.062
error of surface area (%)		0.509	0.538
volume error (%)		0.127	0.126

Founded on the research experiments, that some additional sampling points (improving density of the sampling points) caused the increase of the quality of the derived DEM significantly, but until a certain level of point density the increase of the accuracy is not significant. This condition especially occurs in both regular and progressive sampling methods.

Another comparison factor was the consumed time in sampling point's selection for each sampling method. Regular sampling methods spent 4 hours in sampling point's selection process for three stereo overlapping photographs. Sampling point's selection process here consists of point recognition, point selection, and points matching. The other sampling methods need more time in identification of the sampling points, progressive sampling method need 4 hours and 45 minutes, while selective sampling method used 5 hours and 15 minutes.

Selection of the sampling method has significant impact in quality of derived DEM. Based on the calculation, resulted DEM derived from regular sampling method has 6.2 cm accuracy in elevation interpolation, and 0.126 % in volume difference error. DEM derived from progressive sampling method has 6.7 cm and 0.366 % accuracy, while selective sampling method achieved DEM with accuracy of 5.3 cm and 0.293 %. It can be concluded that based on calculation and field verification, if the accuracy is being a concerned matter, selective sampling method is the best method, but when spending time and accuracy is being a considered matter regular sampling method is being the most effective method.

4.8. Mass-movement Detection

As a slope measurement data collection tool, close-range photogrammetry is also able to be used in slope monitoring, especially to detect mass-movement or landslide on the slope surface. Mass-movement can be detected by calculation of DEMs derived from two difference epoch data. In this thesis, because Area-2 and Area-3 were measured on the same coverage area but performed at different time, it can be used to investigate the possibility of the close-range photogrammetric method to be applied in mass-movement detection.

Velocity and direction of the landslide cannot be accurately identified because there was no permanent point on the slope surface. The most possible way to detect the mass-movement is by calculating the DEMs generated from two different epochs data. By this calculation the distribution of mass-movement, and elevation changed on topographical surfaces was able to be modeled. There are two kind of representations used in this work: by using 3D spatial calculation of overlaying DEMs, and profiling along cross-section and longitudinal-section direction.

In cross sections modeling and longitudinal profiling, elevation from certain points laid on a straight line from both DEMs was modeled in a chart, as shown in Figure 4.15, while position of the straight lines (profiles) was presented in Figure 4.14. Shifting on elevation of the slope surface indicates that there was a landslide on the slope area. Therefore, based on differences in elevations, thickness of gain-loss soil can be examined. Mass-movement and distribution of gain and loss areas can be recognized easily by overlaying both DEMs, than calculated using a simple subtraction process in spatial analyst of ArcView software, as presented in Figure 4.13.

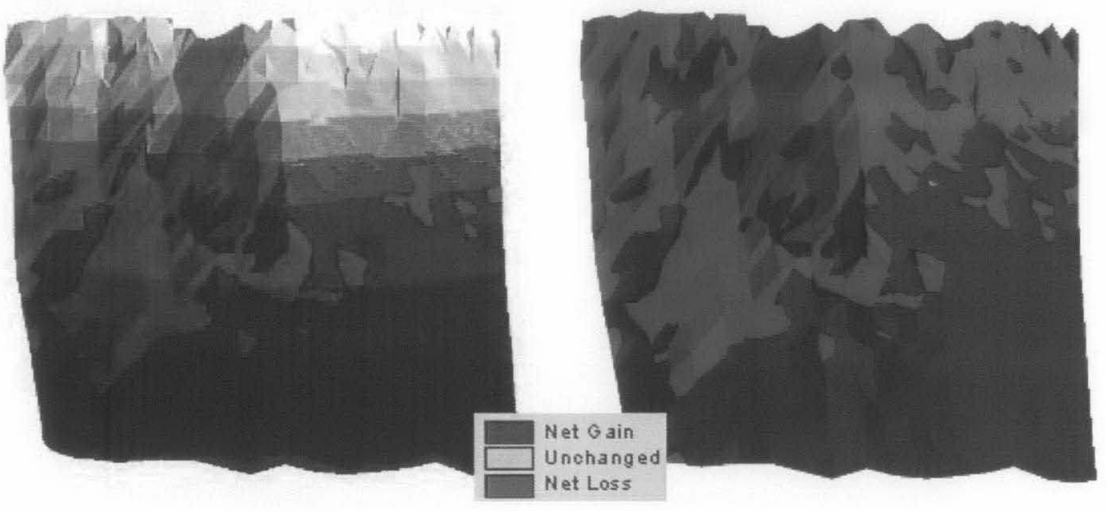

Figure 4.13. The left picture presents overlaying between DEMs of epoch 1 (red graduation) and epoch 2 (blue graduation). Right picture presents the distribution of loss and gain of soil on the slope.

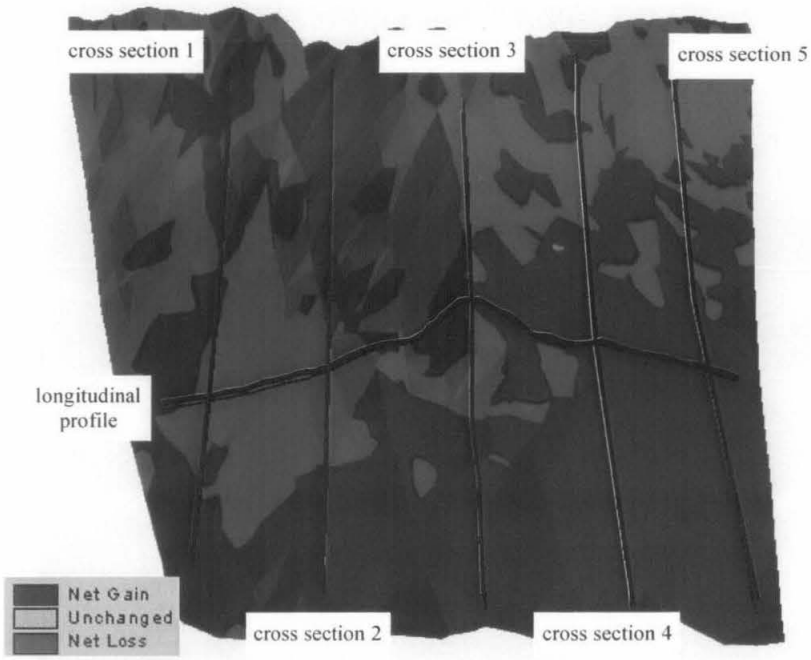

Figure 4.14. Position of the longitudinal profile and cross sections laying on gain-loss soil distribution (in 3D view)

From the pictures presented in Figure 4.15, we can see that during period of 13/05/2007 to 07/04/2008 (330 days) there was a mass movement from top side of the slope moving downward. The blue color (gain) means that there was increasing value of elevation, and also volume of the soil. Meanwhile, the red color (loss) indicates decreasing of the elevation and reducing volume of the soil as well. Volume for the biggest gain area was 19.945 m^3, while volume for the biggest loss area was -24.088 m^3. Details of volume estimation result for loss and gain soils were given on **Appendix G**. Based on the elevation changes on the profiling together with volume estimation of the loss and gain areas, it can be said that the observed slope is categorized in a non-critical slope.

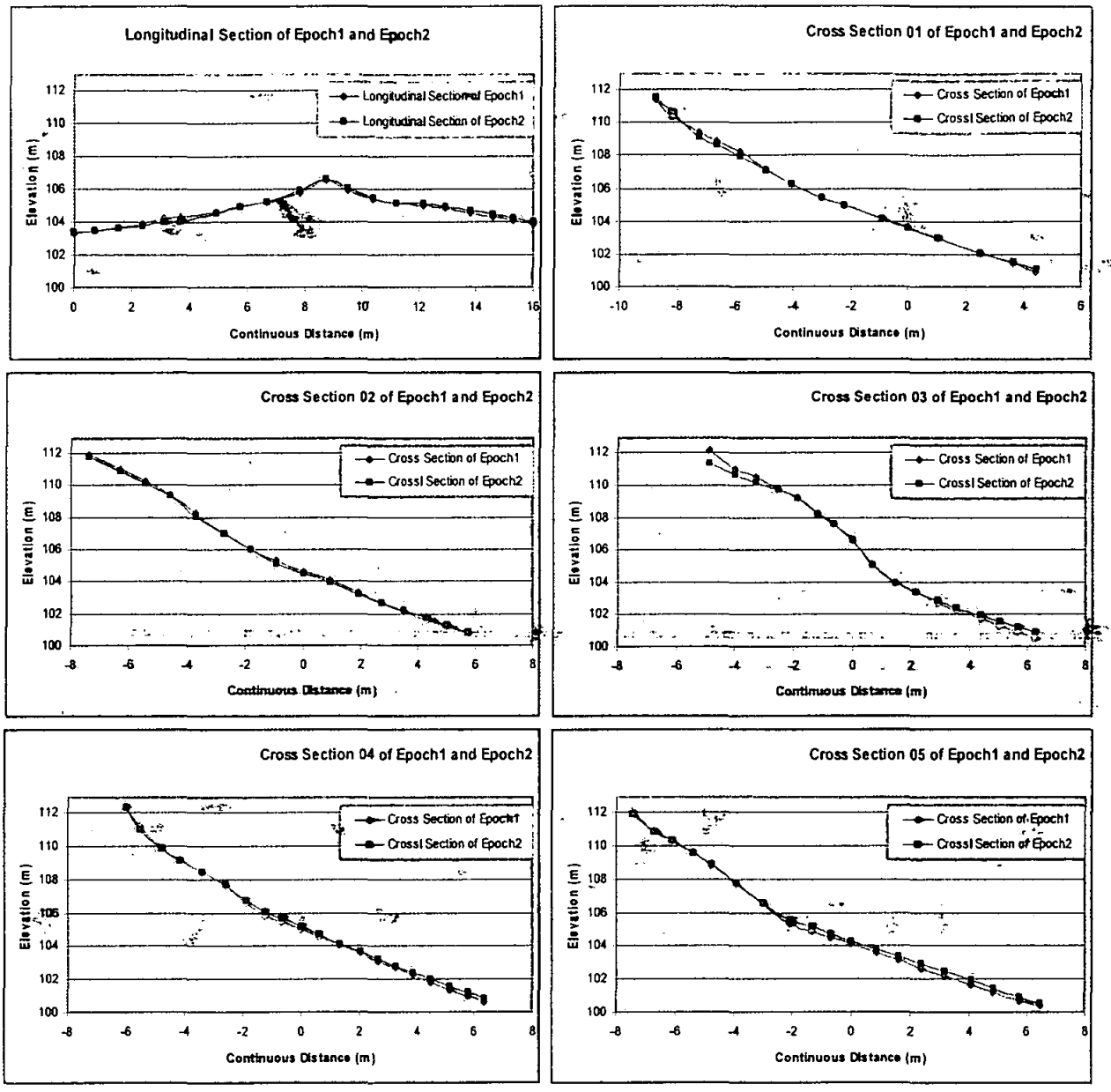

Figure 4.15. Cross and longitudinal profile of the slopes, to indicate change of elevation

What has been discussed in this sub-chapter was constrained for detection of mass-movement on unstable steep slope area, and also volumetric approximation of gain and loss soils on the observed area. Elevation changes were detected by profiling cross-section and longitudinal-section on the derived DEMS. While mass-movement detection

(included defining loss-gain area and volume estimation) was achieved by following spatial calculation of overlaying DEMs. Precise mass-movement monitoring completed with calculation of velocity, direction, and accuracy of the mass-movements is impossible to be performed. It is because of no permanent points (bench-marks) on the observed steep slope area. However, it is the most possible way that can be carried out over an inaccessible steep slope area. The difficulty to define velocity and direction of the landslide due to no permanent points on the slope surface (as mentioned in the previous sentences) is not only occurred in close-range photogrammetric technique, but also in other data collection tools such as: reflector-less total station, terrestrial laser scanner, and ground based radar.

CHAPTER 5

CONCLUSIONS AND RECOMMENDATIONS

5.1. Conclusions

The method presented in this study is based on experimentation of 3D modeling applied for inaccessible steep slope area by means of close-range photogrammetry technique as a DEM data collection tools. Accuracy assessment were carried out by comparing the derived DEM with a reference DEM generated from set of correct data measured by using calibrated reflector-less total station.

Calibration of the main instruments (camera and reflector-less Total Station) used in this technique is absolutely needed to get correction values of systematical errors. Calibration of the reflector-less Total Station obtained correction value of zero-error (acquired by incorrect of reflective signal), as well as scaling factor and constant value of the Total Station (both values show accuracy of the device to get the appropriate data) in distance measurement. Calibration of the camera yield value of radial and tangential error caused by lens's distortion, in which value of both distortions required in image refinement on interior orientation process.

Result of the experiment proves that close-range photogrammetry technique can be used as a high accurately DEM data collection tool. The method is able to be applied in 3D modeling of the unstable steep slope area, with level of accuracy is below than fifteen centimeters in RMS of elevation error and error in volume is less than one percent. Area-1 is a representative of homogeneous relief condition with slope angle of 57.5°-60.8° yielded DEM with 7.365 cm in RMS of elevation error and 0.461 % in volume error. Area-2 has a medium relief slope with slope angle of 35.8°-46.7°, generated DEM with elevation error of 6.200 cm and error in volume is 0.127 %. Area-3 derived DEM with

accuracy in elevation of 5.107 cm and 0.082 % in volume error, topographical condition of this area is medium with slope angle of 35.9°-45.9°. While Area-4 represents a heterogeneous slope with 39.6°-45.4° slope angle, produced DEM with 7.430 cm in RMS of elevation error and 0.982 % error in volume.

According to the experiments the following are observed. It was observed that there was no direct correlation between topographical relief condition and accuracy of the generated DEM. Quality of the derived DEM is only significantly influenced by:

i. Selection of sampling method;
ii. Distance between the camera to the observed objects;
iii. Setting of focal length of the camera;
iv. Density of sampling points.

Increasing density of the sampling points (if number of the sampling point was increased) caused the quality of the derived DEM improved radically, but until a certain level of point density the improvement of DEM's accuracy is not significant. Another factor to be noted was difference setting of focal length and distance between observed objects to the camera influenced the quality of captured images, and of course drastically affected the accuracy of the generated DEM.

All characteristics of topographical relief on slope surface can be presented well by a certain sampling method, in which selection of the sampling method significantly affects the quality of the derived DEM. Regular sampling method spent 4 hours in selection of sampling points, and yielded DEM with RMS of elevation error of 6.208 cm and error in volume of 0.126 %. Progressive sampling method needs 45 minutes more than regular one, and generated DEM with 6.703 cm in elevation's RMS error and 0.366 % in volume difference error. Selective sampling method derived best quality DEM (5.299 cm RMS elevation error and 0.293 % in volume error), but spent longer time in point selection (5 hours and 15 minutes). If the accuracy is the main concern, selective sampling method is the best method. When time spent and accuracy are the concern, regular sampling method is the most effective method. Because it needs shortest time in point's selection and the

accuracy of the resulted DEM is not significantly different compared with selective sampling method.

The technique performed in this thesis is also able to be used in slope monitoring, especially to detect mass movement or landslide on the slope surface. Mass movement can be detected by calculation of DEMs derived from two difference epoch data, measured on the same location. However since there is no permanent points on the slope surface, velocity and direction of the landslide cannot be accurately identified, but distribution of mass movement and elevation changed on the slope surfaces can be modeled by spatial calculation of overlaying DEMs together with profiling of cross-section and longitudinal-section of the generated DEMs.

Limitation of this technique is it requires measurement of several GCPs (which their positions can be recognized clearly on the stereo photographs), in order to define exterior orientation parameters of the cameras. It will be an independent mapping technique if the camera used in this research is a stationery camera, in which all interior and exterior parameters of the cameras are known and fixed (at least there are three cameras observe to the same object). Therefore real time DEM of the observed object can be derived anytime from the overlapping photographs. Another limitation is it spends more time in data processing compare to other DEM data collection techniques, especially in point recognition and sampling point selection processes.

5.2. Recommendations and Future Works

Further studies of applying close-range photogrammetry for larger slope area prone to landslide such as Cameron Highland, Malaysia needs to be carried out. It will be an interesting work, since the images of the unstable slope could be captured by using a difference sheaf of the camera's lenses (by using wide-lens or tele-lens) that might offer higher productivity. However, it needs to be highlighted that applying this method by using wide-lens or tele-lens will provide a better quality of slope images.

The application of close-range photogrammetry in slope monitoring data collection tool on a certain area which has some permanent control points is recommended, since velocity and direction of the mass-movements can be accurately recognized. Different view of capturing angles such as from top side of the slope by using balloon or helicopter is very interesting to be investigated.

References

1. Kasser, M., Egels, Y., 2002, *Digital Photogrammetry*, Taylor & Francis Group, New York.
2. Kraus, K., Briese, C., Attwenger, M., Pfiefer, N., 2004, *Quality Measures for Digital Terrain Models...*
3. Wolf, P.R., Dewitt, B.A., 2000, *Element of Photogrammetry with Application in GIS,* Mc Graw Hill, Singapore.
4. Atkinson, K.B., 2001, *Close Range Photogrammetry and Machine Vision,* Whittles Publishing, Scotland.
5. Hanke, K., Grussenmeyer, C.P., 2002, *Architectural Photogrammetry: Basic Theory, procedures, Tools*, ISPRS Commission 5 Tutorial,
6. Wolf, P.R., Ghilani, C.D., 2006, *Elementary Surveying: An Introduction to Geomatics*, eleventh edition, Pearson Prentice Hall, Upper Saddle River – New Jersey.
7. Ortigao, J.A.R., Sayao, A.S., 2004, *Handbook of Slope Stabilisation*, Springer-Verlag Berlin Heidelberg, New York
8. Anonymous, 2006, *Slope Instability Hazard Assessment, Samoa Islands*, Ministry of Natural Resources, Environment, and Meteorology of Samoa Islands, http://www.mnre.gov.ws/projects/siam-/documents/C4%20Component/NATURAL%20RISK%20MANAGEMENT/Slope%20Instability%20Hazard%20Assessment%20Report.pdf
9. GCO, 1984, *Geotechnical Manual for Slopes,* Geotechnical Control Office, Hong Kong.
10. Duncan, J.M., Buchignani, A.L., 1975, *An Engineering Manual for Slope Stability Studies,* Dept. of Civil Engineering, University of California, Berkeley
11. Vernes, D.J., 1978, *Slope Movement Types and Processes.* In: Schuster, R.L., and Krizek, R.J., *Landslide – Analysis and Control, Transportation Research Board Special Report 176,* National Academy of Science, Washington D.C. p. 12-33
12. Walstra, J., 2006, *Historical Aerial Photographs and Digital Photogrammetry for Landslide Assessment*, Ph.D. Thesis, Loughborough University.

13. Highland, L., 2004, *Landslide Types and Processes*, education information section of the U.S. Geological Survey Landslide Program, http://pubs.usgs.gov/fs/2004/3072/pdf/fs2004-3072.pdf
14. Forward, T.A., 2002, *Quasi-Continuous GPS Steep Slope Monitoring: A Multi-Antenna Array Approach, Chapter-2 Deformation Monitoring of Steep Slopes*, Ph.D. Thesis, p. 8-27, http://adt.curtin.edu.au/theses/available/adt-WCU20021025.152012/ unrestricted/03**chapter2**.pdf
15. Yilmaz, H.M., and Yakar, M., 2008, *Computing of Volume of Excavation Areas by Digital Close Range Photogrammetry*, The Arabian Journal for Science and Engineering, vol. 33, p. 63-79
16. Li, Z., Zhu, Q. and Gold, C., 2005, *Digital Terrain Modelling: Principles and Methodology*, CRC Press, Washington
17. Gili, J.A., Corominas, J., Rius, J., 2000, *Using Global Positioning System Techniques in Landslide Monitoring*, Journal of Engineering Geology, vol. 55, p. 167-192, www.elsevier.nl/locate/enggeo
18. Baldi, P., Fabris, M., Marsella, M., Monticelli, R., 2005, *Monitoring the Morphological Evolution of the Sciara del Fuoco during the 2002-2003 Stromboli Eruption using Multi-temporal Photogrammetry*, ISPRS Journal of Photogrammetry & Remote Sensing, vol. 59, p. 199-211, www.elsivier.com/locate/isprsjprs
19. Tsutsui, Ken, Rukogawa, S., Nakagawa, H., Miyazaki, S., Cheng, C.T., Shiraishi, T., Yang, S.D., 2007, *Detection and Volume Estimation of Large-scale Landslides based on Elevation-change Analysis using DEMs Extracted from High-resolution Satellite Stereo Imagery*, IEEE Transaction on Geoscience and Remote Sensing, vol. 45, p. 1681-1694, http://ieeexplore.ieee.org
20. Barbarella, M., Lenzi, V., Zanni, M., 2004, *Integration of Airborne Laser Data and High Resolution Satellite Images over Landslides Risk Areas*,
21. Kasser, M., Egels, Y., 2002, *Digital Photogrammetry*, Taylor & Francis Group, New York.
22. Rottensteiner, D.I.F., 2001, *Semi-automatic Extraction of Buildings Based on Hybrid Adjustment using 3D Surface Models and Management of Building Data in*

a TIS, Ph.D. Thesis, Vienna University of Technology, www.ipf.tuwien.ac.at\ fr\buildings\ diss\index.html

23. Petrie, G., Kennie, T., 1987, *An Introduction to Terrain Modelling: Applications and Terminology.* In Li, Z., Zhu, Q. and Gold, C., 2005, *Digital Terrain Modelling: Principles and Methodology*, CRC Press, Washington
24. Grussenmeyer, P., Hanke, K., Streilein, 2002, *Architectural Photogrammetry*, in Kasser, M., Egels, Y., 2002, *Digital Photogrammetry, chapter 4: Metrologic Application of Digital Photogrammetry*, p. 300-339, Taylor & Francis Group, New York.
25. Behan, A., Moss, R., 2006, *Close Range Photogrammetric Measurement and 3D Modeling for Irish Medieval Architectural Studies*, The 7th international Symposium on Virtual Reality, Archeology and Cultural Heritage VAST, The Eurographics Association
26. Weibel, R. and Heller, M., 1991. *Digital terrain modelling*, in Maguire, D.J., Goodchild, M.F., and Rhind, D.W., 1991. *Geographical Information Systems: Principles and Applications*, Longman Scientific & Technical, England
27. Renzo, C., 2000, *Archaeological Representation with Augmented Reality based on GIS/DEM contexts - Part 1: General introduction to DEM*, D09 Prospects of Augmented Reality in European Cultural Heritage Sites, p. 59-69,
28. Meneses, A.S., Chasco, F.R., Garcia, B., Caberas, J., Audicana, M.G., 2005, *Quality Control in Digital Terrain Models*, Journal of Surveying Engineering ASCE, vol. 131, p. 118-124
29. Fryer, J.G., 2001, *Camera Calibration*, in Atkinson, K.B., 2001, *Close Range Photogrammetry and Machine Vision,* Whittles Publishing, Scotland
30. Heikkila, J., Silven, O., 1997, A Four Step Camera Calibration Procedure within Implicit Image Correction, http://www.vision.caltech.edu/bouguetj/calib_doc/ papers/ heikkila97.pdf
31. Brown, D.C., 1971, *Close Range Camera Calibration*, www.ifp.uni-stuttgart.dezSzlehrezSzvorlesungenzSzAerozSzBrown71.pdf/close-range-camera-calibration.pdf

32. Ley, R, 1986, *Accuracy assessment of digital terrain models*, Auto-carto London, vol.1, p.455-464
33. Yanalak, M., Baykal, O., 2003, *Digital Elevation Model Based Volume Calculations using Topographical Data*, Journal of Surveying Engineering ASCE, vol. 129, p. 56-64
34. Heikkila, J. and Silven, O., 1997, *A Four Step Camera Calibration Procedure within Implicit Image Correction*, InfoTech Oulu and Department of Electrical Engineering University of Oulu, http://www.vision.caltech.edu/bouguetj/calibdoc/papers/ heikkila97.pdf.
35. Beraldin, J.A., Guidi, G., Ciofi, S., Atzeni, C., 2002, *Improvement of Metric Accuracy of Digital 3D Models through Digital Photogrammetry. A Case Study: Donatello's Maddalena*, National Research Council of Canada, Ottawa.
36. Ji, Q., Zhang, Y., 2001, *Camera Calibration with Genetic Algorithms*, IEEE Transaction on System, Man, and Cybernetics, Part A: System and Humans, vol. 31., p. 120-130, http://www.ecse.rpi.edu/homepages/qji/Papers/genetic_calib_smc.pdf.
37. Meneses, A.S., Chasco, F.R., Garcia, B., Caberas, J., Audicana, M.G., 2005, *Quality Control in Digital Terrain Models*, Journal of Surveying Engineering ASCE, vol. 131, No. 4, p. 118-124.
38. Ray, S.F., 1999, *Scientific Photography and Applied Imaging*, first edition, Focal Press, Oxford.
39. Anonymous, 2005, *PhotoModeler Pro version 5.2.3 Tutorials*, EOS Systems Inc., Vancouver.
40. Gomes, C.J.M., Prado, W.S., Erwes, H., Koatz, G.D., 1999, *A Photogrammetric Project in Brazil: the Use of the PhotoModeler Software*, http://cipa.icomos.org/fileadmin/papers/olinda/99c313.pdf.
41. Wolf, P.R. and Ghilani, C.D., 2006, *Adjustment Computation Spatial Data Analysis*, fourth edition, John Wiley & Sons, Inc., New Jersey.
42. Hanke, K., Grussenmeyer, C.P., 2002, *Architectural Photogrammetry: Basic Theory, procedures, Tools*, ISPRS Commission 5 Tutorial.

43. Jensen, J.R., 1996, *Introductory Digital Image Processing – A Remote Sensing Perspective*, second edition, Prentice Hall Inc., New York.
44. Rebecca, O.C., Gold, C. and Kidner, D., 2006, *An Original Way of Building a TIN with Complex Urban Structures*, ISPRS Technical Commission VI, WG VI/4, Turkey.
45. Anonymous, 2005, *ArcGIS Desktop Tutorials*, Environmental System Research Institute (ESRI) Inc., New York.
46. Anonymous, 2002, *ArcView GIS version 3.2.a Tutorials*, Environmental System Research Institute (ESRI) Inc., New York.
47. Pflipsen, B., 2006, *Volume Computation - A Comparison of Total Station versus Laser Scanner and Different Software*, Master Thesis.
48. Ray, S.F., 1999, *Scientific Photography and Applied Imaging*, first edition, Focal Press, Oxford.
49. Behrens, A., Lasseur, C., Mergelkuhl, D., 2004, *New Developments in Close Range Photogrammetry Applied to Large Physics Detectors*, http://www.slac.stanford.edu/econf/C04100411/papers/019.PDF
50. Kavanagh B.F., 2003, Surveying Principles and Applications, sixth edition, Prentice Hall, New Jersey.
51. Atkinson, K.B., 1999, *Theory of Close Range Photogrammetry*, http://www.lems.brown.edu/vision/people/leymarie/Refs/Photogrammetry.html
52. Zhang Z., A Flexible New Technique for Camera Calibration, 1998. http://research.microsoft.com/ %7Ezhang/Papers/TR98-71.pdf
53. Anonymous, 2008, *Calibration of Electronic Distance Measurement Instruments*, Landgate, Government of West Australia, www.landgate.wa.gov.au
54. Anonymous, 2007, *Pulse Total Station GPT3000 N/LN series: Specification*, Topcon Corporation, www.topcon.co.jp
55. Ormsby, T., 2004, *Getting to Know ArcGIS Desktop*, ESRI Press, California.
56. Yang, C.S., Kao, S.P., Lee, F.B., Hung, P.S., 2004, *Twelve Different Interpolation Methods: A Case Study of Surfer 8.0*,
57. Anonymous, 1998, United States National Mapping Accuracy Standard, http://www.rockyweb.cr.usgs.gov/nmpstds/acrodocs/nmas/NMAS647.PDF

58. Cahyono, B.K., Zahid, M.A., Widjajanti, N., Matori. A.N., 2008, *Calibration of Reflector-less Total Station for Various Material Targets*, Proceeding of International Symposium and Exhibition on Geoinformation

59. Cahyono, B.K., Matori, A.N., Atunggal, D.A., Basith, A., 2008, *Correlation of Sampling Method and Quality in DEM Generation by Using Close-Range Photogrammetric Data*, Proceeding of International Symposium and Exhibition on Geoinformation

60. Cahyono, B.K., Matori, A.N., 2008, *Characterizing Accuracy of DEM Derived from Close-Range Photogrammtetric Data*, Proceeding of National Postgraduate Conference

61. Cahyono, B.K., Matori, A.N., Atunggal, D.A., Basith, A., 2008, *Derivation 3D Model of Instable Open Slope Area from 2D Photographs Using Commercial Pocket Camera*, International Conference of Concrete and Building Technology 2008

Appendix A

Cross-sections Profiling for Area-1

cross-1	elevation	distance
	101.853	0
	102.124	0.598
	102.695	1.196
	104.874	1.794
	106.164	2.392
	107.296	2.99
	108.395	3.588
	109.133	4.186
	109.747	4.784
	110.682	5.382

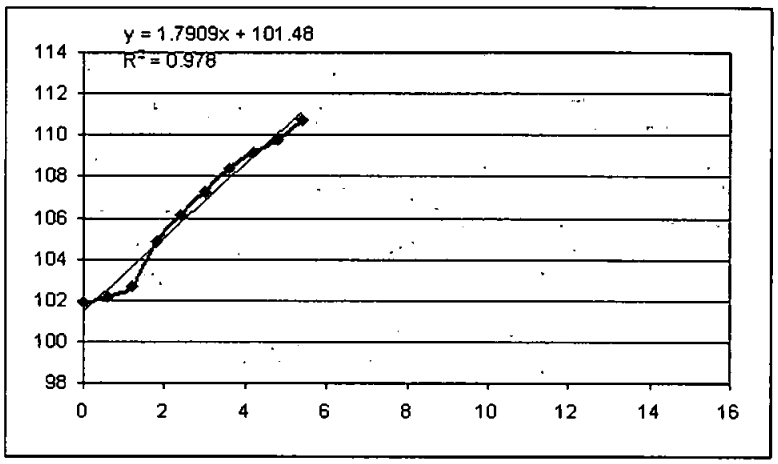

slope-1 58.634 degree

gradient 1.7909 slope 60.822 degree

cross-2	elevation	distance
	101.877	0
	102.309	0.659
	103.827	1.318
	105.05	1.977
	105.81	2.636
	106.589	3.295
	107.488	3.954
	108.911	4.613
	110.209	5.272

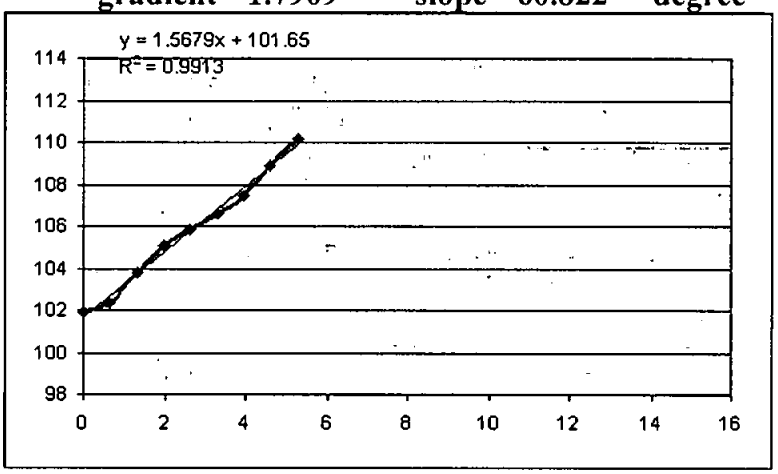

slope-2 57.677 degree

gradient 1.5679 slope 57.470 degree

cross-3	elevation	distance
	101.269	0
	101.757	0.658
	103.204	1.316
	104.698	1.974
	105.59	2.632
	106.452	3.29
	107.371	3.948
	108.296	4.606
	110.123	5.264

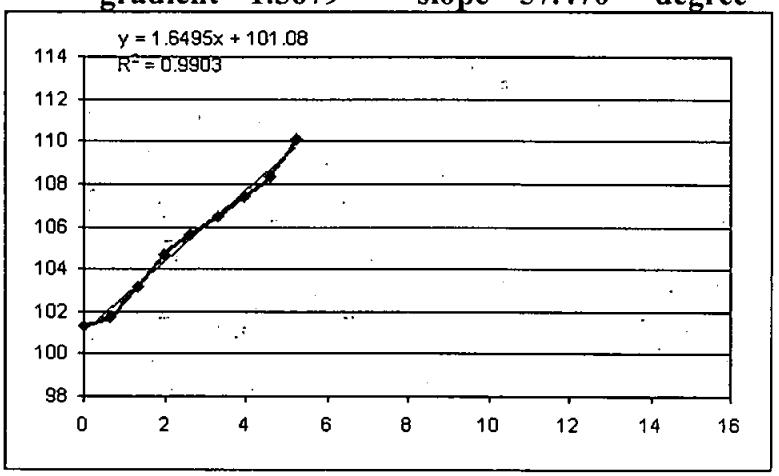

slope-3 59.267 degree

gradient 1.6495 slope 58.774 degree

cross-4	elevation	distance
	101.323	0
	101.745	0.72
	103.572	1.44
	104.564	2.16
	105.462	2.88
	106.663	3.6
	108.063	4.32
	109.723	5.04

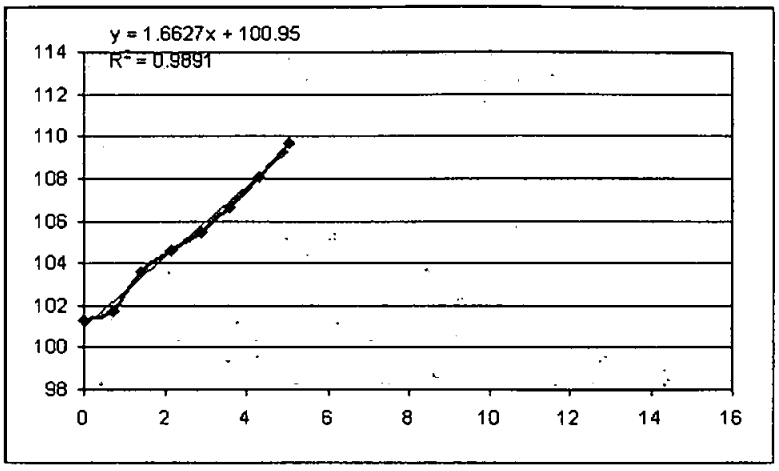

slope-4 59.036 degree **gradient 1.6627 slope 58.976 degree**

cross-5	elevation	distance
	100.545	0
	100.924	0.718
	101.324	1.436
	102.453	2.154
	104.559	2.872
	105.286	3.59
	106.378	4.308
	107.849	5.026
	109.605	5.744

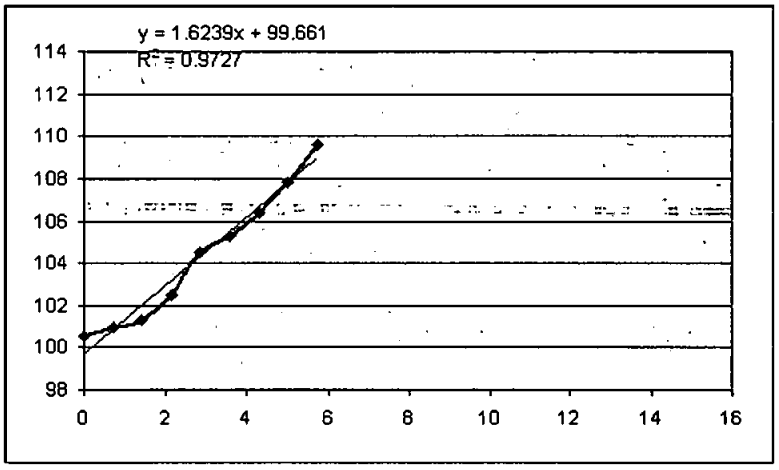

slope-5 57.625 degree **gradient 1.6239 slope 58.375 degree**

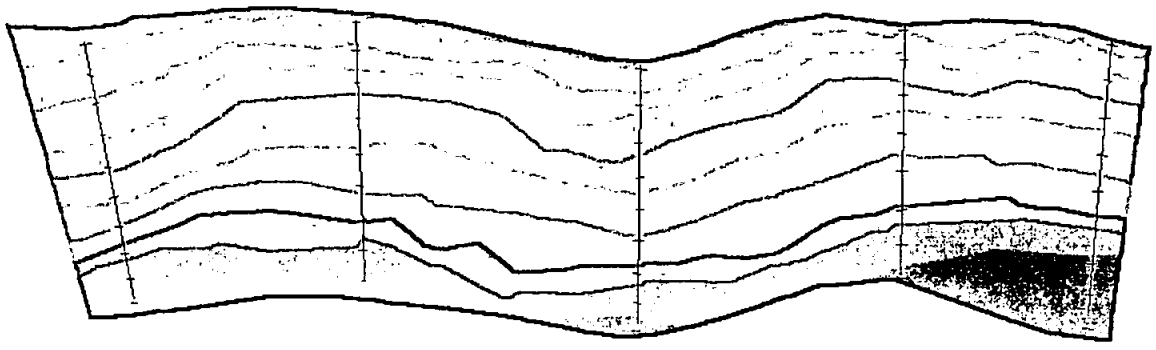

Location of cross-sections 1 to 5 (in left to right direction) on Area-2

Cross-sections Profiling for Area-2

cross-1	elevation	distance
	100.127	0
	100.814	1.219
	101.405	2.438
	101.992	3.657
	102.706	4.876
	103.41	6.095
	104.157	7.314
	104.941	8.533
	105.703	9.752
	106.423	10.971
	107.741	12.19
	108.998	13.409
	110.815	14.628
	112.09	15.847

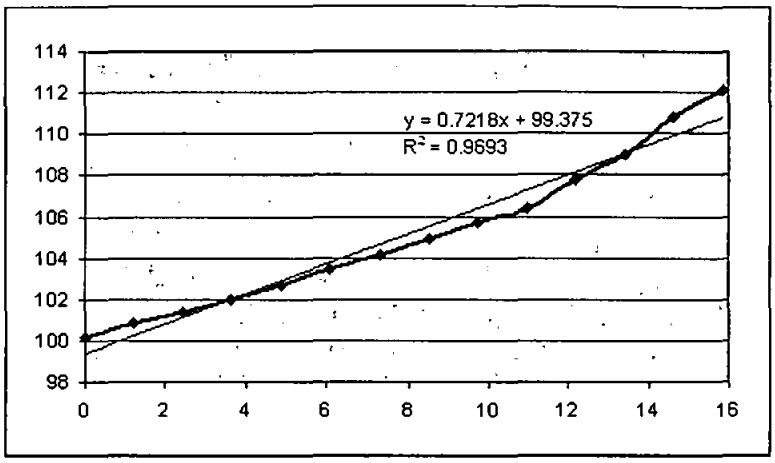

slope-1 37.049 degree **gradient 0.7218 slope 35.822 degree**

cross-2	elevation	distance
	100.319	0
	100.904	1.123
	101.572	2.246
	102.313	3.369
	103.091	4.492
	103.833	5.615
	104.49	6.738
	105.19	7.861
	106.092	8.984
	107.032	10.107
	108.984	11.23
	109.832	12.353
	110.117	13.476
	112.05	14.599

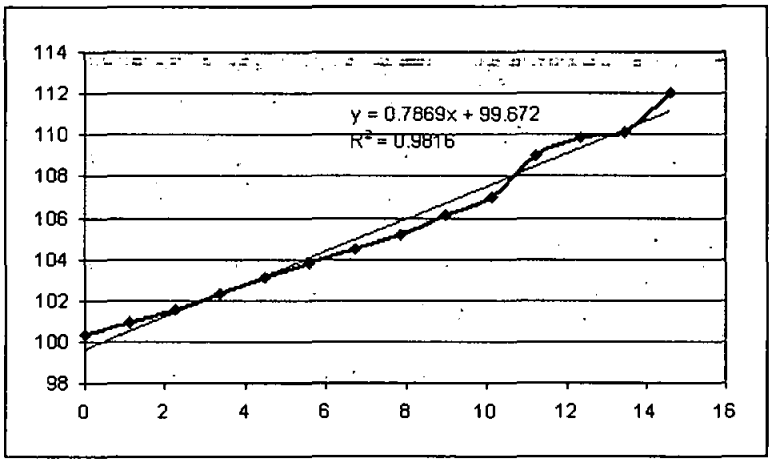

slope-2 38.784 degree **gradient 0.7869 slope 38.199 degree**

cross-3	elevation	distance
	100.097	0
	100.882	1.189
	101.641	2.378
	102.527	3.567
	103.391	4.756
	105.184	5.945
	107.172	7.134
	108.462	8.323
	109.826	9.512
	110.53	10.701
	112.144	11.89
slope-3	45.376	degree

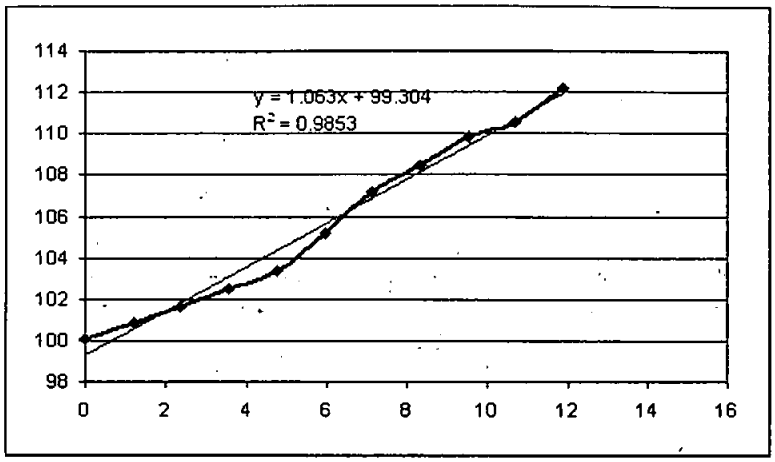

gradient 1.063 slope 46.749 degree

cross-4	elevation	distance
	100.298	0
	101.069	1.186
	101.801	2.372
	102.735	3.558
	103.448	4.744
	104.218	5.93
	105.003	7.116
	105.887	8.302
	107.533	9.488
	108.7	10.674
	110.41	11.86
	112.218	13.046
slope-4	42.418	degree

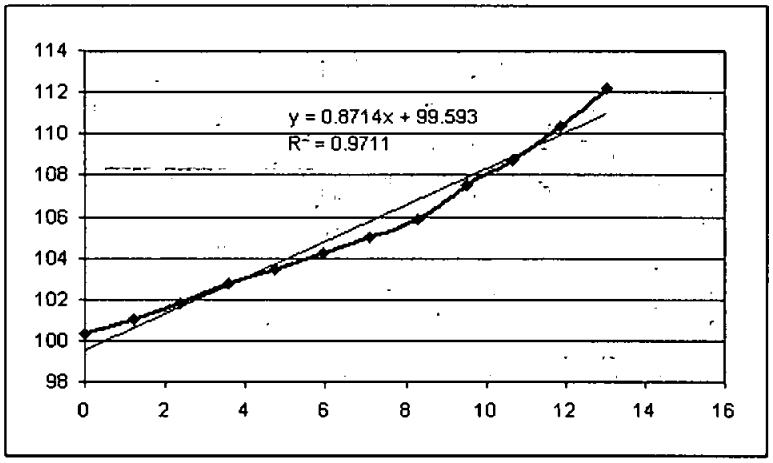

gradient 0.8714 slope 41.069 degree

cross-5	elevation	distance
	99.975	0
	100.297	1.126
	100.729	2.252
	101.343	3.378
	101.975	4.504
	102.633	5.63
	103.245	6.756
	103.767	7.882
	104.466	9.008
	105.323	10.134
	106.564	11.26
	107.855	12.386
	108.799	13.512
	110.607	14.638
	112.511	15.764

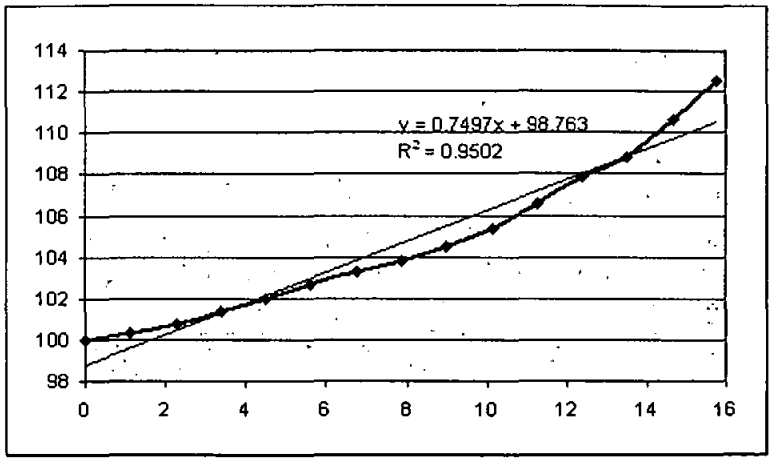

slope-5 38.493 degree **gradient 0.7497 slope 36.859 degree**

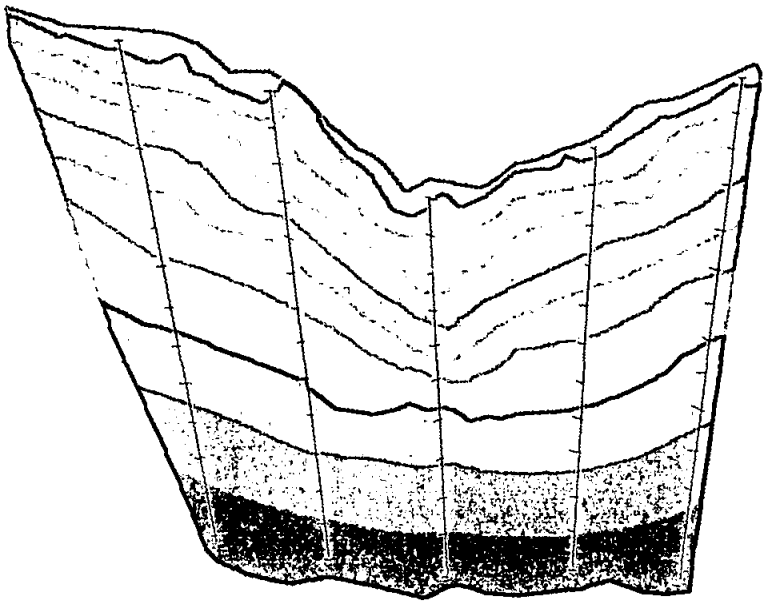

Location of cross-sections 1 to 5 (in left to right direction) on Area-2

Cross-sections Profiling for Area-3

cross-1	elevation	distance
	100.324	0
	100.983	1.219
	101.512	2.438
	102.149	3.657
	102.855	4.876
	103.581	6.095
	104.354	7.314
	105.068	8.533
	105.821	9.752
	106.677	10.971
	107.712	12.19
	109.169	13.409
	111.235	14.628
	112.387	15.847

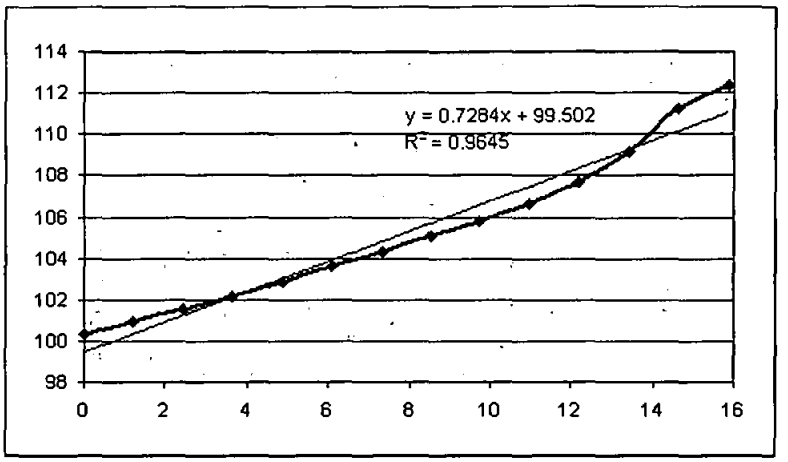

slope-1 37.279 degree **gradient 0.7284 slope 36.070 degree**

cross-2	elevation	distance
	100.403	0
	101.043	1.123
	101.584	2.246
	102.335	3.369
	103.107	4.492
	103.746	5.615
	104.464	6.738
	105.254	7.861
	106.057	8.984
	107.406	10.107
	108.735	11.23
	109.583	12.353
	110.409	13.476
	111.396	14.599

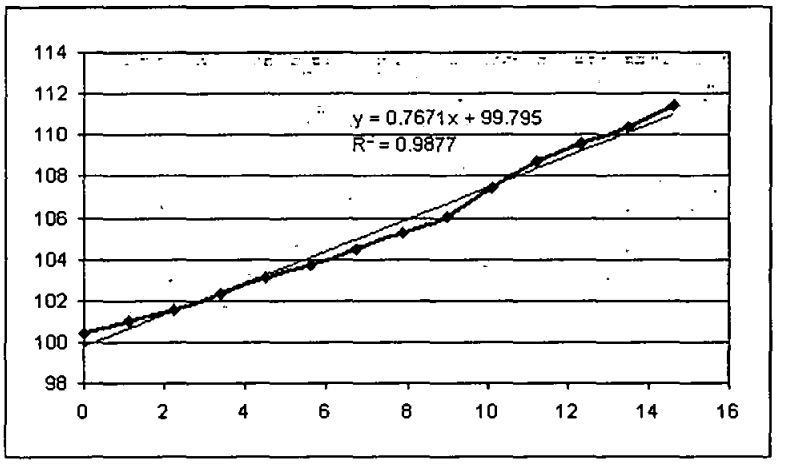

slope-2 36.980 degree **gradient 0.7671 slope 37.492 degree**

cross-3	elevation	distance
	100.458	0
	101.052	1.189
	101.702	2.378
	102.502	3.567
	103.389	4.756
	105.156	5.945
	106.992	7.134
	108.404	8.323
	109.59	9.512
	110.51	10.701
	112.11	11.89

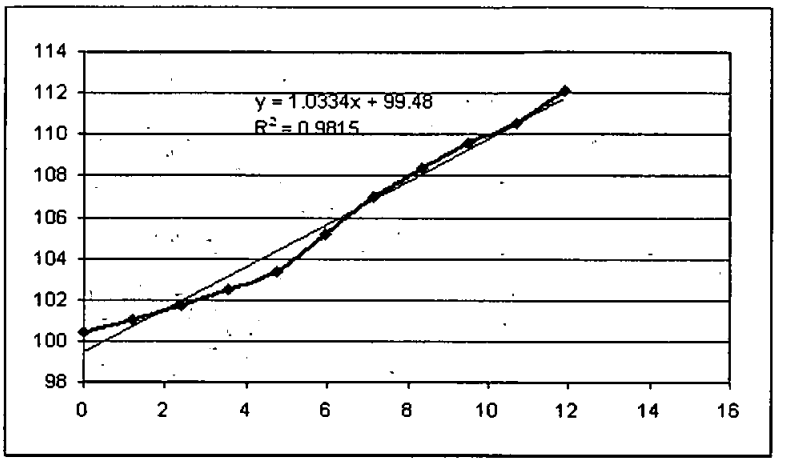

slope-3 44.421 degree **gradient 1.0334 slope 45.941 degree**

cross-4	elevation	distance
	100.56	0
	101.203	1.186
	101.848	2.372
	102.708	3.558
	103.412	4.744
	104.198	5.93
	104.997	7.116
	105.929	8.302
	107.323	9.488
	108.592	10.674
	110.371	11.86
	112.078	13.046

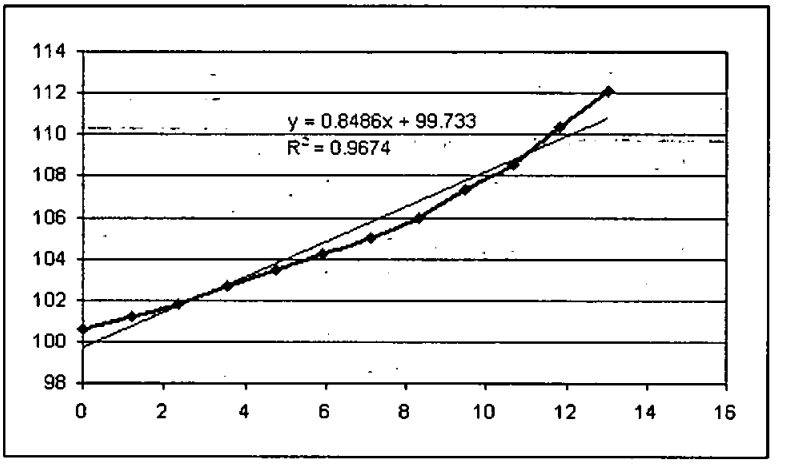

slope-4 41.441 degree **gradient 0.8486 slope 40.318 degree**

cross-5	elevation	distance
	100.002	0
	100.324	1.126
	100.91	2.252
	101.521	3.378
	102.222	4.504
	102.852	5.63
	103.3	6.756
	103.812	7.882
	104.373	9.008
	105.253	10.134
	106.628	11.26
	108.023	12.386
	108.873	13.512
	110.177	14.638
	112.068	15.764

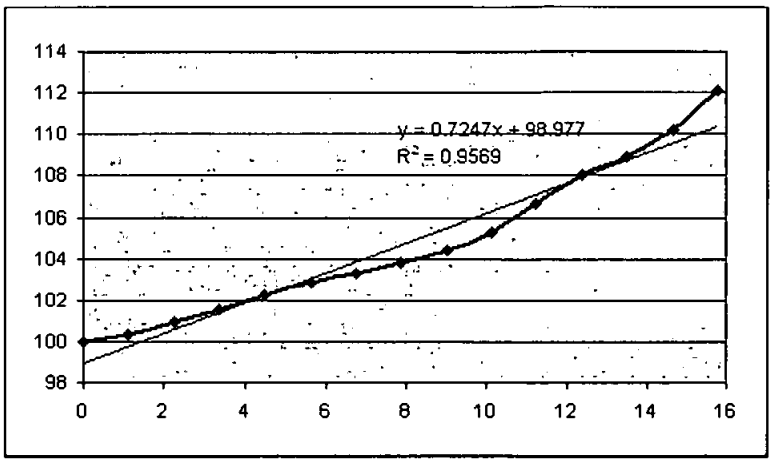

slope-5 37.431 degree **gradient 0.7247 slope 35.931 degree**

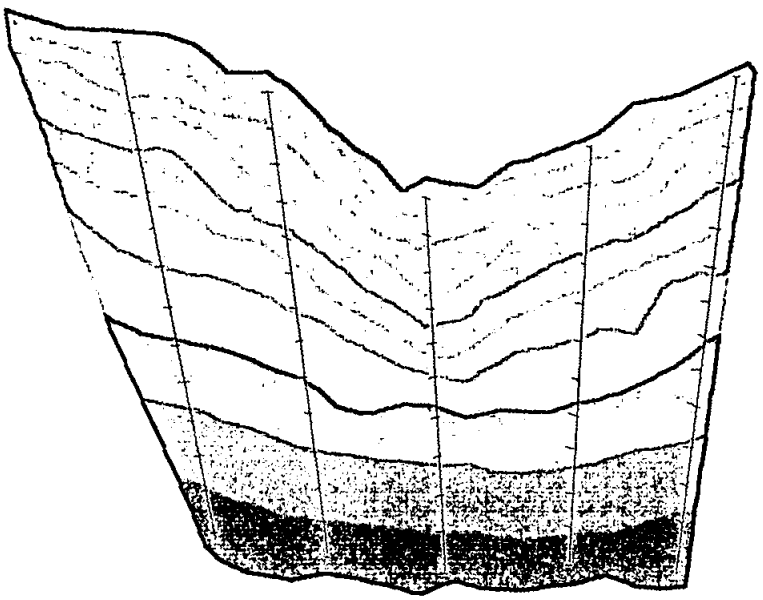

Location of cross-sections 1 to 5 (in left to right direction) on Area-3

Cross-sections Profiling for Area-4

cross-1	elevation	distance
	100.863	0
	101.416	1.099
	102.092	2.198
	102.841	3.297
	103.516	4.396
	104.784	5.495
	105.957	6.594
	106.779	7.693
	107.538	8.792
	108.673	9.891
	109.844	10.99
	111.049	12.089
	112.051	13.188
	113.075	14.287

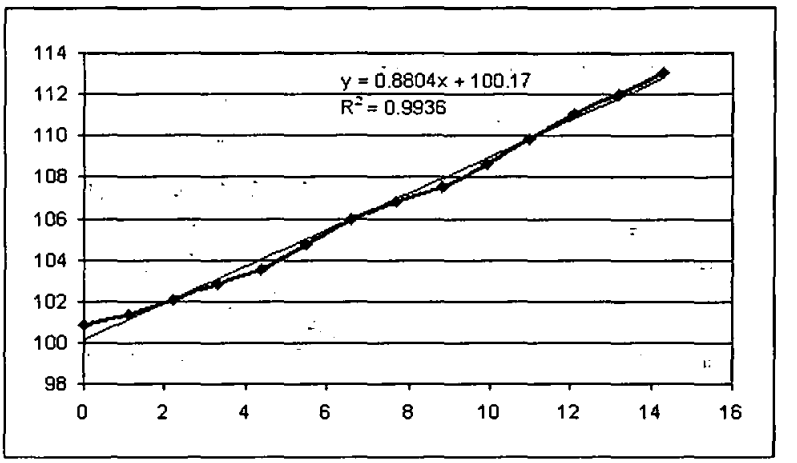

slope-1 40.523 degree **gradient 0.8804 slope 41.361 degree**

cross-2	elevation	distance
	100.802	0
	101.476	1.176
	102.133	2.352
	102.766	3.528
	103.47	4.704
	104.196	5.88
	105.195	7.056
	106.826	8.232
	108.42	9.408
	110.297	10.584
	111.52	11.76
	113.082	12.936

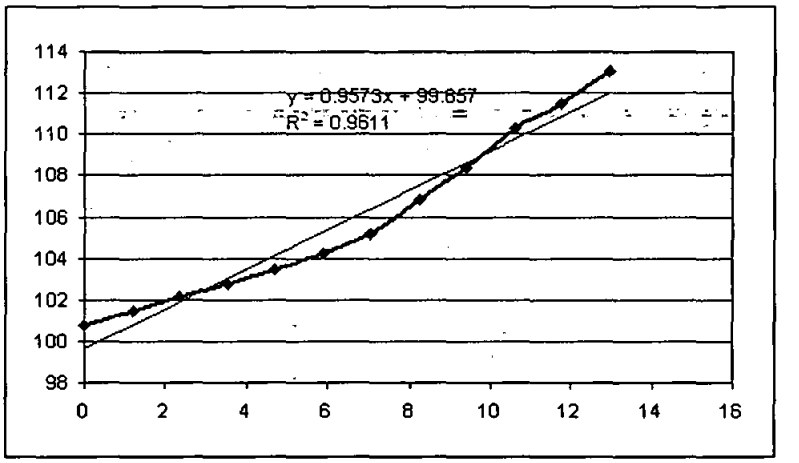

slope-2 43.510 degree **gradient 0.9573 slope 43.750 degree**

cross-3	elevation	distance
	100.862	0
	101.502	1.129
	102.088	2.258
	102.747	3.387
	103.343	4.516
	104.174	5.645
	104.937	6.774
	105.869	7.903
	106.828	9.032
	107.974	10.161
	109.259	11.29
	111.072	12.419
	112.367	13.548
slope-3	40.338	degree

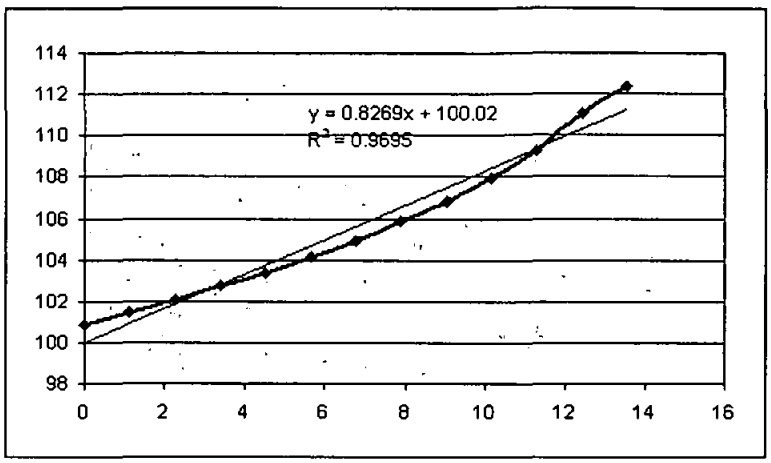

gradient 0.8269 slope 39.587 degree

cross-4	elevation	distance
	100.779	0
	101.435	1.196
	102.005	2.392
	102.831	3.588
	103.504	4.784
	104.303	5.98
	105.199	7.176
	106.108	8.372
	107.815	9.568
	109.545	10.764
	110.244	11.96
	111.064	13.156
	112.258	14.352
slope-4	38.653	degree

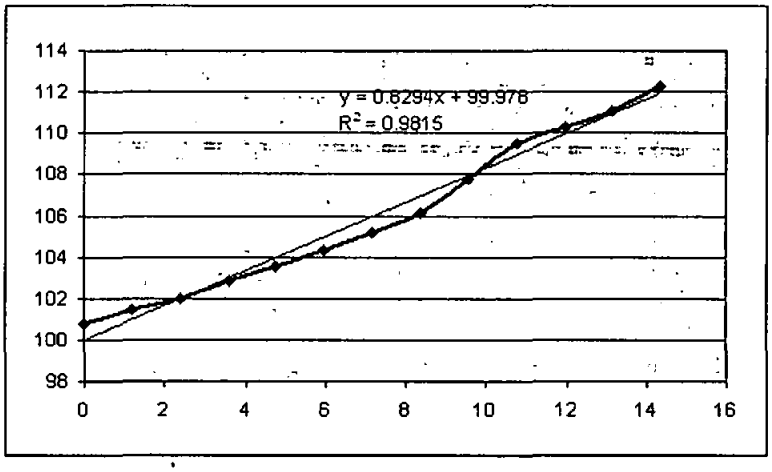

gradient 0.8294 slope 39.672 degree

cross-5	elevation	distance
	100.621	0
	101.142	0.999
	101.658	1.998
	102.27	2.997
	103.006	3.996
	103.985	4.995
	104.909	5.994
	105.643	6.993
	107.225	7.992
	109.047	8.991
	110.148	9.99
	111.099	10.989
	112.334	11.988

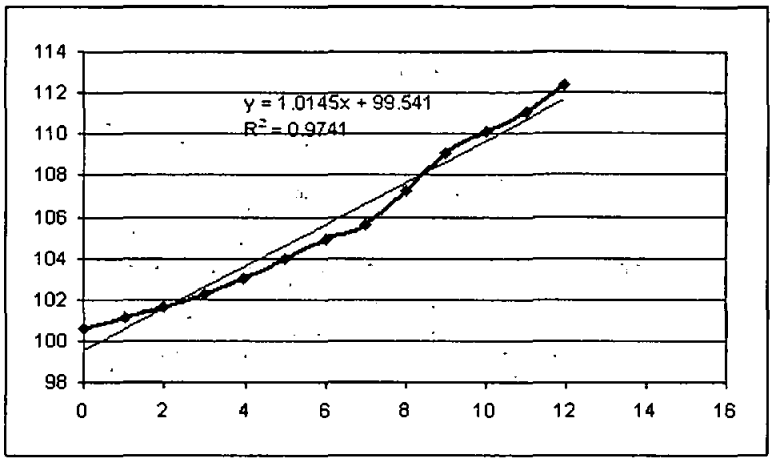

slope-5 44.335 degree **gradient 1.0145 slope 45.412 degree**

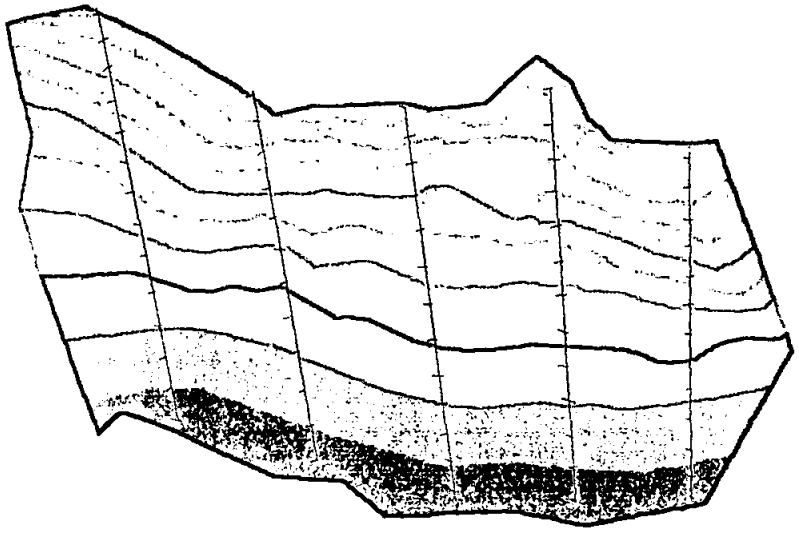

Location of cross-sections 1 to 5 (in left to right direction) on Area-4

Appendix B

Specification of Topcon GPT-3007 N/LN Reflector-less Total Station

	GPT-3002LN/N	GPT-3003LN/N	GPT-3005LN/N	GPT-3007LN/N
Telescope				
Length	150mm			
Objective Lens Diameter	45mm (EDM 50mm)			
Magnification	30x			
Image	Erect			
Field of View	1°30'			
Resolving Power	2.8"			
Min.Focus Distance	1.3m (4.9ft)			
Distance Measurement				
Prism Mode				
Measuring Range (1 prism)	3,000m			
Condition 1: Slight haze with visibility about 20km (12.5miles) moderate sunlight with light heat shimmer.				
Measurement accuracy	Fine : +/-(3mm+2ppm)m.s.e.			
	Coarse: +/-(7mm+2ppm)m.s.e.			
Non Prism Mode (Diffusing Surface)				
Measuring Range	1.5m to 250m			
Measuring Accuracy	Fine Mode :+/-(5mm)m.s.e. (25m or more)			
	'+/-(10mm)m.s.e. (1.5-25m)			
	Coarse : +/-(10mm)m.s.e.			
Measuring Time	Fine 1mm mode : Approx 1.2sec (Initial 3sec)			
	Fine 0.2mm mode: Approx 3.0sec (Initial 4sec)			
	Coarse mode 1mm/10mm : Approx 0.5sec (initial 2.5sec)			
Non Prism Long Mode (Diffusing Surface)				
Measuring Range	5m to 1,200m			
Measuring Accuracy (<500m, Kodak Gray Cardwhite surface (90%))	Fine 1mm mode : +/-(10mm+10ppm)m.s.e.			
	Coarse 5/10mm : +/-(20mm+10ppm)m.s.e.			
	Tracking (10mm)mode : +/-(100mm)m.s.e.			
Measuring Time	Fine 1mm mode : Approx 1.5 to 6sec (Initial 6-8sec)			
	Coarse mode (5/10mm): Approx 1 to 3 sec (Initial 6 to 8sec)			
	Tracking (10mm)mode : Approx 0.4sec (Initial 4 to 7 sec)			

Least Count in Measurement				
Prism Mode / Non Prism Mode	Fine Mode 1mm / 0.2mm			
	Coarse Mode : 10mm/1mm			
Non Prism Long Mode	Fine Mode : 1mm			
	Coarse Mode : 5mm/10mm			
	Tracking Mode : 10mm			
Others				
Measurement Display	12digits : max display 99999999.9999			
Atmospheric Correction Range	-999.9ppm to +999.9ppm, in 0.1ppm increments			
Prism Constant Correction Range	-99.9mm to +99.9mm, in 0.1mm increments			
Angle Measurement				
Method	Absolute Reading			
Detecting System	H: 2sides	H:2sides	H: 1side	
	V: 2sides	V:1side	V: 1side	
Minimum Reading	1"/5" (0.2/1mgon)	5"/10"(1/2mgon)		
Accuracy	2" (0.6mgon)	3" (1mgon)	5" (1.5mgon)	7" (2mgon)
Measuring Time	Less than 0.3sec			
Diameter of Circle	71mm			
Display				
Display Unit	Graphics LCD 160x64 dots with backlight			
	2sides	1side		
Keyboard	Alpha-Numeric Key			
Tilt Correction (Automatic Index)				
Tilt Sensor	Dual Axis	Single Axis		
Method	Liquid type			
Compensating Range	+/-3'			
Correction Unit	1" (0.1mgon)			
Others	Others			
Data Recording (Memory)	Approx 24,000 points			
Instruments Heights	176mm (6.93in)			
Laser Class	Class 1 (for distance measurement)			
	Class 2 (Laser Pointer : On/Off Switchable)			
Level Sensitivity				
Circular Level	10"/2mm			
Plate Level	20"/2mm	40"/2mm		
Size / Weight				
Dimention	336(H)x184(W)x172(L)mm			
Weight	Instrument (with battery) : 5.3kgs			
	Plastic Carrying Case : 3.4kgs (Slightly different depending on market)			

Durability	
Water & Dustproof	IP66 (incl BT-52QA battery) (Based on the standard IEC60529)
Ambient Temperature Range	-20?C to +50?C
Battery BT-52Q	
Output Voltage	DC7.2V
Capacity	2.7Ah (Ni-MH)
Maximum Operating time (when fully recharged) at +20?C	Maximum Operating time (when fully recharged) at +20?C
Distance+Angle Measurement	GPT-3000LNseries : 3.5hours
	GPT-3000N series : 4.2hours
Angle Measurement Only	45hours
Weight	0.3kg
Battery Charger BC-27	
Input Voltage	AC100-220V
Frequency	50/60Hz
Recharging time (at +20?C)	1.8hours (for BT-52QA battery)
Discharging Time (at +20?C)	8hours (for BT-52QA battery fully charged)
Operating Temperature	+10°C to +40°C
Weight	0.5kg

Appendix C

Coordinates of Ground Control Points for Area-1

Control Name	X (m)	Y (m)	Z (m)	RMS Residual (pixels)	Largest Residual (pixels)	Photo Largest Residual
101	986.843	1054.506	111.227	0.061679	0.075845	3
102	987.819	1053.126	108.569	0.0433	0.072614	1
103	998.587	1054.081	110.165	0.047907	0.071885	3
104	1001.562	1050.105	102.089	0.11808	0.175725	3
105	988.477	1050.043	102.625	0.077262	0.096874	1
106	1003.612	1054.406	110.304	0.239762	0.312755	3
107	992.999	1054.127	110.556	0.073202	0.093254	2
108	994.69	1050.404	104.694	0.067519	0.08563	1
109	996.535	1048.82	101.646	0.113756	0.141706	1
110	996.171	1051.846	107.544	0.133688	0.163131	2
112	991.868	1052.984	107.113	0.066419	0.076759	2
113	991.265	1050.206	102.802	0.092708	0.112617	3
114	999.373	1049.87	104	0.234831	0.330802	1
115	1000.55	1052.999	106.541	0.175188	0.248675	3
116	989.241	1051.507	105.573	0.086569	0.096272	2
117	990.038	1054.644	110.419	0.148281	0.183163	1
118	996.497	1053.463	110.237	0.073293	0.094672	3
119	996.756	1049.53	103.598	0.282364	0.321525	3
120	1001.449	1054.084	108.681	0.252748	0.303486	2

Coordinates of Ground Control Points for Area-2

Control Name	X (m)	Y (m)	Z (m)	RMS Residual (pixels)	Largest Residual (pixels)	Photo Largest Residual
2002	1007.455	1053.886	112.7974	0.33468	0.505024	3
2004	1007.793	1041.821	103.6807	0.082458	0.12624	1
2005	1011.152	1050.083	111.6327	0.518362	0.697755	3
2007	1010.842	1041.536	105.0494	0.135458	0.148949	3
2008	1010.734	1038.091	103.4604	0.106503	0.152249	1
2009	1011.781	1033.081	100.733	0.218569	0.323491	1
2012	1017.481	1031.683	101.2923	0.335163	0.461573	1
2013	1017.012	1038.017	105.5428	0.480087	0.568802	1
2014	1012.991	1038.103	104.3459	0.137533	0.189799	3
2015	1015.971	1042.285	111.051	0.312335	0.432382	2
2016	1017.471	1043.331	113.5309	0.280626	0.376175	1
2017	1020.76	1042.224	112.0309	0.527613	0.607651	1
2021	1024.234	1040.124	108.7603	0.297682	0.4	1
2022	1024.212	1037.596	105.4859	0.383785	0.506989	1
2023	1028.786	1042.287	111.9779	0.375279	0.566444	2
2024	1030.908	1040.504	108.7018	0.322351	0.432526	1
2026	1021.413	1029.727	100.8983	0.253827	0.318236	2
2027	1023.453	1042.829	113.1137	0.386543	0.502649	3
2028	1021.831	1033.387	102.5683	0.296836	0.387615	2

Coordinates of Ground Control Points for Area-3

Control Name	X (m)	Y (m)	Z (m)	RMS Residual (pixels)	Largest Residual (pixels)	Photo Largest Residual
101	1016.271	1043.781	113.177	0.172567	0.268091	2
102	1015.033	1038.157	106.506	0.135845	0.167488	2
103	1014.224	1035.206	102.748	0.116722	0.14288	3
105	1025.717	1042.392	112.059	0.207805	0.239832	2
106	1025.686	1038.264	106.506	0.12872	0.183849	1
108	1020.097	1031.773	101.977	0.159448	0.178855	3
109	1016.434	1030.533	100.819	0.18658	0.270646	2
110	1017.761	1032.452	101.974	0.191634	0.252748	1
111	1020.24	1041.864	110.88	0.161358	0.23679	1
112	1020.802	1038.704	106.88	0.238886	0.299854	2
113	1008.225	1052.979	112.658	0.107195	0.165496	1
114	1006.548	1050.721	108.074	0.184643	0.207	2
115	1004.929	1048.743	105.425	0.209317	0.325292	3
118	1012.863	1048.603	112.584	0.119828	0.166337	1
120	1010.959	1037.944	103.36	0.130704	0.157872	2

Coordinates of Ground Control Points for Area-4

Control Name	X (m)	Y (m)	Z (m)	RMS Residual (pixels)	Largest Residual (pixels)	Photo Largest Residual
101	1016.271	1043.781	113.177	0.086381	0.110032	5
102	1015.033	1038.157	106.506	0.075443	0.121399	4
103	1014.224	1035.206	102.748	0.103612	0.161687	4
113	1008.225	1052.979	112.658	0.143508	0.168195	6
114	1006.548	1050.721	108.074	0.172388	0.217379	6
115	1004.929	1048.743	105.425	0.223431	0.284361	6
118	1012.863	1048.603	112.584	0.099149	0.133882	4
120	1010.959	1037.944	103.36	0.057513	0.075265	4
230	1007.622	1047.103	106.27	0.120166	0.178797	6
233	1003.768	1046.296	103.278	0.157477	0.210328	5
234	1010.102	1044.069	105.735	0.065268	0.097049	6
235	1005.84	1039.366	101.665	0.172666	0.235412	4
236	1004.45	1060.625	112.459	0.169506	0.235358	6
237	1001.836	1050.061	103.791	0.142894	0.210122	6
238	1012.352	1045.09	109.178	0.075914	0.109645	6
239	1003.754	1053.353	107.954	0.198786	0.228647	6

Appendix D

Example of Coordinates of Reference Points for Area-1, measured using reflector-less Total Station

```
point_from,point_to,hz_circle,slope_dist,zenith_ang,code,easting,northi
ng,elevation
1,2,265.2955,15.72,90.4145,STN,998.766,984.33,99.706
1,101,346.2545,56.924,80.0445,TIE PNT,1054.506,986.843,111.227
1,102,347.051,54.972,82.314,TIE PNT,1053.126,987.819,108.569
1,103,358.301,54.802,80.4905,TIE PNT,1054.081,998.587,110.165
1,104,1.471,50.134,89.1405,TIE PNT,1050.105,1001.562,102.089
1,105,347.02,51.367,88.3915,TIE PNT,1050.043,988.477,102.625
1,106,3.4755,55.245,80.4445,TIE PNT,1054.406,1003.612,110.304
1,107,352.3745,55.339,80.2945,TIE PNT,1054.127,992.999,110.556
1,108,353.591,50.79,86.181,TIE PNT,1050.404,994.69,104.694
1,109,355.5625,48.945,89.44,TIE PNT,1048.82,996.535,101.646
1,110,355.4635,52.348,83.165,TIE PNT,1051.846,996.171,107.544
1,111,3.2355,52.487,85.312,TIE PNT,1052.234,1003.102,105.517
1,112,351.1625,53.907,83.561,TIE PNT,1052.984,991.868,107.113
1,113,350.075,50.98,88.2645,TIE PNT,1050.206,991.265,102.802
1,114,359.1645,49.942,87.0215,TIE PNT,1049.87,999.373,104
1,115,0.354,53.249,84.285,TIE PNT,1052.999,1000.55,106.541
1,116,348.1205,52.783,85.291,TIE PNT,1051.507,989.241,105.573
1,117,349.4005,56.269,80.4745,TIE PNT,1054.644,990.038,110.419
1,118,356.1505,54.3,80.3915,TIE PNT,1053.463,996.497,110.237
1,119,356.151,49.685,87.291,TIE PNT,1049.53,996.756,103.598
1,120,1.3205,54.589,82.212,TIE PNT,1054.084,1001.449,108.681
1,1001,342.44,58.468,79.4545,GRID,1054.943,982.923,111.811
1,1002,342.44,56.285,80.5615,GRID,1053.077,983.503,110.284
1,1003,342.44,55.151,82.064,GRID,1052.166,983.786,108.989
1,1004,342.44,54.317,83.083,GRID,1051.497,983.994,107.906
1,1005,342.44,53.658,84.0435,GRID,1050.965,984.159,106.957
1,1006,342.44,52.962,85.0345,GRID,1050.387,984.339,105.978
1,1007,342.44,52.37,86.0545,GRID,1049.892,984.492,104.985
1,1008,342.44,51.754,87.0925,GRID,1049.359,984.658,103.987
1,1009,342.44,51.412,88.0405,GRID,1049.067,984.749,103.152
1,1010,342.44,50.2,89,GRID,1047.929,985.102,102.295
1,1011,342.44,48.974,90.04,GRID,1046.766,985.464,101.362
1,1012,342.44,47.27,91.2305,GRID,1045.126,985.974,100.277
1,1013,343.5955,47.643,91.2305,GRID,1045.783,986.871,100.268
1,1014,343.5955,48.977,90.2245,GRID,1047.078,986.5,101.095
1,1015,343.5955,50.5,89.2305,GRID,1048.54,986.081,101.962
1,1016,343.5955,51.548,88.345,GRID,1049.535,985.795,102.696
1,1017,343.5955,51.703,87.345,GRID,1049.655,985.761,103.602
1,1018,343.5955,52.022,86.2725,GRID,1049.911,985.688,104.634
1,1019,344,52.76,85.195,GRID,1050.547,985.505,105.715
1,1020,343.5955,53.546,84.1745,GRID,1051.216,985.313,106.741
1,1021,343.5955,53.81,83.1945,GRID,1051.375,985.268,107.669
1,1022,343.5955,54.827,82.222,GRID,1052.236,985.021,108.697
1,1023,344,56.064,81.1225,GRID,1053.257,984.728,109.99
1,1024,343.5955,57.247,80.0815,GRID,1054.215,984.453,111.225
1,1025,344.003,57.633,79.4745,GRID,1054.525,984.373,111.629
1,1026,345.21,57.117,79.5415,GRID,1054.404,985.778,111.431
1,1027,345.21,56.162,81.102,GRID,1053.691,985.964,110.039
1,1028,345.21,54.613,82.2355,GRID,1052.373,986.309,108.644
```

1,1029,345.21,53.434,84.0025,GRID,1051.413,986.559,106.998
1,1030,345.21,52.598,85.1345,GRID,1050.711,986.743,105.794
1,1031,345.21,52.108,86.343,GRID,1050.323,986.844,104.532
1,1032,345.21,51.791,87.4315,GRID,1050.067,986.912,103.479
1,1033,345.21,51.395,89.013,GRID,1049.716,987.003,102.293
1,1034,345.21,49.978,90.072,GRID,1048.352,987.36,101.313
1,1035,345.21,48.123,91.2415,GRID,1046.544,987.832,100.239
1,1036,346.4215,47.564,91.242,GRID,1046.275,989.065,100.253
1,1037,346.4215,49.499,90.122,GRID,1048.171,988.617,101.241
1,1038,346.4215,50.953,89.0855,GRID,1049.581,988.284,102.177
1,1039,346.4215,51.842,87.5745,GRID,1050.42,988.085,103.262
1,1040,346.4215,52.315,86.411,GRID,1050.828,987.989,104.443
1,1041,346.4215,52.752,85.283,GRID,1051.177,987.906,105.582
1,1042,346.4215,53.503,84.1745,GRID,1051.81,987.757,106.737
1,1043,346.4215,54.125,83.145,GRID,1052.309,987.639,107.783
1,1044,346.4215,55.074,82.0905,GRID,1053.094,987.453,108.94
1,1045,346.4215,56.311,81.0425,GRID,1054.137,987.207,110.157
1,1046,346.4215,57.039,80.0315,GRID,1054.675,987.079,111.271
1,1047,348.101,56.875,80.0545,GRID,1054.837,988.514,111.202
1,1048,348.101,56.207,81.2235,GRID,1054.391,988.607,109.847
1,1049,348.101,55.103,82.523,GRID,1053.514,988.791,108.254
1,1050,348.101,54.115,84.144,GRID,1052.697,988.962,106.846
1,1051,348.101,52.794,85.2915,GRID,1051.511,989.21,105.573
1,1052,348.101,52.128,86.512,GRID,1050.944,989.329,104.279
1,1053,348.101,51.512,88.122,GRID,1050.393,989.444,103.032
1,1054,348.101,49.734,89.4225,GRID,1048.676,989.804,101.673
1,1055,348.101,47.157,91.194,GRID,1046.142,990.335,100.327
1,1056,350.0955,47.724,91.194,GRID,1047.009,991.851,100.313
1,1057,350.0955,49.208,90.061,GRID,1048.485,991.595,101.331
1,1058,350.0955,50.889,88.4535,GRID,1050.129,991.31,102.521
1,1059,350.0955,51.239,87.274,GRID,1050.436,991.257,103.69
1,1060,350.0955,51.834,86.164,GRID,1050.964,991.166,104.784
1,1061,350.0955,52.561,85.211,GRID,1051.618,991.052,105.678
1,1062,350.0955,53.958,84.085,GRID,1052.887,990.832,106.921
1,1063,350.0955,54.722,82.573,GRID,1053.51,990.724,108.127
1,1064,350.0955,55.321,81.5,GRID,1053.955,990.647,109.277
1,1065,350.0955,55.952,80.453,GRID,1054.414,990.567,110.405
1,1066,350.0955,56.483,80.1145,GRID,1054.84,990.494,111.038
1,1067,351.51,56.515,80.1745,GRID,1055.143,992.103,110.946
1,1068,351.51,54.947,81.405,GRID,1053.819,992.292,109.369
1,1069,351.51,54.303,83.012,GRID,1053.355,992.359,108.016
1,1070,351.51,53.318,84.374,GRID,1052.547,992.475,106.411
1,1071,351.51,51.685,85.5025,GRID,1051.027,992.692,105.168
1,1072,351.51,50.533,87.0615,GRID,1049.958,992.846,103.973
1,1073,351.51,50.228,88.281,GRID,1049.703,992.882,102.761
1,1074,351.51,49.492,89.4355,GRID,1048.991,992.984,101.651
1,1075,351.51,47.227,91.292,GRID,1046.734,993.307,100.192
1,1076,353.303,46.714,91.292,GRID,1046.398,994.721,100.206
1,1077,353.303,48.561,90.1055,GRID,1048.248,994.51,101.265
1,1078,353.303,49.35,88.5205,GRID,1049.023,994.422,102.394
1,1079,353.303,49.56,87.3935,GRID,1049.201,994.401,103.444
1,1080,353.303,50.78,86.265,GRID,1050.356,994.27,104.566
1,1081,353.303,51.821,85.161,GRID,1051.313,994.161,105.693
1,1082,353.303,52.901,84.1515,GRID,1052.297,994.049,106.716
1,1083,353.303,53.945,83.0305,GRID,1053.205,993.946,107.945
1,1084,353.303,54.593,81.434,GRID,1053.678,993.892,109.274
1,1085,353.303,55.473,80.1555,GRID,1054.322,993.819,110.799

Example of Coordinates of Reference Points for Area-2, measured using reflector-less Total Station

```
point_from,point_to,hz_circle,slope_dist,zenith_ang,code,easting,northi
ng,elevation
1,2,85.3029,15.951,89.5758,STN,1001.249,1015.902,100.014
1,1001,341.3029,70.578,80.2104,GRID,1065.987,977.931,113.208
1,1002,341.3028,69.804,80.3826,GRID,1065.319,978.155,112.731
1,1003,341.3029,69.511,80.5329,GRID,1065.091,978.231,112.383
1,1004,341.3029,69.185,81.1219,GRID,1064.841,978.314,111.957
1,1005,341.3029,69.053,81.2922,GRID,1064.766,978.34,111.598
1,1006,341.3029,68.803,81.4703,GRID,1064.58,978.402,111.211
1,1007,341.3029,68.1,82.2129,GRID,1064.01,978.593,110.434
1,1008,341.3028,67.579,82.4817,GRID,1063.585,978.734,109.843
1,1009,341.3028,66.948,83.1929,GRID,1063.06,978.91,109.16
1,1010,341.3028,66.348,83.5001,GRID,1062.558,979.078,108.505
1,1011,341.3028,66.017,84.0743,GRID,1062.28,979.171,108.131
1,1012,341.3028,65.435,84.294,GRID,1061.77,979.341,107.656
1,1013,341.3028,64.458,85.0308,GRID,1060.902,979.632,106.938
1,1014,341.3028,63.742,85.4227,GRID,1060.281,979.839,106.149
1,1015,341.3028,63.563,85.5822,GRID,1060.132,979.889,105.842
1,1016,341.3028,63.091,86.2542,GRID,1059.717,980.028,105.309
1,1017,341.3028,62.366,86.5007,GRID,1059.056,980.249,104.821
1,1018,341.3028,61.694,87.1012,GRID,1058.438,980.456,104.424
1,1019,341.3028,59.289,87.5722,GRID,1056.192,981.207,103.493
1,1020,341.3028,57.455,88.4205,GRID,1054.474,981.781,102.68
1,1021,341.3028,56.199,89.2101,GRID,1053.294,982.176,102.015
1,1022,341.3028,54.69,90.164,GRID,1051.866,982.654,101.113
1,1023,341.3028,53.443,90.5915,GRID,1050.676,983.052,100.457
1,1024,341.3028,52.234,91.4204,GRID,1049.515,983.44,99.828
1,1025,341.3028,46.939,92.275,GRID,1044.474,985.126,99.36
1,1026,341.3028,37.89,92.5412,GRID,1035.887,987.998,99.459
1,1027,341.3028,30.853,93.3102,GRID,1029.205,990.233,99.485
1,1028,341.3028,25.759,94.0725,GRID,1024.366,991.851,99.526
1,1029,341.3028,21.501,94.5633,GRID,1020.315,993.206,99.526
1,1030,342.3614,21.262,94.5625,GRID,1020.214,993.667,99.547
1,1031,342.3614,27.187,93.591,GRID,1025.881,991.891,99.488
1,1032,342.3614,31.531,92.551,GRID,1030.05,990.585,99.772
1,1033,342.3614,50.968,91.5806,GRID,1048.608,984.771,99.628
1,1034,342.3614,52.685,91.055,GRID,1050.266,984.252,100.369
1,1035,342.3614,54.382,90.0606,GRID,1051.894,983.741,101.282
1,1036,342.3613,55.978,89.0932,GRID,1053.412,983.266,102.2
1,1037,342.3613,57.609,88.1201,GRID,1054.947,982.785,103.187
1,1038,342.3613,59.797,87.1232,GRID,1056.994,982.143,104.29
1,1039,342.3613,61.603,86.2915,GRID,1058.674,981.617,105.152
1,1040,342.3613,62.808,85.4331,GRID,1059.769,981.274,106.06
1,1041,342.3613,63.897,84.5656,GRID,1060.737,980.97,107.004
1,1042,342.3613,64.978,84.0847,GRID,1061.683,980.674,108.005
1,1043,342.3613,65.889,83.2544,GRID,1062.462,980.43,108.918
1,1044,342.3613,66.926,82.431,GRID,1063.35,980.152,109.86
1,1045,342.3613,67.657,81.525,GRID,1063.915,979.975,110.934
1,1046,342.3613,68.278,81.0435,GRID,1064.366,979.833,111.97
1,1047,342.3613,69.19,80.1826,GRID,1065.083,979.609,113.027
1,1048,343.4556,68.18,80.1339,GRID,1064.511,981.216,112.951
1,1049,343.4557,67.851,80.4337,GRID,1064.294,981.279,112.312
1,1050,343.4557,67.364,81.1331,GRID,1063.921,981.388,111.655
```

1,1735,6.4744,67.809,81.4309,GRID,1066.63,1007.94,111.145
1,1736,6.4744,68.032,81.1841,GRID,1066.779,1007.958,111.656
1,1737,6.4744,68.276,80.5658,GRID,1066.952,1007.978,112.119
1,1738,6.4744,68.751,80.415,GRID,1067.37,1008.028,112.492
1,2001,339.2021,61.861,88.3258,GCP,1057.863,978.18,102.944
1,2002,341.3615,69.227,81.0706,GCP,1064.902,978.416,112.067
1,2003,345.0855,49.504,92.0548,GCP,1047.818,987.32,99.567
1,2004,344.2102,56.78,88.0717,GCP,1054.646,984.692,103.24
1,2005,345.2254,66.265,81.4003,GCP,1063.443,983.453,110.981
1,2006,348.3804,66.194,80.5828,GCP,1064.093,987.117,111.763
1,2007,347.1943,57.393,86.4644,GCP,1055.907,987.43,104.603
1,2008,348.1722,54.04,88.1137,GCP,1052.889,989.037,103.082
1,2009,351.1237,49.676,91.032,GCP,1049.084,992.41,100.463
1,2010,352.532,33.552,93.1402,GCP,1033.241,995.853,99.485
1,2011,2.2925,38.218,92.4904,GCP,1038.136,1001.659,99.499
1,2012,357.4216,50.723,90.221,GCP,1050.681,997.969,101.051
1,2013,354.1843,56.322,86.0916,GCP,1055.918,994.43,105.156
1,2014,350.2939,54.825,87.1757,GCP,1054.012,990.956,103.962
1,2015,351.432,60.438,81.1738,GCP,1059.119,991.399,110.527
1,2016,352.3818,62.363,79.1742,GCP,1060.773,992.148,112.963
1,2017,355.4941,62.41,80.3929,GCP,1061.419,995.52,111.509
1,2018,0.525,54.329,89.0044,GCP,1054.315,1000.835,102.315
1,2019,2.353,50.986,90.4541,GCP,1050.93,1002.305,100.701
1,2020,357.4558,64.306,79.5758,GCP,1063.274,997.532,112.582
1,2021,359.3455,61.682,83.3208,GCP,1061.288,999.553,108.323
1,2022,0.4708,59.203,86.2206,GCP,1059.079,1000.81,105.128
1,2023,2.0407,66.217,81.1328,GCP,1065.399,1002.362,111.481
1,2024,4.2843,65.442,83.5644,GCP,1064.878,1005.082,108.281
1,2025,8.3421,46.702,92.1458,GCP,1046.144,1006.956,99.545
1,2026,2.3457,50.983,90.4542,GCP,1050.926,1002.297,100.701
1,2027,357.4517,64.297,79.581,GCP,1063.265,997.52,112.577
1,2028,0.5346,54.295,89.014,GCP,1054.281,1000.849,102.3
1,3001,335.5531,79.966,81.2822,BREAK-LINE,1072.203,967.74,113.236
1,3002,336.3234,79.08,81.2052,BREAK-LINE,1071.719,968.879,113.275
1,3003,337.2603,78,81.1508,BREAK-LINE,1071.19,970.416,113.241
1,3004,338.0626,77.209,81.0541,BREAK-LINE,1070.777,971.558,113.331
1,3005,338.5941,76.226,80.5756,BREAK-LINE,1070.278,973.015,113.348
1,3006,339.3147,74.644,81.0255,BREAK-LINE,1069.079,974.214,112.993
1,3007,340.1149,74.394,80.4747,BREAK-LINE,1069.093,975.121,113.277
1,3008,341.1834,70.708,80.1713,BREAK-LINE,1066.019,977.666,113.308
1,3009,342.1614,69.398,80.1948,BREAK-LINE,1065.162,979.167,113.035
1,3010,343.02,69.438,80.0943,BREAK-LINE,1065.439,980.035,113.243
1,3011,344.0204,68.842,80.0305,BREAK-LINE,1065.191,981.349,113.272
1,3012,345.0513,69.015,80.0802,BREAK-LINE,1065.704,982.502,113.204
1,3013,346.0042,68.12,79.5859,BREAK-LINE,1065.092,983.785,113.227
1,3014,347.312,66.399,79.4028,BREAK-LINE,1063.78,985.886,113.28
1,3015,348.1759,67.267,79.5237,BREAK-LINE,1064.844,986.571,113.201
1,3016,348.4724,67.232,79.544,BREAK-LINE,1064.929,987.132,113.156
1,3017,349.22,66.503,79.4807,BREAK-LINE,1064.329,987.923,113.153
1,3018,349.5257,65.186,79.322,BREAK-LINE,1063.105,988.739,113.214
1,3019,350.551,63.59,79.2059,BREAK-LINE,1061.711,990.137,113.131
1,3020,351.4658,62.681,79.1336,BREAK-LINE,1060.944,991.199,113.095
1,3021,352.0547,63.38,79.1646,BREAK-LINE,1061.682,991.437,113.168
1,3022,352.3845,62.567,79.1316,BREAK-LINE,1060.957,992.133,113.08
1,3023,353.0735,62.627,79.1612,BREAK-LINE,1061.089,992.636,113.038
1,3024,353.2616,62.438,79.3029,BREAK-LINE,1060.992,992.984,112.748
1,3025,353.2901,64.614,79.2834,BREAK-LINE,1063.116,992.79,113.18

Example of Coordinates of Reference Points for Area-3 and Area-4, measured using reflector-less Total Station

```
point_from,point_to,hz_circle,slope_dist,zenith_ang,code,easting,northi
ng,elevation
1,2,296.3,46.765,90.082,STN,1020.866,958.149,99.895
1,101,20.2315,48.161,75.5305,TIE PNT,1043.781,1016.271,113.177
1,102,21.301,41.326,82.5655,TIE PNT,1038.157,1015.033,106.506
1,103,22,37.995,88.0055,TIE PNT,1035.206,1014.224,102.748
1,104,22.09,34.066,91.2335,TIE PNT,1031.542,1012.84,100.604
1,105,31.1435,50.709,77.541,TIE PNT,1042.392,1025.717,112.059
1,106,33.5225,46.364,83.4305,TIE PNT,1038.264,1025.686,106.506
1,107,34.28,42.356,86.3555,TIE PNT,1034.859,1023.928,103.946
1,108,32.1855,37.6,89.101,TIE PNT,1031.773,1020.097,101.977
1,109,28.1725,34.68,91.005,TIE PNT,1030.533,1016.434,100.819
1,110,28.413,36.999,89.094,TIE PNT,1032.452,1017.761,101.974
1,111,25.4805,47.451,78.3055,TIE PNT,1041.864,1020.24,110.88
1,112,28.1525,44.276,82.56,TIE PNT,1038.704,1020.802,106.88
1,113,8.493,54.778,78.1025,TIE PNT,1052.979,1008.225,112.658
1,114,7.212,51.573,82.36,TIE PNT,1050.721,1006.548,108.074
1,115,5.463,49.154,85.2025,TIE PNT,1048.743,1004.929,105.425
1,116,4.2005,49.12,87.022,TIE PNT,1048.913,1003.708,103.97
1,117,10.241,36.334,91.2545,TIE PNT,1035.726,1006.559,100.526
1,118,14.4925,51.499,77.294,TIE PNT,1048.603,1012.863,112.584
1,119,8.5435,48.114,84.2725,TIE PNT,1047.311,1007.417,106.08
1,120,16.0635,39.543,87.122,TIE PNT,1037.944,1010.959,103.36
1,1001,32.385,51.978,77.265,GRID,1042.719,1027.37,112.73
1,1002,32.3905,51.295,78.0525,GRID,1042.259,1027.078,112.018
1,1003,32.3905,50.827,78.5355,GRID,1041.994,1026.909,111.219
1,1004,32.39,50.121,79.4425,GRID,1041.526,1026.609,110.359
1,1005,32.3905,49.255,80.364,GRID,1040.915,1026.217,109.467
1,1006,32.3905,48.033,81.2645,GRID,1039.992,1025.626,108.577
1,1007,32.3905,47.216,82.2155,GRID,1039.402,1025.248,107.705
1,1008,32.39,46.697,82.512,GRID,1039.012,1024.998,107.24
1,1009,32.3905,46.005,83.264,GRID,1038.481,1024.658,106.685
1,1010,32.3905,45.522,83.573,GRID,1038.115,1024.423,106.223
1,1011,32.39,44.885,84.3105,GRID,1037.619,1024.105,105.721
1,1012,32.39,43.938,85.0425,GRID,1036.858,1023.618,105.205
1,1013,32.39,43.138,85.435,GRID,1036.219,1023.208,104.644
1,1014,32.3905,42.083,86.404,GRID,1035.372,1022.666,103.871
1,1015,32.39,40.389,87.34,GRID,1033.976,1021.771,103.147
1,1016,32.3905,39.092,88.0525,GRID,1032.895,1021.079,102.735
1,1017,32.39,38.211,88.4045,GRID,1032.164,1020.61,102.313
1,1018,32.39,37.443,89.2605,GRID,1031.524,1020.2,101.802
1,1019,32.39,36.196,90.2015,GRID,1030.475,1019.528,101.219
1,1020,32.39,35.372,91.095,GRID,1029.776,1019.079,100.714
1,1021,32.39,33.949,91.5535,GRID,1028.568,1018.306,100.291
1,1022,32.39,31.872,92.4345,GRID,1026.804,1017.175,99.915
1,1023,31.2535,32.155,92.434,GRID,1027.407,1016.747,99.902
1,1024,31.2535,34.033,92.0235,GRID,1029.021,1017.733,100.219
1,1025,31.2535,34.953,91.2745,GRID,1029.816,1018.219,100.54
1,1026,31.2535,35.768,90.4335,GRID,1030.518,1018.648,100.979
1,1027,31.2535,36.475,90.012,GRID,1031.124,1019.018,101.418
1,1028,31.2535,37.484,89.085,GRID,1031.981,1019.542,101.99
1,1029,31.2535,38.355,88.21,GRID,1032.715,1019.99,102.537
1,1030,31.2535,39.415,87.335,GRID,1033.602,1020.532,103.108
```

1,1031,31.2535,40.971,86.4455,GRID,1034.904,1021.328,103.756
1,1032,31.2535,42.308,86.005,GRID,1036.014,1022.006,104.373
1,1033,31.2535,43.796,85.1925,GRID,1037.246,1022.759,105.003
1,1034,31.2535,44.5,84.3005,GRID,1037.797,1023.096,105.696
1,1035,31.2535,44.954,83.4725,GRID,1038.134,1023.301,106.295
1,1036,31.2535,45.531,83.0925,GRID,1038.575,1023.571,106.857
1,1037,31.2535,46.315,82.28,GRID,1039.179,1023.94,107.504
1,1038,31.2535,47.022,81.55,GRID,1039.725,1024.274,108.044
1,1039,31.2535,47.574,81.131,GRID,1040.118,1024.514,108.694
1,1040,31.2535,48.438,80.35,GRID,1040.775,1024.915,109.358
1,1041,31.2535,49.112,80.1235,GRID,1041.297,1025.234,109.784
1,1042,31.2535,49.762,79.31,GRID,1041.753,1025.513,110.486
1,1043,31.2535,50.4,78.4225,GRID,1042.173,1025.769,111.302
1,1044,31.2535,50.847,77.5345,GRID,1042.423,1025.922,112.094
1,1045,31.2535,51.697,77.07,GRID,1043.003,1026.276,112.959
1,1046,30.005,50.474,77.07,GRID,1042.604,1024.612,112.686
1,1047,30.0055,51.003,76.2815,GRID,1042.937,1024.804,113.364
1,1048,30.005,50.092,77.561,GRID,1042.417,1024.504,111.902
1,1049,30.005,49.717,78.4455,GRID,1042.221,1024.391,111.132
1,1050,30.005,48.793,79.46,GRID,1041.577,1024.019,110.1
1,1051,30.0055,46.914,80.481,GRID,1040.1,1023.165,108.93
1,1052,30.005,46.792,80.531,GRID,1040.005,1023.11,108.844
1,1053,30.005,46.115,81.423,GRID,1039.513,1022.826,108.082
1,1054,30.005,45.19,82.403,GRID,1038.81,1022.42,107.193
1,1055,30.0055,44.505,83.3345,GRID,1038.293,1022.122,106.422
1,1056,30.005,43.87,84.3545,GRID,1037.818,1021.847,105.564
1,1057,30.005,41.802,85.39,GRID,1036.092,1020.85,104.602
1,1058,30.005,40.204,86.4705,GRID,1034.757,1020.079,103.687
1,1059,30.005,39.199,87.322,GRID,1033.91,1019.59,103.116
1,1060,30.005,38.823,87.474,GRID,1033.591,1019.405,102.927
1,1061,30.005,37.623,88.412,GRID,1032.569,1018.815,102.293
1,1062,30.005,36.499,89.412,GRID,1031.603,1018.257,101.63
1,1063,30.005,35.153,90.461,GRID,1030.436,1017.582,100.96
1,1064,30.005,34.309,91.4145,GRID,1029.695,1017.154,100.417
1,1065,30.005,33.188,92.3345,GRID,1028.709,1016.585,99.948
1,1066,28.3715,33.14,92.3345,GRID,1029.061,1015.858,99.95
1,1067,28.3715,33.907,91.4915,GRID,1029.749,1016.233,100.355
1,1068,28.3715,34.868,90.5425,GRID,1030.604,1016.7,100.88
1,1069,28.3715,35.73,89.595,GRID,1031.364,1017.115,101.434
1,1070,28.3715,37.021,89.0255,GRID,1032.492,1017.73,102.047
1,1071,28.3715,38.013,88.125,GRID,1033.352,1018.2,102.617
1,1072,28.3715,39.025,87.1545,GRID,1034.216,1018.671,103.296
1,1073,28.3715,39.769,86.3705,GRID,1034.848,1019.016,103.778
1,1074,28.3715,40.699,85.531,GRID,1035.633,1019.444,104.352
1,1075,28.3715,42.051,85.0145,GRID,1036.773,1020.066,105.076
1,1076,28.3715,42.378,83.5755,GRID,1036.993,1020.186,105.887
1,1077,28.3715,44.307,83.032,GRID,1038.607,1021.067,106.789
1,1078,28.3715,45.089,81.563,GRID,1039.188,1021.384,107.753
1,1079,28.3715,45.8,81.0105,GRID,1039.71,1021.669,108.582
1,1080,28.3715,46.809,80.033,GRID,1040.472,1022.085,109.514
1,1081,28.3715,47.517,79.102,GRID,1040.968,1022.355,110.359
1,1082,28.3715,48.34,78.161,GRID,1041.546,1022.671,111.26
1,1083,28.3715,49.638,77.293,GRID,1042.538,1023.212,112.183
1,1084,28.371,50.562,76.355,GRID,1043.175,1023.559,113.152
1,1085,27.33,49.678,76.355,GRID,1042.844,1022.351,112.947
1,1086,27.33,48.548,77.3055,GRID,1042.025,1021.924,111.927
1,1087,27.2925,48.117,78.0045,GRID,1041.753,1021.726,111.426

Appendix E

Example of Sampling Points of Area-1 Measured Using Close-range Photogrammetry Method

```
X (m),Y (m),Z (m),X_Precision,Y_Precision,Z_Precision,Angle
(deg.),RMS_Residual (pixels),Largest_Residual
(pixels),Photo_Largest_Residual,Precision_Vector_Length
986.843,1054.506,111.227,fixed,fixed,fixed,17.025,0.062,0.076,3,fixed
987.819,1053.126,108.569,fixed,fixed,fixed,17.704,0.043,0.073,1,fixed
998.587,1054.081,110.165,fixed,fixed,fixed,17.687,0.048,0.072,3,fixed
1001.562,1050.105,102.089,fixed,fixed,fixed,19.244,0.118,0.176,3,fixed
988.477,1050.043,102.625,fixed,fixed,fixed,19.054,0.077,0.097,1,fixed
1003.612,1054.406,110.304,fixed,fixed,fixed,17.242,0.24,0.313,3,fixed
992.999,1054.127,110.556,fixed,fixed,fixed,17.64,0.073,0.093,2,fixed
994.69,1050.404,104.694,fixed,fixed,fixed,19.329,0.068,0.086,1,fixed
996.535,1048.82,101.646,fixed,fixed,fixed,20.056,0.114,0.142,1,fixed
996.171,1051.846,107.544,fixed,fixed,fixed,18.67,0.134,0.163,2,fixed
991.868,1052.984,107.113,fixed,fixed,fixed,18.153,0.066,0.077,2,fixed
991.265,1050.206,102.802,fixed,fixed,fixed,19.273,0.093,0.113,3,fixed
999.373,1049.87,104,fixed,fixed,fixed,19.48,0.235,0.331,1,fixed
1000.55,1052.999,106.541,fixed,fixed,fixed,18.136,0.175,0.249,3,fixed
989.241,1051.507,105.573,fixed,fixed,fixed,18.532,0.087,0.096,2,fixed
990.038,1054.644,110.419,fixed,fixed,fixed,17.317,0.148,0.183,1,fixed
996.497,1053.463,110.237,fixed,fixed,fixed,17.938,0.073,0.095,3,fixed
996.756,1049.53,103.598,fixed,fixed,fixed,19.726,0.282,0.322,3,fixed
1001.449,1054.084,108.681,fixed,fixed,fixed,17.611,0.253,0.303,2,fixed
983.325,1054.226,111.409,0.002,0.006,0.001,16.653,0.066,0.087,3,0.006
986.061,1047.254,101.389,0.001,0.004,0.001,19.784,0.015,0.018,2,0.005
1007.028,1054.008,110.305,0.001,0.006,0.001,16.969,0.107,0.143,1,0.006
1006.336,1049.071,101.092,0.001,0.005,0.001,19.002,0.08,0.111,3,0.005
987.065,1054.682,111.266,0.001,0.006,0.001,16.994,0.043,0.052,3,0.006
988.719,1047.828,101.011,0.001,0.004,0.001,19.981,0.029,0.04,2,0.004
988.308,1054.86,111.194,0.001,0.006,0.001,17.065,0.015,0.016,1,0.006
989.952,1047.564,100.912,0.001,0.004,0.001,20.253,0.049,0.059,1,0.004
985.702,1054.332,111.358,0.001,0.006,0.001,16.94,0.141,0.181,1,0.006
987.832,1047.14,100.514,0.001,0.004,0.001,20.135,0.03,0.039,2,0.004
984.66,1054.288,111.408,0.001,0.006,0.001,16.819,0.107,0.139,3,0.006
986.941,1047.113,100.89,0.001,0.004,0.001,20,0.047,0.063,3,0.005
989.661,1054.931,111.074,0.001,0.005,0.001,17.162,0.051,0.069,1,0.006
991.294,1048.11,101.067,0.001,0.004,0.001,20.156,0.06,0.078,3,0.004
991.01,1054.568,110.984,0.001,0.005,0.001,17.373,0.173,0.212,1,0.006
992.581,1047.606,100.648,0.001,0.004,0.001,20.48,0.12,0.154,1,0.004
992.293,1055.036,110.854,0.001,0.005,0.001,17.298,0.203,0.281,2,0.006
994.162,1047.051,100.48,0.001,0.004,0.001,20.821,0.081,0.114,3,0.004
994.071,1054.123,110.504,0.001,0.005,0.001,17.677,0.11,0.144,1,0.005
995.185,1047.619,100.903,0.001,0.004,0.001,20.588,0.059,0.076,3,0.004
995.449,1054.507,110.822,0.001,0.005,0.001,17.551,0.024,0.033,2,0.005
996.477,1047.292,100.616,0.001,0.004,0.001,20.743,0.025,0.031,3,0.004
997.017,1053.453,110.498,0.001,0.005,0.001,17.919,0.035,0.048,2,0.005
997.426,1047.223,100.645,0.001,0.004,0.001,20.757,0.065,0.084,1,0.004
998.24,1054.126,110.59,0.001,0.005,0.001,17.658,0.109,0.144,3,0.005
998.95,1046.918,100.412,0.001,0.004,0.001,20.829,0.133,0.168,1,0.004
999.601,1054.431,110.403,0.001,0.005,0.001,17.515,0.099,0.131,3,0.005
999.932,1047.607,100.532,0.001,0.004,0.001,20.444,0.082,0.112,1,0.004
1000.91,1054.625,110.37,0.001,0.005,0.001,17.382,0.242,0.312,3,0.006
```

1000.896,1047.796,100.511,0.001,0.004,0.001,20.276,0.039,0.047,3,0.004
1002.332,1054.424,110.269,0.001,0.005,0.001,17.351,0.078,0.101,3,0.006
1002.059,1047.82,100.348,0.001,0.004,0.001,20.139,0.108,0.138,1,0.004
1003.603,1054.419,110.162,0.001,0.006,0.001,17.246,0.149,0.194,3,0.006
1003.36,1048.216,100.351,0.001,0.004,0.001,19.804,0.088,0.123,1,0.005
1004.695,1054.449,110.257,0.001,0.006,0.001,17.121,0.211,0.274,3,0.006
1004.541,1048.125,100.357,0.001,0.005,0.001,19.667,0.121,0.163,1,0.005
1005.752,1054.319,110.269,0.001,0.006,0.001,17.04,0.034,0.048,3,0.006
1005.373,1048.245,100.392,0.001,0.005,0.001,19.483,0.161,0.206,1,0.005
983.728,1053.417,110.55,0.002,0.005,0.001,16.988,0.072,0.09,3,0.006
984.164,1052.559,109.346,0.001,0.005,0.001,17.37,0.016,0.022,2,0.005
984.53,1051.747,108.122,0.001,0.005,0.001,17.738,0.158,0.202,3,0.005
984.489,1051.109,107.137,0.001,0.005,0.001,17.979,0.055,0.067,1,0.005
984.791,1050.626,106.19,0.001,0.005,0.001,18.225,0.054,0.071,3,0.005
985.022,1050,104.992,0.001,0.005,0.001,18.516,0.008,0.009,1,0.005
985.175,1049.593,104.064,0.001,0.005,0.001,18.708,0.135,0.17,3,0.005
985.222,1049.404,103.255,0.001,0.005,0.001,18.798,0.02,0.025,3,0.005
985.522,1048.558,102.267,0.001,0.004,0.001,19.174,0.03,0.04,3,0.005
984.804,1053.497,110.489,0.001,0.005,0.001,17.12,0.031,0.043,1,0.006
985.124,1053.157,109.472,0.001,0.005,0.001,17.32,0.043,0.062,1,0.006
985.497,1051.635,108.156,0.001,0.005,0.001,17.919,0.055,0.068,3,0.005
985.585,1051.342,107.075,0.001,0.005,0.001,18.076,0.078,0.104,1,0.005
985.725,1050.773,106.121,0.001,0.005,0.001,18.326,0.189,0.25,1,0.005
985.906,1050.181,105.065,0.001,0.005,0.001,18.595,0.04,0.053,3,0.005
986.068,1049.886,103.973,0.001,0.005,0.001,18.752,0.068,0.09,3,0.005
986.077,1049.803,103.243,0.001,0.005,0.001,18.796,0.053,0.07,1,0.005
985.987,1049.654,102.504,0.001,0.005,0.001,18.844,0.072,0.092,1,0.005
986.476,1048.132,101.574,0.001,0.004,0.001,19.509,0.027,0.038,1,0.005
985.854,1053.81,110.502,0.001,0.005,0.001,17.162,0.168,0.211,1,0.006
985.941,1053.645,109.745,0.001,0.005,0.001,17.263,0.059,0.073,3,0.006
986.201,1052.417,108.67,0.001,0.005,0.001,17.737,0.03,0.039,2,0.005
986.554,1051.575,107.354,0.001,0.005,0.001,18.123,0.129,0.158,1,0.005
986.68,1051.045,106.415,0.001,0.005,0.001,18.36,0.089,0.11,3,0.005
986.718,1050.535,105.513,0.001,0.005,0.001,18.577,0.061,0.078,1,0.005
986.874,1050.361,104.558,0.001,0.005,0.001,18.688,0.093,0.121,3,0.005
986.891,1050.103,103.533,0.001,0.005,0.001,18.806,0.172,0.221,1,0.005
986.913,1049.962,102.763,0.001,0.005,0.001,18.871,0.027,0.036,1,0.005
987.317,1048.318,101.297,0.001,0.004,0.001,19.573,0.049,0.068,2,0.005
987.205,1054.259,110.277,0.001,0.005,0.001,17.192,0.156,0.208,3,0.006
987.353,1053.61,109.5,0.001,0.005,0.001,17.451,0.077,0.108,3,0.005
987.482,1053.012,108.739,0.001,0.005,0.001,17.696,0.139,0.189,1,0.005
987.666,1052.341,107.799,0.001,0.005,0.001,17.983,0.015,0.021,2,0.005
987.745,1051.829,107.002,0.001,0.005,0.001,18.201,0.073,0.083,1,0.005
987.814,1051.611,106.16,0.001,0.005,0.001,18.317,0.015,0.021,1,0.005
987.866,1051.166,105.404,0.001,0.005,0.001,18.506,0.126,0.16,3,0.005
987.854,1050.876,104.675,0.001,0.005,0.001,18.63,0.043,0.052,1,0.005
987.896,1050.694,103.9,0.001,0.005,0.001,18.718,0.161,0.203,1,0.005
988.001,1050.263,103.127,0.001,0.005,0.001,18.905,0.106,0.131,3,0.005
988.145,1049.742,102.255,0.001,0.004,0.001,19.13,0.139,0.175,1,0.005
988.477,1048.677,101.617,0.001,0.004,0.001,19.598,0.012,0.014,3,0.005
988.359,1054.408,110.319,0.001,0.005,0.001,17.258,0.169,0.208,1,0.006
988.383,1054.361,109.597,0.001,0.005,0.001,17.313,0.017,0.023,2,0.006
988.495,1053.761,108.741,0.001,0.005,0.001,17.557,0.159,0.196,1,0.005
988.581,1053.424,107.943,0.001,0.005,0.001,17.712,0.123,0.151,1,0.005
988.662,1052.802,107.106,0.001,0.005,0.001,17.963,0.142,0.197,3,0.005
988.888,1051.869,106.229,0.001,0.005,0.001,18.344,0.094,0.115,1,0.005
989.019,1051.261,105.291,0.001,0.005,0.001,18.607,0.02,0.025,3,0.005

Example of Sampling Points of Area-2 Measured Using Close-range Photogrammetry Method

```
X (m),Y (m),Z (m),X_Precision,Y_Precision,Z_Precision,RMS_Residual
(pixels),Largest_Residual
(pixels),Photo_Largest_Residual,Precision_Vector_Length
1016.271,1043.781,113.177,fixed,fixed,fixed,0.173,0.268,2,fixed
1015.033,1038.157,106.506,fixed,fixed,fixed,0.136,0.167,2,fixed
1014.224,1035.206,102.748,fixed,fixed,fixed,0.117,0.143,3,fixed
1025.717,1042.392,112.059,fixed,fixed,fixed,0.208,0.240,2,fixed
1025.686,1038.264,106.506,fixed,fixed,fixed,0.129,0.184,1,fixed
1020.097,1031.773,101.977,fixed,fixed,fixed,0.159,0.179,3,fixed
1016.434,1030.533,100.819,fixed,fixed,fixed,0.187,0.271,2,fixed
1017.761,1032.452,101.974,fixed,fixed,fixed,0.192,0.253,1,fixed
1020.240,1041.864,110.880,fixed,fixed,fixed,0.161,0.237,1,fixed
1020.802,1038.704,106.880,fixed,fixed,fixed,0.239,0.300,2,fixed
1008.225,1052.979,112.658,fixed,fixed,fixed,0.107,0.165,1,fixed
1006.548,1050.721,108.074,fixed,fixed,fixed,0.185,0.207,2,fixed
1004.929,1048.743,105.425,fixed,fixed,fixed,0.209,0.325,3,fixed
1012.863,1048.603,112.584,fixed,fixed,fixed,0.120,0.166,1,fixed
1010.959,1037.944,103.360,fixed,fixed,fixed,0.131,0.158,2,fixed
1012.760,1031.521,100.599,0.001,0.002,0.000,0.116,0.150,2,0.002
1007.623,1047.139,106.274,0.001,0.004,0.001,0.085,0.116,2,0.004
1005.907,1054.751,111.600,0.001,0.006,0.001,0.127,0.151,1,0.006
1004.259,1037.461,100.150,0.001,0.003,0.000,0.187,0.230,2,0.003
1027.342,1042.898,112.853,0.002,0.004,0.001,0.087,0.113,3,0.005
1027.426,1038.059,106.197,0.002,0.003,0.001,0.123,0.166,3,0.004
1013.158,1028.914,99.806,0.001,0.002,0.000,0.050,0.057,1,0.002
1025.082,1042.703,112.882,0.002,0.004,0.001,0.069,0.090,3,0.004
1023.106,1032.518,101.995,0.001,0.002,0.000,0.133,0.163,2,0.003
1025.195,1035.507,103.944,0.002,0.003,0.000,0.137,0.178,3,0.003
1026.349,1042.942,112.943,0.002,0.004,0.001,0.047,0.060,2,0.004
1011.658,1051.555,113.285,0.001,0.005,0.001,0.130,0.185,1,0.005
1008.891,1032.245,99.834,0.001,0.002,0.000,0.043,0.059,1,0.002
1008.861,1053.007,113.169,0.001,0.005,0.001,0.050,0.071,2,0.006
1007.062,1035.073,100.347,0.001,0.003,0.000,0.034,0.042,1,0.003
1015.395,1050.153,113.570,0.001,0.005,0.001,0.122,0.156,2,0.005
1011.757,1030.691,99.916,0.001,0.002,0.000,0.071,0.098,2,0.002
1006.759,1054.659,112.841,0.001,0.006,0.001,0.094,0.114,3,0.006
1004.914,1037.433,100.087,0.001,0.003,0.000,0.135,0.183,2,0.003
1007.559,1055.147,113.686,0.001,0.006,0.001,0.055,0.076,1,0.006
1005.710,1035.654,100.058,0.001,0.003,0.000,0.058,0.085,1,0.003
1008.253,1053.698,113.252,0.001,0.005,0.001,0.034,0.050,1,0.006
1006.381,1035.157,100.141,0.001,0.003,0.000,0.079,0.112,1,0.003
1010.364,1052.197,113.445,0.001,0.005,0.001,0.063,0.077,1,0.005
1008.069,1034.195,100.424,0.001,0.002,0.000,0.097,0.113,3,0.003
1009.696,1052.300,113.288,0.001,0.005,0.001,0.050,0.062,2,0.005
1007.612,1034.985,100.539,0.001,0.003,0.000,0.110,0.143,3,0.003
1011.225,1053.105,113.701,0.001,0.005,0.001,0.063,0.087,2,0.006
1008.601,1033.281,100.169,0.001,0.002,0.000,0.039,0.044,1,0.002
1013.409,1049.364,113.483,0.001,0.005,0.001,0.011,0.015,2,0.005
1010.371,1031.001,99.815,0.001,0.002,0.000,0.037,0.052,1,0.002
1012.549,1050.605,113.617,0.001,0.005,0.001,0.036,0.048,2,0.005
1009.648,1031.484,99.780,0.001,0.002,0.000,0.076,0.097,1,0.002
1014.297,1049.721,113.591,0.001,0.005,0.001,0.074,0.102,1,0.005
1011.058,1030.314,99.726,0.001,0.002,0.000,0.056,0.078,2,0.002
```

1015.619,1045.534,113.219,0.001,0.004,0.001,0.067,0.087,2,0.004
1012.886,1031.118,100.241,0.001,0.002,0.000,0.030,0.038,3,0.002
1023.168,1042.717,112.822,0.002,0.004,0.001,0.022,0.025,1,0.004
1020.079,1042.446,112.182,0.002,0.003,0.001,0.033,0.043,1,0.004
1018.371,1042.581,112.235,0.001,0.003,0.001,0.025,0.034,2,0.004
1024.096,1043.031,113.106,0.002,0.004,0.001,0.048,0.054,3,0.004
1017.077,1043.942,113.172,0.001,0.004,0.001,0.034,0.044,1,0.004
1014.160,1029.967,100.071,0.001,0.002,0.000,0.126,0.139,2,0.002
1015.826,1029.984,100.552,0.001,0.002,0.000,0.031,0.039,2,0.002
1016.985,1028.090,99.957,0.001,0.002,0.000,0.034,0.047,2,0.002
1019.167,1029.256,100.554,0.001,0.002,0.000,0.032,0.045,2,0.002
1020.321,1030.112,100.941,0.001,0.002,0.000,0.147,0.202,2,0.002
1022.042,1032.056,101.697,0.001,0.002,0.000,0.030,0.039,1,0.003
1022.215,1042.684,112.705,0.002,0.004,0.001,0.036,0.044,1,0.004
1017.767,1043.216,113.166,0.001,0.004,0.001,0.025,0.033,2,0.004
1014.876,1028.863,99.950,0.001,0.002,0.000,0.032,0.044,2,0.002
1019.471,1043.345,113.102,0.002,0.004,0.001,0.029,0.031,2,0.004
1016.570,1029.415,100.132,0.001,0.002,0.000,0.062,0.083,2,0.002
1017.722,1027.742,99.957,0.001,0.002,0.000,0.110,0.138,3,0.002
1021.135,1043.041,112.956,0.002,0.004,0.001,0.074,0.092,3,0.004
1014.983,1037.862,105.877,0.001,0.003,0.001,0.043,0.059,1,0.003
1015.450,1039.960,109.227,0.001,0.003,0.001,0.051,0.067,3,0.003
1016.123,1043.060,112.348,0.001,0.003,0.001,0.105,0.137,1,0.004
1015.967,1042.680,111.733,0.001,0.003,0.001,0.022,0.030,2,0.004
1015.854,1042.339,111.003,0.001,0.003,0.001,0.052,0.071,1,0.004
1015.619,1040.912,110.049,0.001,0.003,0.001,0.049,0.065,1,0.003
1015.216,1039.579,108.556,0.001,0.003,0.001,0.145,0.180,1,0.003
1015.157,1039.012,107.880,0.001,0.003,0.001,0.053,0.066,3,0.003
1015.025,1038.564,107.203,0.001,0.003,0.001,0.071,0.089,1,0.003
1014.623,1038.296,106.489,0.001,0.003,0.001,0.035,0.048,1,0.003
1014.819,1037.602,105.265,0.001,0.003,0.001,0.029,0.040,2,0.003
1014.796,1037.403,104.507,0.001,0.003,0.000,0.185,0.233,1,0.003
1014.585,1036.620,103.913,0.001,0.003,0.000,0.118,0.165,1,0.003
1014.366,1035.746,103.296,0.001,0.002,0.000,0.021,0.029,2,0.003
1014.172,1034.937,102.592,0.001,0.002,0.000,0.047,0.061,2,0.003
1013.911,1033.818,101.931,0.001,0.002,0.000,0.057,0.074,3,0.002
1013.883,1032.996,101.559,0.001,0.002,0.000,0.046,0.061,2,0.002
1013.735,1031.985,100.922,0.001,0.002,0.000,0.199,0.223,2,0.002
1013.464,1030.971,100.282,0.001,0.002,0.000,0.066,0.078,2,0.002
1016.968,1043.581,112.557,0.001,0.004,0.001,0.044,0.057,1,0.004
1016.845,1043.022,111.715,0.001,0.003,0.001,0.020,0.028,2,0.004
1016.717,1042.329,110.965,0.001,0.003,0.001,0.034,0.043,1,0.004
1016.575,1041.139,109.972,0.001,0.003,0.001,0.051,0.064,1,0.004
1016.278,1040.227,109.367,0.001,0.003,0.001,0.058,0.073,3,0.003
1016.183,1039.602,108.487,0.001,0.003,0.001,0.169,0.180,3,0.003
1016.077,1039.101,107.806,0.001,0.003,0.001,0.041,0.049,3,0.003
1015.933,1038.647,107.100,0.001,0.003,0.001,0.056,0.070,1,0.003
1015.836,1038.075,106.377,0.001,0.003,0.001,0.050,0.059,1,0.003
1015.742,1037.792,105.882,0.001,0.003,0.001,0.030,0.040,2,0.003
1015.602,1037.421,105.285,0.001,0.003,0.001,0.034,0.044,2,0.003
1015.451,1036.935,104.663,0.001,0.003,0.000,0.034,0.045,3,0.003
1015.391,1036.176,103.853,0.001,0.003,0.000,0.102,0.127,3,0.003
1015.253,1035.502,103.391,0.001,0.002,0.000,0.092,0.118,1,0.003
1014.990,1034.342,102.666,0.001,0.002,0.000,0.055,0.073,1,0.003
1014.793,1033.375,102.033,0.001,0.002,0.000,0.085,0.107,1,0.002
1014.503,1032.431,101.471,0.001,0.002,0.000,0.038,0.046,2,0.002
1014.557,1031.541,100.911,0.001,0.002,0.000,0.018,0.024,3,0.002

Example of Sampling Points of Area-3 Measured Using Close-range Photogrammetry Method

```
X_(m),Y_(m),Z_(m),X_Precision,Y_Precision,Z_Precision,RMS_Residual_(pix
els),Largest_Residual_(pixels),Photo_Largest_Residual,Precision_Vector_
Length
1007.637,1053.634,112.893,0.001,0.010,0.002,0.029,0.039,1,0.010
1014.190,1035.588,103.117,0.001,0.005,0.001,0.155,0.190,1,0.006
1024.171,1040.067,108.657,0.002,0.006,0.001,0.054,0.076,1,0.007
1024.007,1028.076,100.478,0.002,0.004,0.001,0.013,0.014,2,0.005
1024.946,1029.604,101.132,0.002,0.005,0.001,0.085,0.117,1,0.005
1025.458,1030.230,101.548,0.002,0.005,0.001,0.209,0.271,3,0.005
1026.243,1031.583,102.309,0.002,0.005,0.001,0.046,0.055,1,0.005
1027.085,1032.820,103.034,0.002,0.005,0.001,0.035,0.048,2,0.006
1027.341,1033.128,103.428,0.002,0.005,0.001,0.043,0.055,1,0.006
1028.168,1034.471,104.215,0.002,0.005,0.001,0.047,0.052,1,0.006
1028.725,1035.246,104.928,0.002,0.005,0.001,0.071,0.079,3,0.006
1029.400,1036.265,105.686,0.002,0.006,0.001,0.023,0.029,1,0.006
1030.133,1037.173,106.358,0.002,0.006,0.001,0.045,0.056,2,0.006
1030.757,1038.161,107.160,0.002,0.006,0.001,0.093,0.122,3,0.007
1031.342,1038.880,107.553,0.003,0.006,0.001,0.132,0.177,2,0.007
1031.749,1039.295,108.398,0.003,0.006,0.001,0.020,0.024,1,0.007
1032.032,1040.067,109.220,0.003,0.007,0.001,0.203,0.269,3,0.007
1032.242,1040.478,109.846,0.003,0.007,0.001,0.051,0.070,2,0.007
1032.730,1040.776,110.284,0.003,0.007,0.001,0.151,0.212,3,0.007
1033.151,1041.344,111.166,0.003,0.007,0.002,0.031,0.041,2,0.008
1033.303,1041.380,111.986,0.003,0.007,0.002,0.025,0.031,1,0.008
1022.992,1026.481,99.927,0.002,0.004,0.001,0.012,0.015,2,0.005
1033.636,1041.536,112.826,0.003,0.007,0.002,0.037,0.041,3,0.008
1032.193,1042.086,112.113,0.003,0.007,0.002,0.108,0.133,3,0.008
1031.946,1041.693,111.412,0.003,0.007,0.002,0.034,0.047,1,0.008
1031.476,1041.442,110.498,0.003,0.007,0.001,0.080,0.108,3,0.007
1031.396,1041.073,109.795,0.003,0.007,0.001,0.045,0.061,3,0.007
1031.001,1040.775,109.038,0.003,0.007,0.001,0.039,0.048,2,0.007
1030.213,1039.468,107.913,0.002,0.006,0.001,0.066,0.087,3,0.007
1029.554,1038.591,107.213,0.002,0.006,0.001,0.126,0.163,1,0.007
1029.158,1037.827,106.549,0.002,0.006,0.001,0.016,0.020,1,0.006
1028.324,1036.639,105.636,0.002,0.006,0.001,0.166,0.208,1,0.006
1027.610,1035.531,104.806,0.002,0.005,0.001,0.028,0.040,3,0.006
1026.834,1034.709,104.232,0.002,0.005,0.001,0.178,0.223,1,0.006
1026.210,1033.641,103.494,0.002,0.005,0.001,0.019,0.026,2,0.006
1025.831,1032.574,102.775,0.002,0.005,0.001,0.095,0.124,1,0.005
1025.113,1031.265,102.066,0.002,0.005,0.001,0.024,0.033,2,0.005
1024.426,1030.525,101.566,0.002,0.005,0.001,0.028,0.037,2,0.005
1023.816,1029.596,101.086,0.002,0.005,0.001,0.030,0.044,3,0.005
1022.770,1027.749,100.393,0.002,0.004,0.001,0.054,0.073,2,0.005
1022.606,1028.992,100.809,0.002,0.005,0.001,0.087,0.112,3,0.005
1023.186,1030.078,101.298,0.002,0.005,0.001,0.019,0.025,1,0.005
1023.820,1031.262,101.830,0.002,0.005,0.001,0.042,0.051,3,0.005
1024.749,1032.262,102.506,0.002,0.005,0.001,0.029,0.034,1,0.005
1025.042,1033.338,103.080,0.002,0.005,0.001,0.044,0.059,1,0.005
1025.621,1034.324,103.740,0.002,0.005,0.001,0.031,0.043,2,0.006
1026.238,1035.275,104.410,0.002,0.005,0.001,0.035,0.049,2,0.006
1027.061,1036.384,105.136,0.002,0.006,0.001,0.019,0.025,1,0.006
1027.751,1037.820,106.083,0.002,0.006,0.001,0.068,0.088,1,0.006
1028.220,1038.610,106.705,0.002,0.006,0.001,0.007,0.009,2,0.007
```

1028.740,1039.341,107.504,0.002,0.006,0.001,0.036,0.047,1,0.007
1028.909,1039.676,108.093,0.002,0.006,0.001,0.055,0.075,1,0.007
1029.151,1040.029,108.797,0.002,0.006,0.001,0.039,0.046,2,0.007
1029.423,1040.542,109.601,0.002,0.007,0.001,0.029,0.040,3,0.007
1030.357,1041.897,110.428,0.003,0.007,0.001,0.133,0.144,1,0.007
1030.563,1042.254,111.027,0.003,0.007,0.001,0.010,0.013,2,0.008
1030.794,1042.538,111.739,0.003,0.007,0.002,0.049,0.065,3,0.008
1030.816,1042.562,112.366,0.003,0.007,0.002,0.035,0.041,3,0.008
1030.165,1043.311,112.531,0.003,0.007,0.002,0.041,0.052,3,0.008
1029.977,1043.358,111.979,0.003,0.007,0.002,0.041,0.050,3,0.008
1029.404,1042.091,111.054,0.002,0.007,0.001,0.157,0.194,3,0.007
1028.683,1041.027,110.300,0.002,0.007,0.001,0.034,0.041,2,0.007
1028.504,1040.626,109.645,0.002,0.007,0.001,0.034,0.040,3,0.007
1028.168,1040.005,108.761,0.002,0.006,0.001,0.085,0.117,1,0.007
1027.886,1039.707,108.153,0.002,0.006,0.001,0.035,0.042,3,0.007
1027.471,1039.154,107.417,0.002,0.006,0.001,0.076,0.096,3,0.007
1027.141,1038.506,106.630,0.002,0.006,0.001,0.054,0.073,1,0.006
1026.547,1037.382,105.643,0.002,0.006,0.001,0.022,0.024,3,0.006
1025.762,1036.193,104.888,0.002,0.006,0.001,0.027,0.035,1,0.006
1025.304,1035.186,104.202,0.002,0.005,0.001,0.162,0.199,3,0.006
1024.788,1034.293,103.583,0.002,0.005,0.001,0.093,0.129,3,0.006
1024.441,1033.683,103.168,0.002,0.005,0.001,0.016,0.022,2,0.006
1023.688,1032.211,102.270,0.002,0.005,0.001,0.025,0.032,2,0.005
1022.874,1030.970,101.610,0.002,0.005,0.001,0.009,0.013,3,0.005
1022.307,1029.820,101.069,0.002,0.005,0.001,0.045,0.061,1,0.005
1021.815,1028.469,100.477,0.002,0.005,0.001,0.038,0.049,3,0.005
1020.979,1029.297,100.681,0.001,0.005,0.001,0.019,0.027,1,0.005
1021.540,1031.115,101.458,0.002,0.005,0.001,0.049,0.058,2,0.005
1022.189,1032.081,101.919,0.002,0.005,0.001,0.038,0.048,1,0.005
1022.804,1033.000,102.435,0.002,0.005,0.001,0.114,0.156,1,0.005
1023.309,1033.942,102.998,0.002,0.005,0.001,0.035,0.045,1,0.005
1023.845,1034.937,103.630,0.002,0.005,0.001,0.041,0.056,2,0.006
1024.251,1035.591,104.169,0.002,0.005,0.001,0.023,0.030,2,0.006
1024.745,1036.431,104.784,0.002,0.006,0.001,0.050,0.070,2,0.006
1025.188,1037.336,105.442,0.002,0.006,0.001,0.083,0.087,3,0.006
1025.611,1038.003,106.110,0.002,0.006,0.001,0.052,0.067,3,0.006
1025.702,1038.600,106.731,0.002,0.006,0.001,0.068,0.087,1,0.006
1026.205,1039.095,107.311,0.002,0.006,0.001,0.072,0.089,3,0.007
1026.404,1039.572,107.852,0.002,0.006,0.001,0.073,0.093,3,0.007
1026.734,1039.998,108.491,0.002,0.006,0.001,0.015,0.021,2,0.007
1026.985,1040.470,109.156,0.002,0.006,0.001,0.016,0.021,2,0.007
1027.271,1040.955,109.717,0.002,0.007,0.001,0.041,0.055,1,0.007
1027.538,1041.357,110.407,0.002,0.007,0.001,0.049,0.066,1,0.007
1027.812,1041.817,111.033,0.002,0.007,0.001,0.052,0.068,3,0.007
1027.933,1041.954,111.648,0.002,0.007,0.002,0.094,0.129,2,0.007
1028.391,1042.844,112.440,0.002,0.007,0.002,0.038,0.052,3,0.008
1020.017,1029.233,100.499,0.001,0.005,0.001,0.019,0.025,2,0.005
1020.625,1030.348,101.008,0.001,0.005,0.001,0.021,0.023,3,0.005
1021.157,1031.402,101.514,0.001,0.005,0.001,0.029,0.040,2,0.005
1021.994,1032.982,102.303,0.002,0.005,0.001,0.044,0.060,2,0.005
1022.418,1034.110,102.941,0.002,0.005,0.001,0.079,0.104,1,0.005
1023.046,1035.156,103.636,0.002,0.005,0.001,0.038,0.050,3,0.006
1023.594,1036.221,104.493,0.002,0.006,0.001,0.039,0.045,3,0.006
1023.860,1036.831,105.010,0.002,0.006,0.001,0.159,0.217,2,0.006
1024.446,1037.830,105.949,0.002,0.006,0.001,0.165,0.227,2,0.006
1024.773,1038.481,106.668,0.002,0.006,0.001,0.098,0.123,3,0.006
1025.088,1038.931,107.183,0.002,0.006,0.001,0.041,0.047,1,0.006

Example of Sampling Points of Area-4 Measured Using Close-range Photogrammetry Method

```
X (m),Y (m),Z (m),X Precision,Y Precision,Z Precision,RMS Residual
(pixels),Largest Residual (pixels),Photo Largest Residual,Precision
Vector Length
1016.271,1043.781,113.177,fixed,fixed,fixed,0.086,0.11,5,fixed
1015.033,1038.157,106.506,fixed,fixed,fixed,0.075,0.121,4,fixed
1014.224,1035.206,102.748,fixed,fixed,fixed,0.104,0.162,4,fixed
1008.225,1052.979,112.658,fixed,fixed,fixed,0.144,0.168,6,fixed
1006.548,1050.721,108.074,fixed,fixed,fixed,0.172,0.217,6,fixed
1004.929,1048.743,105.425,fixed,fixed,fixed,0.223,0.284,6,fixed
1012.863,1048.603,112.584,fixed,fixed,fixed,0.099,0.134,4,fixed
1010.959,1037.944,103.36,fixed,fixed,fixed,0.058,0.075,4,fixed
1007.622,1047.103,106.27,fixed,fixed,fixed,0.12,0.179,6,fixed
1003.768,1046.296,103.278,fixed,fixed,fixed,0.157,0.21,5,fixed
1010.102,1044.069,105.735,fixed,fixed,fixed,0.065,0.097,6,fixed
1005.84,1039.366,101.665,fixed,fixed,fixed,0.173,0.235,4,fixed
1004.45,1060.625,112.459,fixed,fixed,fixed,0.17,0.235,6,fixed
1001.836,1050.061,103.791,fixed,fixed,fixed,0.143,0.21,6,fixed
1012.352,1045.09,109.178,fixed,fixed,fixed,0.076,0.11,6,fixed
1003.754,1053.353,107.954,fixed,fixed,fixed,0.199,0.229,6,fixed
1017.656,1043.365,113.252,0.007,0.005,0.002,0.126,0.148,4,0.008
1013.177,1034.994,102.303,0.005,0.003,0.001,0.181,0.213,4,0.006
1014.677,1035.569,103.262,0.005,0.003,0.001,0.169,0.205,4,0.006
1017.083,1043.882,113.195,0.007,0.005,0.002,0.045,0.061,5,0.008
1015.666,1045.34,113.379,0.006,0.005,0.002,0.034,0.046,5,0.008
1009.307,1033.509,100.424,0.005,0.003,0.001,0.142,0.189,6,0.005
1016.483,1048.412,113.653,0.007,0.006,0.002,0.153,0.188,4,0.009
1007.525,1034.468,100.23,0.004,0.003,0.001,0.064,0.082,6,0.005
1016.125,1049.04,113.478,0.007,0.006,0.002,0.04,0.053,5,0.009
1006.602,1034.995,100.109,0.004,0.003,0.001,0.062,0.08,6,0.005
1015.634,1049.806,113.487,0.007,0.006,0.002,0.117,0.144,4,0.009
1005.761,1035.467,99.995,0.004,0.003,0.001,0.106,0.15,6,0.005
1013.155,1049.404,113.396,0.006,0.006,0.002,0.046,0.059,4,0.008
1005.312,1036.172,100.087,0.004,0.003,0.001,0.193,0.262,6,0.005
1012.582,1050.371,113.594,0.006,0.006,0.002,0.104,0.144,6,0.008
1004.621,1036.578,99.942,0.004,0.003,0.001,0.099,0.141,6,0.005
1011.314,1034.413,101.515,0.005,0.003,0.001,0.016,0.017,6,0.006
1017.094,1045.245,113.656,0.007,0.005,0.002,0.122,0.158,4,0.009
1015.494,1046.505,113.101,0.006,0.005,0.002,0.026,0.035,6,0.008
1008.81,1034.411,100.62,0.004,0.003,0.001,0.106,0.142,4,0.005
1012.307,1051.206,113.364,0.006,0.006,0.002,0.063,0.088,6,0.009
1004.262,1037.525,100.128,0.004,0.003,0.001,0.081,0.101,6,0.005
1010.83,1051.314,113.018,0.006,0.006,0.002,0.087,0.118,6,0.008
1003.595,1038.039,100.126,0.004,0.003,0.001,0.03,0.033,5,0.005
1010.254,1051.984,113.265,0.006,0.006,0.002,0.077,0.108,4,0.008
1002.761,1038.081,99.879,0.004,0.003,0.001,0.089,0.112,6,0.005
1009.227,1052.628,113.196,0.005,0.006,0.002,0.203,0.262,6,0.008
1002.436,1038.949,100.109,0.004,0.003,0.001,0.034,0.043,4,0.005
1008.38,1053.306,113.228,0.005,0.006,0.002,0.157,0.194,6,0.008
1001.301,1039.013,99.803,0.004,0.003,0.001,0.055,0.073,5,0.005
1007.552,1054.422,113.263,0.005,0.006,0.002,0.087,0.12,4,0.008
1000.892,1039.95,99.847,0.004,0.004,0.001,0.103,0.136,6,0.005
1007.46,1055.595,113.671,0.005,0.006,0.002,0.068,0.097,4,0.009
999.877,1040.217,99.873,0.004,0.004,0.001,0.125,0.168,4,0.005
```

1006.915,1056.412,113.452,0.005,0.007,0.002,0.197,0.263,6,0.009
1000.481,1041.923,100.139,0.004,0.004,0.001,0.103,0.104,6,0.005
1007.136,1057.849,113.458,0.005,0.007,0.002,0.092,0.125,6,0.009
1000.201,1042.942,100.301,0.004,0.004,0.001,0.078,0.093,4,0.005
1006.858,1059.029,113.696,0.006,0.007,0.002,0.11,0.154,4,0.01
999.483,1043.391,100.172,0.004,0.004,0.001,0.045,0.06,4,0.005
1006.128,1059.384,113.447,0.005,0.007,0.002,0.061,0.075,6,0.009
998.87,1043.971,100.05,0.003,0.004,0.001,0.091,0.115,5,0.005
1006.174,1060.992,113.609,0.006,0.008,0.002,0.136,0.181,6,0.01
998.455,1044.508,99.994,0.003,0.004,0.001,0.138,0.187,4,0.005
1004.948,1061.186,113.434,0.005,0.008,0.002,0.129,0.173,4,0.01
998.296,1045.325,99.875,0.003,0.004,0.001,0.127,0.179,6,0.006
1004.27,1061.965,113.372,0.005,0.008,0.002,0.114,0.152,6,0.01
997.718,1046.223,100.046,0.003,0.004,0.001,0.069,0.094,6,0.006
1003.802,1062.867,113.581,0.005,0.008,0.002,0.125,0.169,6,0.01
996.882,1046.36,100.057,0.003,0.004,0.001,0.08,0.105,6,0.006
1003.084,1062.321,111.738,0.005,0.008,0.002,0.079,0.109,6,0.01
996.186,1046.623,99.96,0.003,0.005,0.001,0.094,0.131,6,0.006
1002.01,1060.824,109.31,0.005,0.008,0.002,0.142,0.193,4,0.009
994.916,1046.328,99.861,0.003,0.005,0.001,0.102,0.142,6,0.006
1000.703,1059.305,107.093,0.004,0.007,0.001,0.057,0.076,4,0.008
995.567,1048.805,100.662,0.003,0.005,0.001,0.084,0.108,6,0.006
1018.14,1043.205,113.188,0.007,0.005,0.002,0.115,0.129,4,0.009
1016.112,1036.068,103.959,0.006,0.003,0.001,0.095,0.121,6,0.007
998.483,1056.759,105.021,0.004,0.006,0.001,0.075,0.097,6,0.007
995.054,1048.736,100.55,0.003,0.005,0.001,0.129,0.181,4,0.006
997.841,1055.317,104.339,0.004,0.006,0.001,0.19,0.238,6,0.007
997.452,1054.169,103.666,0.004,0.006,0.001,0.224,0.278,6,0.007
997.112,1053.31,103.036,0.003,0.005,0.001,0.108,0.135,4,0.007
996.504,1051.899,102.304,0.003,0.005,0.001,0.043,0.062,4,0.006
995.855,1050.662,101.575,0.003,0.005,0.001,0.082,0.105,6,0.006
995.412,1049.532,101.046,0.003,0.005,0.001,0.032,0.041,6,0.006
998.834,1055.571,104.815,0.004,0.006,0.001,0.135,0.168,4,0.007
998.416,1054.432,104.114,0.004,0.006,0.001,0.114,0.147,6,0.007
997.999,1053.568,103.506,0.004,0.006,0.001,0.096,0.12,6,0.007
997.371,1052.508,102.756,0.003,0.005,0.001,0.027,0.036,4,0.006
997.038,1051.485,102.179,0.003,0.005,0.001,0.035,0.046,6,0.006
996.207,1049.977,101.258,0.003,0.005,0.001,0.082,0.109,6,0.006
999.516,1056.875,105.526,0.004,0.006,0.001,0.052,0.067,4,0.008
999.867,1057.866,106.21,0.004,0.007,0.001,0.103,0.126,4,0.008
1001.695,1059.326,107.743,0.005,0.007,0.001,0.078,0.105,6,0.009
1001.051,1058.034,106.917,0.004,0.007,0.001,0.047,0.062,5,0.008
1000.557,1057.066,106.141,0.004,0.006,0.001,0.059,0.078,6,0.008
1000.071,1055.934,105.468,0.004,0.006,0.001,0.147,0.187,4,0.007
999.551,1054.488,104.568,0.004,0.006,0.001,0.105,0.148,6,0.007
998.998,1053.522,103.828,0.004,0.006,0.001,0.012,0.017,5,0.007
998.528,1052.556,103.206,0.004,0.005,0.001,0.083,0.102,6,0.006
997.868,1051.289,102.387,0.003,0.005,0.001,0.025,0.036,6,0.006
997.404,1050.337,101.652,0.003,0.005,0.001,0.041,0.053,6,0.006
996.923,1049.136,100.901,0.003,0.005,0.001,0.028,0.032,4,0.006
996.938,1048.647,100.285,0.003,0.005,0.001,0.042,0.051,5,0.006
1001.558,1059.652,108.445,0.005,0.007,0.001,0.045,0.061,6,0.009
1002.573,1060.373,109.896,0.005,0.007,0.002,0.177,0.225,4,0.009
1002.834,1061.246,110.678,0.005,0.008,0.002,0.021,0.028,6,0.009
1002.413,1059.474,108.857,0.005,0.007,0.001,0.07,0.086,6,0.009
1002.344,1059.01,108.206,0.005,0.007,0.001,0.023,0.032,4,0.009
1002.138,1057.972,107.376,0.004,0.007,0.001,0.193,0.242,4,0.008

Appendix F

Calculation of Elevation Interpolation Error for Area-1

PT_#	X_ts	Y_ts	Z_ts	Y_photo	Y_ts - Y_photo	abs(Y_ts - Y_photo)	(Y_ts - Y_photo)^2
1015	1048.540	986.081	101.962	986.082	-0.001	0.001	0.000001
1024	1054.215	984.453	111.225	984.571	-0.118	0.118	0.013924
1031	1050.323	986.844	104.532	986.778	0.066	0.066	0.004356
104	1050.105	1001.562	102.089	1001.562	0.000	0.000	0.000000
1043	1052.309	987.639	107.783	987.624	0.015	0.015	0.000225
1045	1054.137	987.207	110.157	987.208	-0.001	0.001	0.000001
1049	1053.514	988.791	108.254	988.668	0.123	0.123	0.015129
105	1050.043	988.477	102.625	988.477	0.000	0.000	0.000000
1051	1051.511	989.210	105.573	989.227	-0.017	0.017	0.000289
1062	1052.887	990.832	106.921	990.837	-0.005	0.005	0.000025
1068	1053.819	992.292	109.369	992.194	0.098	0.098	0.009604
1081	1051.313	994.161	105.693	994.246	-0.085	0.085	0.007225
1084	1053.678	993.892	109.274	993.859	0.033	0.033	0.001089
1088	1052.962	995.283	108.895	995.217	0.066	0.066	0.004356
109	1048.820	996.535	101.646	996.535	0.000	0.000	0.000000
1092	1050.394	995.512	104.816	995.553	-0.041	0.041	0.001681
1104	1051.056	996.788	106.088	996.677	0.111	0.111	0.012321
1111	1052.863	997.984	108.256	997.912	0.072	0.072	0.005184
1114	1050.234	998.084	104.469	998.231	-0.147	0.147	0.021609
1123	1051.264	999.526	105.120	999.487	0.039	0.039	0.001521
1125	1054.343	999.497	110.096	999.395	0.102	0.102	0.010404
1139	1051.703	1001.778	104.797	1001.848	-0.070	0.070	0.004900
114	1049.870	999.373	104.000	999.372	0.001	0.001	0.000001
1141	1054.162	1001.862	108.884	1001.809	0.053	0.053	0.002809
1145	1054.286	1004.543	109.247	1004.537	0.006	0.006	0.000036
1150	1052.001	1004.352	105.190	1004.413	-0.061	0.061	0.003721
1154	1049.778	1004.165	101.370	1004.352	-0.187	0.187	0.034969
1160	1050.821	1005.082	104.218	1005.155	-0.073	0.073	0.005329
1162	1052.873	1005.287	106.747	1005.215	0.072	0.072	0.005184
1168	1053.768	1006.647	109.251	1006.515	0.132	0.132	0.017424
117	1054.644	990.038	110.419	990.038	0.000	0.000	0.000000
1172	1050.861	1006.288	104.452	1006.179	0.109	0.109	0.011881
1176	1048.562	1006.004	100.672	1006.072	-0.068	0.068	0.004624
1071	1051.027	992.692	105.168	992.752	-0.060	0.060	0.003600
1040	1050.828	987.989	104.443	987.937	0.052	0.052	0.002704
118	1053.463	996.497	110.237	996.497	0.000	0.000	0.000000

sum	0.216000	2.084000	0.206126
average	0.005684	0.054842	0.005424
RMS			0.073650
max	0.132000	0.187000	0.034969
min	-0.187000	0.000000	0.000000

Calculation of Elevation Interpolation Error for Area-2

NO	X_ts	Y_ts	Z_ts	Y_photo	Z_ts - Z_photo	abs(Z_ts - Z_photo)	(Z - Z_rerata)^2
1	1008.883	1048.075	107.399	1047.945	0.130	0.130	0.016823
2	1008.144	1045.081	105.029	1045.101	-0.021	0.021	0.000428
3	1011.133	1047.413	108.527	1047.500	-0.087	0.087	0.007499
4	1010.254	1044.343	105.670	1044.329	0.015	0.015	0.000224
6	1012.501	1045.773	109.282	1045.850	-0.077	0.077	0.005970
7	1011.084	1041.314	104.603	1041.327	-0.013	0.013	0.000172
8	1010.031	1034.413	100.616	1034.467	-0.054	0.054	0.002928
9	1012.672	1042.145	106.687	1042.211	-0.066	0.066	0.004346
10	1013.196	1043.680	108.598	1043.733	-0.053	0.053	0.002815
11	1012.894	1039.869	105.221	1039.875	-0.006	0.006	0.000039
12	1011.262	1032.234	99.881	1032.282	-0.048	0.048	0.002277
13	1011.974	1034.082	101.065	1034.104	-0.022	0.022	0.000472
14	1012.501	1035.450	101.991	1035.490	-0.039	0.039	0.001543
16	1014.005	1039.355	106.435	1039.257	0.098	0.098	0.009656
17	1014.556	1040.784	108.392	1040.775	0.009	0.009	0.000086
18	1015.060	1042.093	109.634	1042.156	-0.063	0.063	0.003970
19	1014.163	1036.431	103.243	1036.399	0.032	0.032	0.001047
21	1014.120	1033.898	101.642	1033.825	0.073	0.073	0.005360
20	1016.036	1040.986	109.915	1040.808	0.179	0.179	0.031893
22	1016.091	1038.459	106.290	1038.481	-0.022	0.022	0.000476
23	1016.766	1040.023	108.346	1040.153	-0.130	0.130	0.017007
24	1018.824	1042.187	110.495	1042.268	-0.082	0.082	0.006645
25	1017.650	1039.591	107.741	1039.513	0.078	0.078	0.006116
26	1016.413	1036.856	104.224	1036.940	-0.084	0.084	0.006973
27	1015.537	1034.923	102.715	1034.953	-0.030	0.030	0.000921
28	1015.260	1031.376	100.433	1031.425	-0.049	0.049	0.002416
29	1016.816	1034.605	102.863	1034.621	-0.016	0.016	0.000259
30	1018.308	1037.699	105.242	1037.684	0.015	0.015	0.000228
31	1020.032	1041.273	109.489	1041.304	-0.031	0.031	0.000955
32	1020.267	1038.994	107.027	1038.960	0.035	0.035	0.001196
33	1018.526	1035.565	103.824	1035.563	0.002	0.002	0.000003
34	1020.533	1036.480	104.457	1036.444	0.035	0.035	0.001259
35	1022.355	1037.747	105.230	1037.808	-0.061	0.061	0.003739
36	1019.854	1033.291	102.274	1033.302	-0.011	0.011	0.000120
37	1018.504	1030.884	100.719	1030.899	-0.014	0.014	0.000198
38	1007.926	1041.778	103.240	1041.778	0.000	0.000	0.000000
39	1010.804	1038.079	103.082	1038.079	0.000	0.000	0.000000
40	1024.114	1040.074	108.323	1040.074	0.000	0.000	0.000000

sum	-0.377048	1.780360	0.146059
average	-0.009922	0.046852	0.003844
RMS			0.061997305
max	0.178587	0.178587	0.031893
min	-0.130412	0.000008	0.000000

Calculation of Elevation Interpolation Error for Area-3

PT_#	X_ts	Y_ts	Z_ts	Y_photo	Y_ts - Y_photo	abs(Y_ts - Y_photo)	(Y - Y_rerata)^2
4237	1012.533	1045.339	108.955	1045.338	0.001	0.001	0.000000
4244	1011.818	1041.253	104.984	1041.253	0.000	0.000	0.000000
4447	1010.828	1047.855	108.457	1047.855	0.000	0.000	0.000000
4451	1010.232	1044.142	105.555	1044.142	0.000	0.000	0.000000
4489	1009.301	1048.026	107.390	1048.026	0.000	0.000	0.000000
4499	1008.375	1037.877	101.680	1037.877	0.000	0.000	0.000000
4517	1008.327	1045.105	105.219	1045.105	0.000	0.000	0.000000
4520	1008.128	1041.466	103.256	1041.466	0.000	0.000	0.000000
1027	1019.018	1031.124	101.010	1031.122	0.002	0.002	0.000004
1033	1022.759	1037.246	104.595	1037.303	-0.057	0.057	0.003280
1039	1024.514	1040.118	108.286	1040.164	-0.046	0.046	0.002096
1057	1020.850	1036.092	104.194	1036.129	-0.037	0.037	0.001341
1060	1019.405	1033.591	102.519	1033.615	-0.024	0.024	0.000556
1092	1020.206	1038.831	106.816	1038.911	-0.080	0.080	0.006337
1096	1018.282	1035.135	103.443	1035.155	-0.020	0.020	0.000388
1107	1015.169	1031.738	100.763	1031.735	0.003	0.003	0.000007
1112	1016.847	1035.249	103.390	1035.198	0.051	0.051	0.002594
1115	1018.069	1037.807	105.435	1037.769	0.038	0.038	0.001441
1121	1019.769	1041.363	109.649	1041.330	0.033	0.033	0.001062
1131	1017.665	1039.144	107.131	1039.121	0.023	0.023	0.000530
1137	1016.420	1036.387	103.920	1036.381	0.006	0.006	0.000037
1140	1015.593	1034.554	102.548	1034.574	-0.020	0.020	0.000381
1173	1016.176	1038.196	105.936	1038.262	-0.066	0.066	0.004396
1179	1016.983	1040.102	108.531	1040.142	-0.040	0.040	0.001577
1192	1016.637	1041.074	109.531	1041.055	0.019	0.019	0.000346
120	1010.959	1037.944	102.952	1037.944	0.000	0.000	0.000000
1201	1014.852	1036.669	103.790	1036.566	0.103	0.103	0.010681
1215	1013.278	1035.596	102.349	1035.591	0.005	0.005	0.000022
1236	1014.783	1042.159	109.363	1042.130	0.029	0.029	0.000868
1238	1014.232	1040.587	107.667	1040.584	0.003	0.003	0.000008
1241	1013.777	1039.290	105.661	1039.484	-0.194	0.194	0.037639
1244	1013.207	1037.663	103.576	1037.672	-0.009	0.009	0.000079
1248	1011.887	1033.899	100.998	1033.944	-0.045	0.045	0.001982
1249	1011.375	1032.439	100.423	1032.404	0.035	0.035	0.001257
1262	1012.841	1039.838	105.075	1039.920	-0.082	0.082	0.006723
1278	1013.586	1043.954	109.355	1043.992	-0.038	0.038	0.001407
1283	1012.906	1041.752	106.845	1041.665	0.087	0.087	0.007544
1184	1017.973	1042.440	111.533	1042.507	-0.067	0.067	0.004521

sum	-0.385439	1.259643	0.099102
average	-0.010143	0.033148	0.002608
RMS			0.051068
max	0.103350	0.194008	0.037639
min	-0.194008	0.000015	0.000000

Calculation of Elevation Interpolation Error for Area-4

NO	X_ts	Y_ts	Z_ts	Y_photo	Y_ts - Y_photo	abs(Y_ts - Y_photo)	(Y_ts - Y_photo)^2
1	1012.954	1047.522	110.595	1047.512	0.010	0.010	0.000099
2	1012.104	1043.239	107.005	1043.142	0.096	0.096	0.009303
3	1011.818	1041.253	105.392	1041.242	0.011	0.011	0.000115
4	1011.565	1045.383	108.625	1045.410	-0.026	0.026	0.000697
6	1010.986	1048.533	109.646	1048.377	0.157	0.157	0.024557
7	1009.446	1042.042	104.512	1042.055	-0.013	0.013	0.000168
8	1008.420	1038.719	102.469	1038.732	-0.013	0.013	0.000172
9	1009.613	1051.672	112.495	1051.495	0.177	0.177	0.031333
10	1009.220	1050.443	110.562	1050.384	0.059	0.059	0.003522
11	1008.566	1045.831	106.121	1045.843	-0.012	0.012	0.000137
12	1007.115	1035.655	100.740	1035.558	0.097	0.097	0.009417
13	1014.852	1036.669	104.198	1036.547	0.122	0.122	0.014884
14	1014.532	1038.957	107.107	1038.880	0.077	0.077	0.005929
16	1015.417	1041.330	110.174	1041.356	-0.026	0.026	0.000676
17	1015.439	1044.028	112.287	1044.027	0.001	0.001	0.000001
18	1013.916	1039.684	106.784	1039.551	0.133	0.133	0.017689
19	1012.877	1036.722	103.289	1036.671	0.051	0.051	0.002601
21	1015.101	1048.853	112.202	1049.020	-0.167	0.167	0.027889
20	1013.718	1044.377	110.322	1044.310	0.067	0.067	0.004489
22	1011.740	1037.979	103.883	1037.936	0.043	0.043	0.001849
23	1010.882	1035.204	101.763	1035.201	0.003	0.003	0.000009
24	1006.699	1041.937	103.358	1041.911	0.026	0.026	0.000676
25	1007.329	1052.636	110.702	1052.690	-0.054	0.054	0.002916
26	1006.787	1048.746	106.466	1048.670	0.076	0.076	0.005776
27	1004.575	1039.297	101.127	1039.324	-0.027	0.027	0.000729
28	1005.101	1043.812	103.352	1043.787	0.025	0.025	0.000625
29	1004.914	1053.999	110.082	1053.984	0.015	0.015	0.000225
30	1004.545	1049.938	105.259	1049.888	0.050	0.050	0.002500
31	1002.863	1046.818	102.900	1046.747	0.071	0.071	0.005041
32	1003.190	1052.168	106.343	1052.063	0.105	0.105	0.011025
33	1003.437	1056.206	108.733	1056.088	0.118	0.118	0.013924
34	1001.643	1042.172	100.802	1042.162	0.010	0.010	0.000100
35	1000.364	1046.349	101.464	1046.310	0.039	0.039	0.001521
36	1000.397	1050.650	102.968	1050.607	0.043	0.043	0.001849
37	998.989	1053.687	103.968	1053.634	0.053	0.053	0.002809
38	997.050	1050.117	101.468	1050.121	-0.004	0.004	0.000016
39	1009.766	1044.758	106.077	1044.825	-0.067	0.067	0.004489
40	1004.929	1048.743	105.425	1048.743	0.000	0.000	0.000000

sum	1.326003	2.144444	0.209758
avreage	0.034895	0.056433	0.005520
RMS			0.074296
max	0.177011	0.177011	0.031333
min	-0.167000	0.000000	0.000000

Calculation of Volumetric Error for Area-1

photogrammetry	101 meter above	planimetric area	121.671	
		surface area	248.711	
		volume	577.79	
	110 meter above	planimetric area	6.842	
		surface area	15.549	
		volume	3.386	
	between 101 to 110 m	planimetric area	114.829	
		surface area	233.162	
		volume	574.404	
total station	101 meter above	planimetric area	121.279	
		surface area	243.731	
		volume	580.358	
	110 meter above	planimetric area	7.174	
		surface area	16.928	
		volume	3.292	
	between 101 to 110 m	planimetric area	114.105	
		surface area	226.803	
		volume	577.066	
error in:		planimetric area	0.724 m^2	0.634503 %
		surface area	6.359 m^2	2.803755 %
		volume	2.662 m^3	0.461299 %

Calculation of Volumetric Error for Area-2

photogrammetry	101 meter above	planimetric area	245.611	
		surface area	374.403	
		volume	1280.754	
	112 meter above	planimetric area	10.983	
		surface area	20.04	
		volume	4.217	
	between 101 to 112 m	planimetric area	234.628	
		surface area	354.363	
		volume	1276.537	
total station	101 meter above	planimetric area	244.872	
		surface area	373.663	
		volume	1279.422	
	112 meter above	planimetric area	11.096	
		surface area	21.095	
		volume	4.507	
	between 101 to 112 m	planimetric area	233.776	
		surface area	352.568	
		volume	1274.915	
error in:		planimetric area	0.852 m^2	0.364451 %
		surface area	1.795 m^2	0.509122 %
		volume	1.622 m^3	0.127224 %

Calculation of Volumetric Error for Area-3

photogrammetry	101 meter above	planimetric area	248.031	
		surface area	375.049	
		volume	1284.707	
	112 meter above	planimetric area	10.764	
		surface area	19.023	
		volume	3.859	
	between 101 to 112 m	planimetric area	237.267	
		surface area	356.026	
		volume	1280.848	
total station	101 meter above	planimetric area	274.981	
		surface area	372.822	
		volume	1283.698	
	112 meter above	planimetric area	10.539	
		surface area	18.77	
		volume	3.896	
	between 101 to 112 m	planimetric area	264.442	
		surface area	354.052	
		volume	1279.802	
error in:		planimetric area	27.175 m^2	10.27636 %
		surface area	1.974 m^2	0.557545 %
		volume	1.046 m^3	0.081731 %

Calculation of Volumetric Error for Area-4

photogrammetry	101 meter above	planimetric area	306.277	
		surface area	450.504	
		volume	1534.512	
	112 meter above	planimetric area	16.923	
		surface area	30.327	
		volume	8.706	
	between 101 to 112 m	planimetric area	289.354	
		surface area	420.177	
		volume	1525.806	
total station	101 meter above	planimetric area	307.061	
		surface area	445.53	
		volume	1549.878	
	112 meter above	planimetric area	17.472	
		surface area	30.378	
		volume	8.938	
	between 101 to 112 m	planimetric area	289.589	
		surface area	415.152	
		volume	1540.94	
error in:		planimetric area	0.235 m^2	0.081149 %
		surface area	5.025 m^2	1.2104 %
		volume	15.134 m^3	0.982128 %

Appendix G

Profiling of Longitudinal-Section on Area-2 and Area-3

Long_Section	X	Y	Z_Area2	Z_Area3	distance	comulative_dist
beganing	1006.96	1041.75	103.329	103.354	0.000	0.000
int sight 01	1007.6	1041.41	103.451	103.424	0.725	0.725
cross 01	1008.35	1041.11	103.677	103.587	0.808	1.532
int sight 11	1009.14	1040.76	103.929	103.761	0.864	2.397
int sight 12	1009.83	1040.52	104.199	103.995	0.731	3.127
int sight 13	1010.32	1040.22	104.286	104.101	0.575	3.702
cross 02	1011.46	1039.78	104.647	104.512	1.222	4.924
int sight 21	1012.2	1039.43	105.018	104.929	0.819	5.742
int sight 22	1013.04	1039.03	105.217	105.233	0.930	6.673
int sight 23	1014.08	1038.59	105.776	105.896	1.129	7.802
cross 03	1014.92	1038.24	106.537	106.584	0.910	8.712
int sight 31	1015.61	1037.9	105.920	106.064	0.769	9.481
int sight 32	1016.45	1037.55	105.390	105.452	0.910	10.391
int sight 33	1017.19	1037.26	105.120	105.149	0.795	11.186
cross 04	1018.08	1036.86	104.994	105.183	0.976	12.162
int sight 41	1018.77	1036.51	104.845	104.904	0.774	12.935
int sight 42	1019.56	1036.17	104.561	104.682	0.860	13.795
int sight 43	1020.31	1035.82	104.272	104.446	0.828	14.623
cross 05	1020.95	1035.62	104.095	104.251	0.671	15.294
ending	1021.59	1035.33	103.836	103.985	0.703	15.996

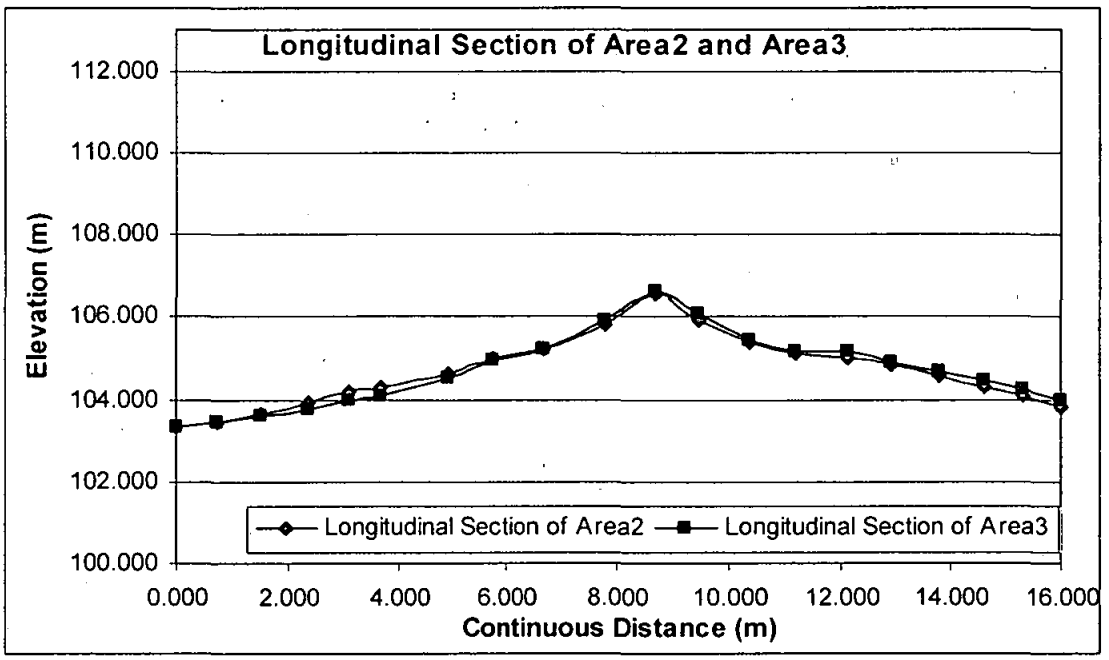

Profiling of Cross-section 01 on Area-2 and Area-3

Cross_Section_01	X	Y	Z_Area2	Z_Area3	distance	comulative_dist
beganing	1011.7	1049.17	111.405	111.565	0.000	-8.732
1	1011.47	1048.68	110.360	110.597	0.541	-8.190
2	1011.1	1047.77	109.404	109.065	0.982	-7.208
3	1010.85	1047.24	108.893	108.643	0.586	-6.622
4	1010.52	1046.48	108.230	107.969	0.829	-5.793
5	1010.19	1045.65	107.217	107.108	0.893	-4.900
6	1009.86	1044.83	106.251	106.243	0.884	-4.016
7	1009.45	1043.9	105.427	105.445	1.016	-3.000
8	1009.14	1043.18	104.956	104.942	0.784	-2.216
9	1008.65	1041.96	104.202	104.118	1.315	-0.901
cross 01	1008.35	1041.11	103.677	103.587	0.901	0.000
11	1007.89	1040.21	102.994	102.961	1.011	1.011
12	1007.31	1038.85	102.060	102.049	1.479	2.489
13	1006.86	1037.8	101.417	101.498	1.142	3.632
ending	1006.57	1037.04	100.945	101.067	0.813	4.445

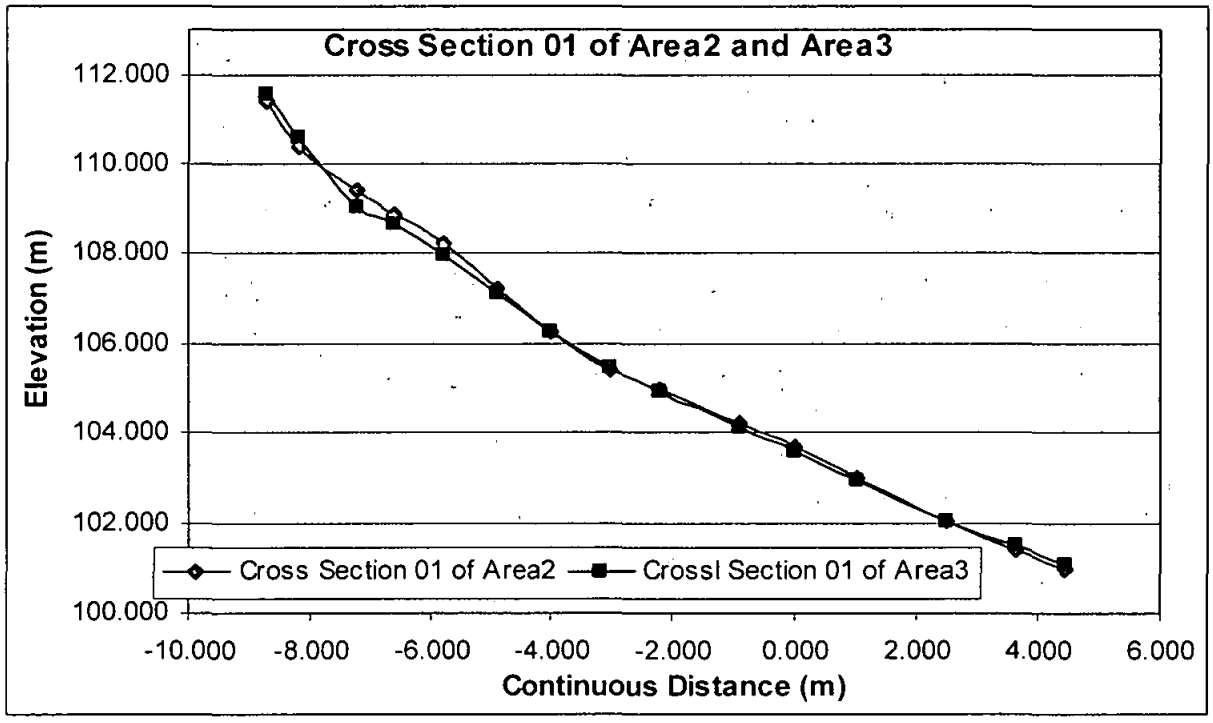

Profiling of Cross-section 02 on Area-2 and Area-3

Cross_Section_02	X	Y	Z_Area2	Z_Area3	distance	comulative_dist
beganing	1014.29	1046.56	111.924	111.764	0.000	-7.350
1	1013.88	1045.57	111.056	110.869	1.072	-6.279
2	1013.53	1044.77	110.243	110.149	0.873	-5.406
3	1013.2	1044	109.445	109.330	0.838	-4.568
4	1012.83	1043.18	108.268	108.072	0.900	-3.668
5	1012.48	1042.31	106.981	106.967	0.938	-2.730
6	1012.09	1041.49	106.011	106.019	0.908	-1.822
7	1011.78	1040.66	105.322	105.104	0.886	-0.936
cross 02	1011.46	1039.78	104.647	104.512	0.936	0.000
11	1011.04	1038.93	104.070	103.923	0.948	0.948
12	1010.63	1038.03	103.352	103.217	0.989	1.937
13	1010.32	1037.28	102.645	102.660	0.812	2.749
14	1010.03	1036.58	102.143	102.167	0.758	3.506
15	1009.7	1035.86	101.620	101.719	0.792	4.298
16	1009.43	1035.22	101.182	101.324	0.695	4.993
ending	1009.14	1034.54	100.738	100.872	0.739	5.732

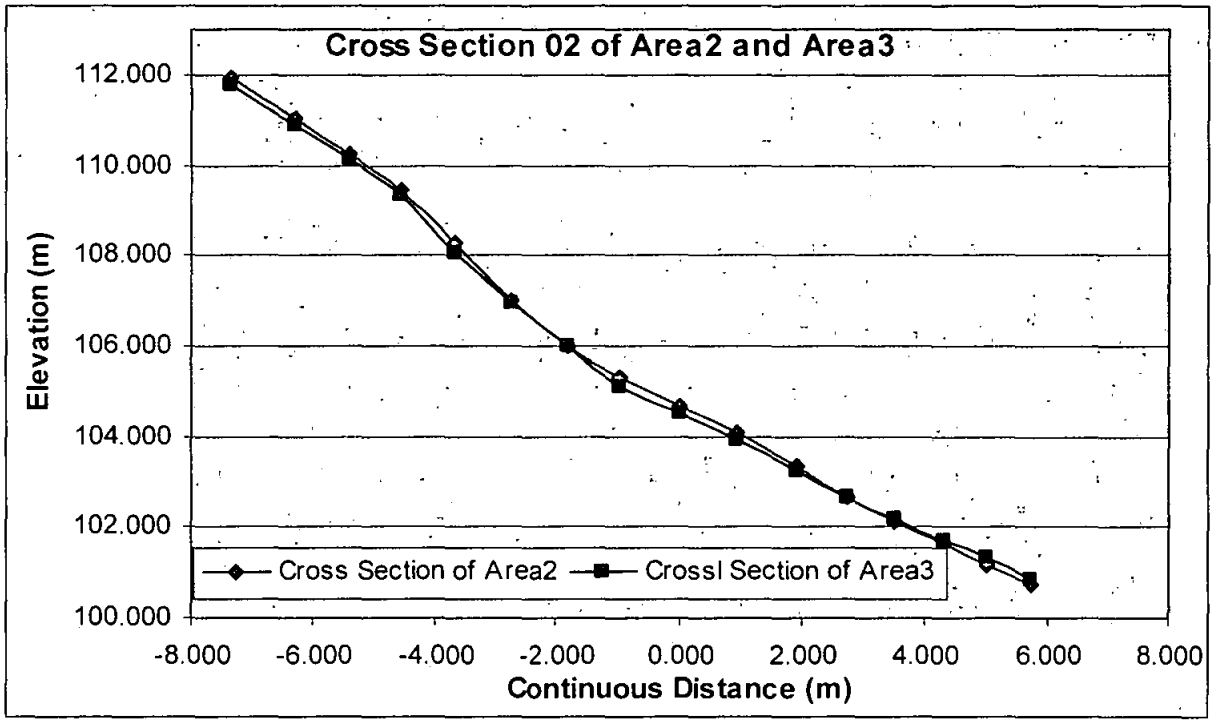

Profiling of Cross-section 03 on Area-2 and Area-3

Cross_Section_03	X	Y	Z_Area2	Z_Area3	distance	comulative_dist
beganing	1016.81	1042.68	112.174	111.380	0.000	-4.828
1	1016.46	1041.9	110.951	110.615	0.855	-3.973
2	1016.17	1041.22	110.533	110.131	0.739	-3.234
3	1015.88	1040.54	109.749	109.691	0.739	-2.495
4	1015.63	1039.94	109.211	109.148	0.650	-1.845
5	1015.35	1039.32	108.276	108.223	0.680	-1.164
6	1015.12	1038.83	107.566	107.602	0.541	-0.623
cross 03	1014.92	1038.24	106.537	106.584	0.623	0.000
11	1014.62	1037.61	105.074	105.069	0.698	0.698
12	1014.31	1036.87	103.978	103.929	0.802	1.500
13	1014.03	1036.25	103.403	103.417	0.680	2.180
14	1013.72	1035.53	102.681	102.859	0.784	2.964
15	1013.49	1034.98	102.229	102.421	0.596	3.560
16	1013.14	1034.24	101.747	101.932	0.819	4.379
17	1012.89	1033.62	101.298	101.576	0.669	5.048
18	1012.65	1033.04	100.888	101.177	0.628	5.675
ending	1012.42	1032.48	100.514	100.868	0.605	6.281

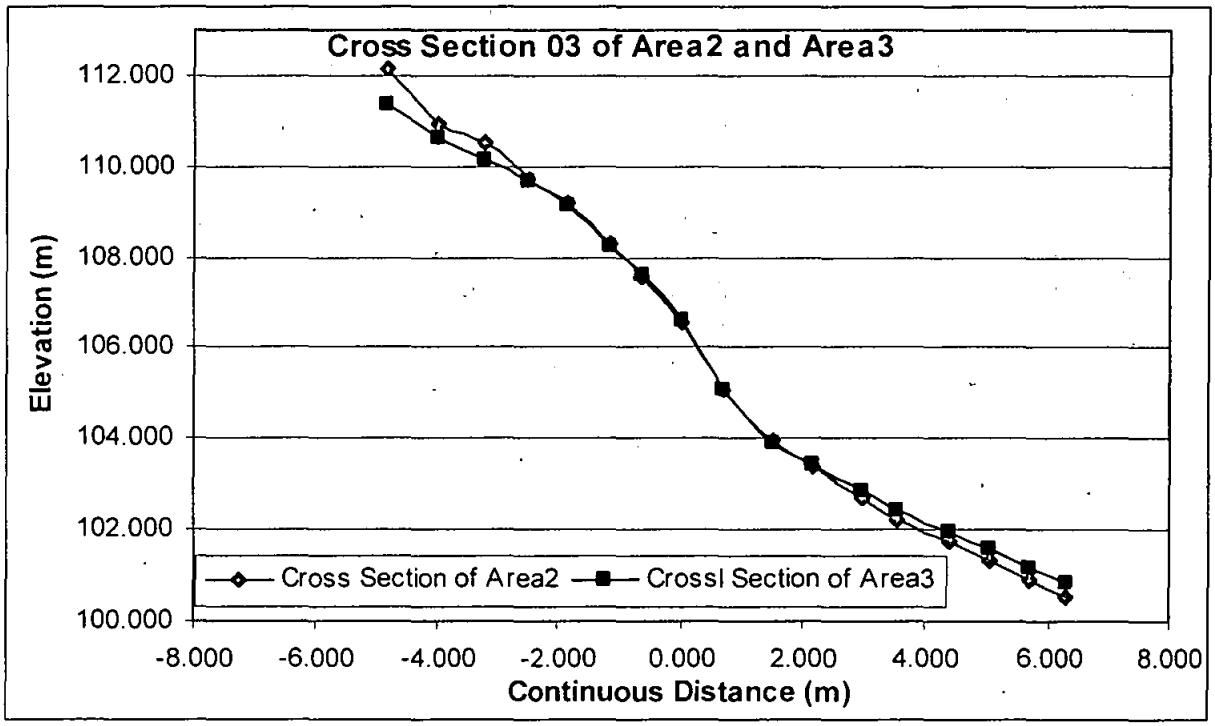

Profiling of Cross-section 04 on Area-2 and Area-3

Cross_Section_04	X	Y	Z_Area2	Z_Area3	distance	comulative_dist
beganing	1020.52	1041.54	112.310	112.334	0.000	-5.982
1	1020.23	1041.92	111.171	111.016	0.478	-5.504
2	1019.94	1041.24	109.862	109.832	0.739	-4.765
3	1019.67	1040.66	109.163	109.105	0.640	-4.125
4	1019.4	1039.96	108.468	108.435	0.750	-3.375
5	1019.03	1039.24	107.637	107.666	0.810	-2.566
6	1018.81	1038.62	106.565	106.692	0.658	-1.908
7	1018.56	1038.01	105.827	106.019	0.659	-1.249
8	1018.31	1037.51	105.465	105.701	0.559	-0.689
cross 04	1018.08	1036.86	104.994	105.183	0.689	0.000
11	1017.82	1036.32	104.567	104.670	0.599	0.599
12	1017.53	1035.64	104.034	104.114	0.739	1.339
13	1017.24	1035	103.553	103.648	0.703	2.041
14	1016.99	1034.44	103.099	103.217	0.613	2.654
15	1016.79	1033.88	102.658	102.781	0.595	3.249
16	1016.54	1033.33	102.244	102.390	0.604	3.853
17	1016.27	1032.77	101.827	102.016	0.622	4.475
18	1016.03	1032.13	101.367	101.581	0.684	5.159
19	1015.76	1031.54	100.939	101.182	0.649	5.807
ending	1015.53	1031.02	100.575	100.836	0.569	6.376

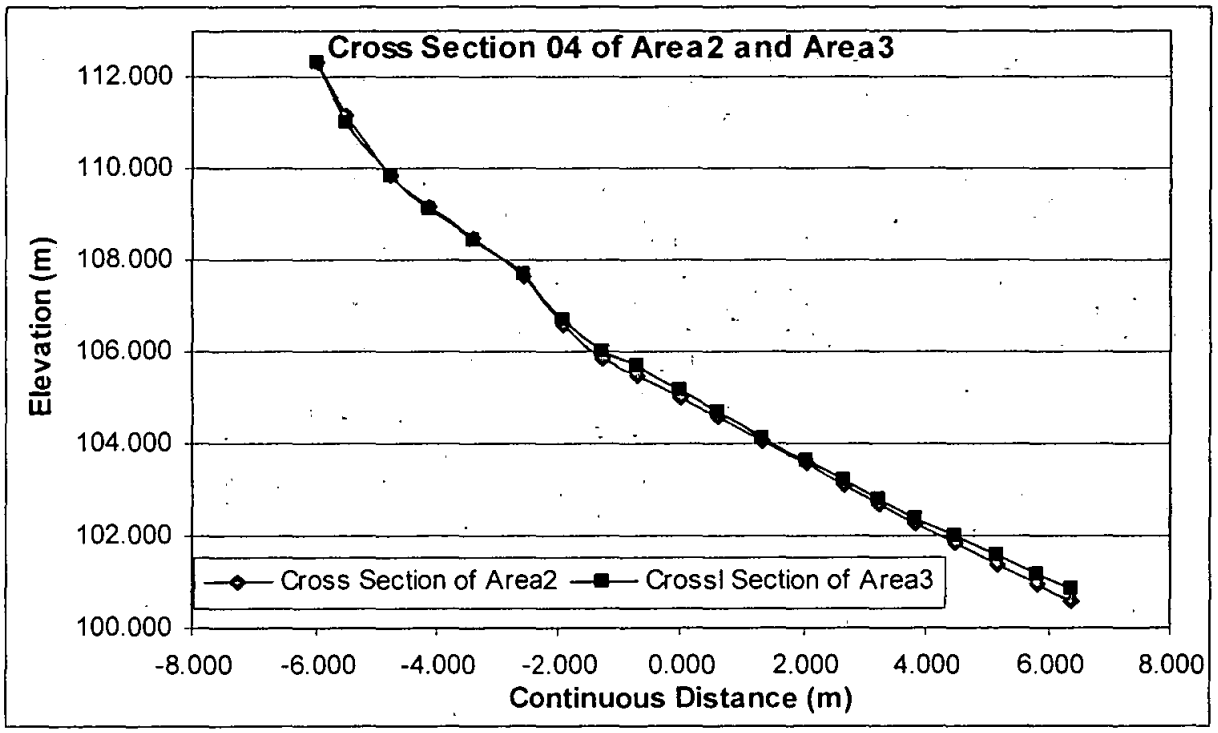

Profiling of Cross-section 05 on Area-2 and Area-3

Cross_Section_05	X	Y	Z_Area2	Z_Area3	distance	comulative_dist
beganing	1023.91	1042.45	112.019	111.890	0.000	-7.448
1	1023.62	1041.78	110.896	110.802	0.730	-6.718
2	1023.38	1041.23	110.316	110.278	0.600	-6.118
3	1023.09	1040.55	109.643	109.564	0.739	-5.378
4	1022.82	1039.96	108.839	108.906	0.649	-4.729
5	1022.46	1039.2	107.729	107.777	0.841	-3.889
6	1022.12	1038.36	106.523	106.549	0.906	-2.982
7	1021.74	1037.56	105.282	105.561	0.886	-2.097
8	1021.42	1036.86	104.863	105.152	0.770	-1.327
9	1021.17	1036.27	104.504	104.742	0.641	-0.686
cross 05	1020.95	1035.62	104.095	104.251	0.686	0.000
11	1020.54	1034.83	103.575	103.796	0.890	0.890
12	1020.26	1034.16	103.101	103.378	0.726	1.616
13	1019.95	1033.44	102.649	102.947	0.784	2.400
14	1019.61	1032.72	102.193	102.477	0.796	3.196
15	1019.23	1031.92	101.677	101.937	0.886	4.082
16	1018.91	1031.2	101.215	101.440	0.788	4.870
17	1018.57	1030.38	100.642	100.893	0.888	5.758
ending	1018.28	1029.71	100.341	100.504	0.730	6.488

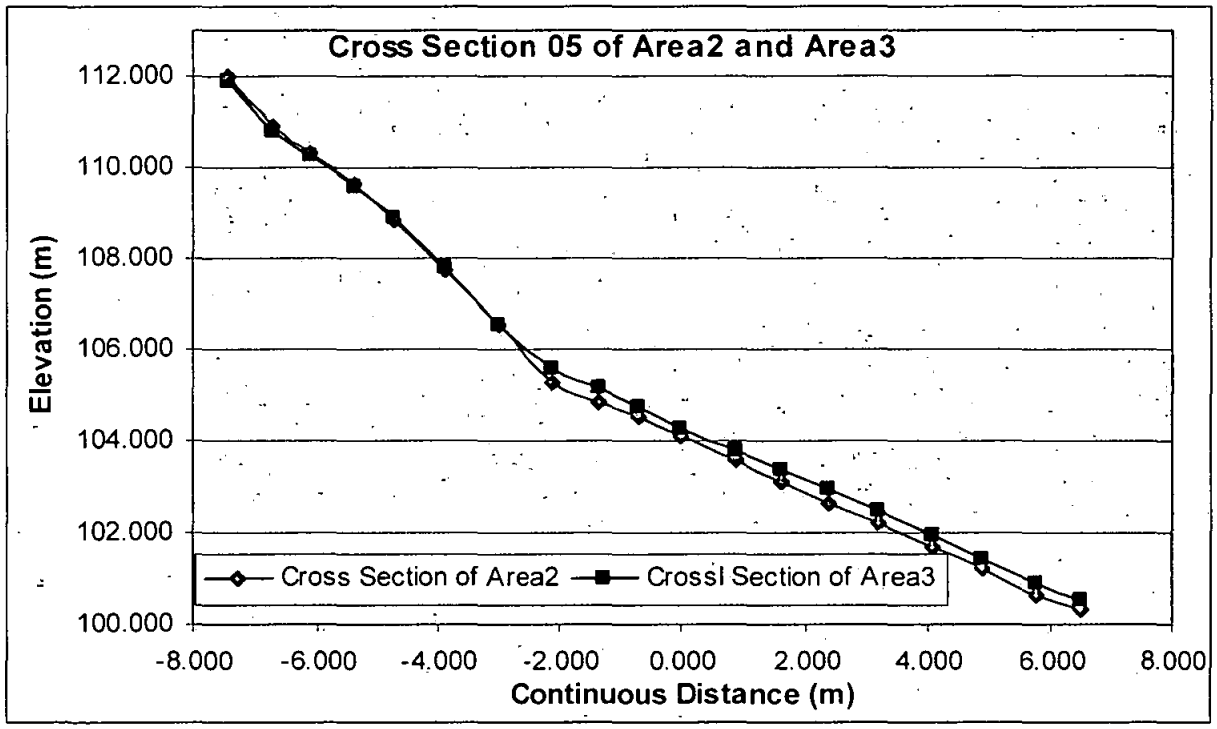

Loss and Gain Volume Estimation

Area (m2)	Volume (m3)	Loss or Gain	Area_id
133.747	19.945	Gain Area	47
3.408	0.318	Gain Area	3
1.868	0.186	Gain Area	14
0.809	0.178	Gain Area	27
2.281	0.121	Gain Area	46
1.785	0.12	Gain Area	29
1.236	0.117	Gain Area	11
2.074	0.084	Gain Area	40
0.753	0.081	Gain Area	26
1.367	0.064	Gain Area	52
0.68	0.048	Gain Area	33
1.121	0.048	Gain Area	73
0.282	0.026	Gain Area	28
0.266	0.02	Gain Area	36
0.234	0.011	Gain Area	38
0.147	0.007	Gain Area	4
0.155	0.007	Gain Area	64
0.228	0.007	Gain Area	62
0.181	0.004	Gain Area	49
0.086	0.003	Gain Area	30
0.146	0.003	Gain Area	39
0.163	0.003	Gain Area	87
0.041	0.002	Gain Area	43
0.046	0.001	Gain Area	24
0.056	0.001	Gain Area	2

Area (m2)	Volume (m3)	Loss or Gain	Area_id
0.001	0	Unchanged Area	35
0.002	0	Unchanged Area	102
0.004	0	Unchanged Area	6
0.004	0	Unchanged Area	42
0.005	0	Unchanged Area	19
0.02	0	Unchanged Area	21
0.022	0	Unchanged Area	61
0.025	0	Unchanged Area	22
0.028	0	Unchanged Area	12
0.048	0	Unchanged Area	82
0.085	-0.001	Loss Area	117
0.191	-0.002	Loss Area	118
0.393	-0.007	Loss Area	74
0.477	-0.007	Loss Area	110
0.494	-0.007	Loss Area	85
0.268	-0.008	Loss Area	83
0.47	-0.02	Loss Area	51
0.558	-0.027	Loss Area	89
1.084	-0.04	Loss Area	103
1.728	-0.078	Loss Area	80
142.189	-24.088	Loss Area	1